

Vignesh Balasubramaniyan

# Load transfer from coupled analysis to structural design of FWTs

Master's thesis in Marine Technology

Supervisor: Prof. Zhen Gao

Co-supervisor: Prof. Erin Bachynski-Polić

August 2022



Vignesh Balasubramaniyan

# Load transfer from coupled analysis to structural design of FWTs

Master's thesis in Marine Technology

Supervisor: Prof. Zhen Gao

Co-supervisor: Prof. Erin Bachynski-Polić

August 2022

Norwegian University of Science and Technology

Faculty of Engineering

Department of Marine Technology



Norwegian University of  
Science and Technology







# PROJECT THESIS IN MARINE TECHNOLOGY SPRING 2022

for

**Stud. Tech. Vignesh Balasubramaniyan**

## **Load transfer from coupled analysis to structural design of FWTs**

*Overføring av laster fra koblet analyse til konstruksjonsdesign for flytende havvindturbiner*

Historically, the hull of a floating wind turbine has been considered as a rigid body in aero-hydro-servo-elastic analysis. These analyses thus provide limited information about the global loads from wind, waves, inertia, and effects from the tower and mooring system. In the oil and gas industry, the loads are typically dominated by wave and inertia effects, and a frequency domain or design wave approach can be used. The applicability of such methods, and improved ways of estimating the global loads for input into a finite element model of the hull, will be further examined in the thesis. A case study considering the 15MW IEA turbines supported by the VolturnUS-S semi-submersible will be studied. The proposed tasks to be carried out include:

1. As needed, revise and extend the literature review into wave and wind statistical description (spectra), wind and wave loads, floating offshore wind turbine dynamics, fatigue and ultimate strength, relevant guidelines and standards, and existing approaches for estimating loads in the hull.
2. Establish a metocean design basis for studying relevant fatigue and extreme loads in the hull, and select several cross sections within the hull and tower for comparisons.
3. Based on the established WADAM model and the provided mass model in Genie, develop a WASIM model of the chosen FWT and compare the responses in regular waves to the previously obtained results (extended to more frequencies) from WADAM and SIMA.
4. For a small number of environmental (wind and wave) conditions, obtain loads at the selected cross sections in the hull and tower by using the motion response from SIMA as input to WASIM.
5. In collaboration with fellow student Yu Ma, develop a SIMA model with the hull modelled using flexible beams. Extract loads at the same locations using the SIMA model, and compare to the WASIM results.
6. Conclusions and recommendations for further work.

The work scope may prove to be larger than initially anticipated. Subject to approval from the supervisors, topics may be deleted from the list above or reduced in extent.

In the project report, the candidate shall present his personal contribution to the resolution of problems within the scope of the project work



Theories and conclusions should be based on mathematical derivations and/or logic reasoning identifying the various steps in the deduction.

The candidate should utilise the existing possibilities for obtaining relevant literature.

### **Project report format**

The project report should be organised in a rational manner to give a clear exposition of results, assessments, and conclusions. The text should be brief and to the point, with a clear language. Telegraphic language should be avoided.

The report shall contain the following elements: A text defining the scope, preface, list of contents, summary, main body of thesis, conclusions with recommendations for further work, list of symbols and acronyms, references and (optional) appendices. All figures, tables and equations shall be numerated.

The supervisors may require that the candidate, in an early stage of the work, presents a written plan for the completion of the work.

The original contribution of the candidate and material taken from other sources shall be clearly defined. Work from other sources shall be properly referenced using an acknowledged referencing system.

The report shall be submitted in electronic format (.pdf):

- Signed by the candidate
- The text defining the scope shall be included (this document)
- Drawings and/or computer models that are not suited to be part of the report in terms of appendices shall be provided on separate (.zip) files.

### **Ownership**

NTNU has according to the present rules the ownership of the project reports. Any use of the report has to be approved by NTNU (or external partner when this applies). The department has the right to use the report as if the work was carried out by a NTNU employee, if nothing else has been agreed in advance.

### **Thesis supervisors:**

Prof. Zhen Gao, NTNU, [zhen.gao@ntnu.no](mailto:zhen.gao@ntnu.no)

Prof. Erin Bachynski-Polić, NTNU, [erin.bachynski@ntnu.no](mailto:erin.bachynski@ntnu.no)

Svein Ersdal, Aker Solutions, [svein.ersdal@akersolutions.com](mailto:svein.ersdal@akersolutions.com)

Andreas Watle, Aker Solutions, [andreas.watle@akersolutions.com](mailto:andreas.watle@akersolutions.com)




Trondheim, August 2022

Zhen Gao

Erin Bachynski-Polić

Svein Ersdal

Andreas Watle

 08/08/2022

Candidate – date and signature:

# Preface

The Master's thesis is submitted as the concluding work of the Master's degree coursework in the department of Marine Technology at the Norwegian University of Science and Technology (NTNU), Trondheim, Norway.

The thesis was initially supervised by Ms. Erin Bachynski-Polić. She helped me in commencing the thesis work. I would like to thank Ms. Erin Bachynski-Polić for providing me with a reference model, technical documents, and some useful Matlab codes. I also thank her for her valuable advice in structuring my thesis work. I would like to express my gratitude to Mr. Zhen Gao, the main supervisor for this thesis work. Mr. Zhen Gao's experience and knowledge in the field of the offshore wind turbine was very useful in carrying out this thesis work. I am grateful to him for his guidance throughout this thesis work.

I would like to thank NTNU Alumni Mr. Kristian Freng Svendsen, whose Master's thesis provided the prerequisite knowledge to start this thesis work. I would like to thank the Master's student and my classmate Mr. Yu Ma for sharing his analysis concerning flexible body modeling of offshore wind turbines in SIMA. The analysis done by Yu Ma was used for a comparative study in this thesis work.

Last but not least, I would want to express my gratitude to the Marine Technology department at NTNU, which provided me with a wealth of academic resources, office space to carry out my thesis work, and also access to the super-fast computer lab, which helped significantly in this thesis work.



---

Vignesh Balasubramanian  
August 2022  
Trondheim, Norway



# Abstract

It is of research interest to establish a technique to capture the loads on the structural members of the offshore wind turbine when they are exposed to simultaneous wind and wave action. Unlike other floating offshore structures, which are dominated by wave loads, offshore wind turbines are subjected to wind turbine loads in addition to the wave loads. In this thesis, simultaneous wind and wave action (called the coupled domain) results in wind turbine loads like thrust and torque in addition to wave loads. The thesis aims to demonstrate a procedure to include the wind, wave, inertia, and effects from the tower and mooring system on the offshore wind turbine and estimate the loads on the cross-section of the pontoon of an offshore wind turbine.

Most current numerical solutions cannot handle both coupled analysis and load transfer. For example, most analyses assume the floater as a rigid body and perform coupled analysis using numerical tools like SIMA. Numerical tools like SIMA, which can handle coupled analysis, do not facilitate obtaining the cross-section load on a rigid body. The thesis addresses the challenge of handling coupled analysis and load transfer for a floating offshore wind structure. This thesis work proposes using three different numerical tools, SIMA, WASIM, and WADAM, to attain the goal of the thesis. SIMA can handle coupled analysis, but cross-sectional loads on a rigid body cannot be obtained in SIMA. WASIM and WADAM can obtain cross-sectional loads on a rigid body. The goal of the thesis is attained by using these tools in conjunction. This thesis work is divided into three stages. In stage one, the model used in SIMA, WASIM, and WADAM are validated by comparing the hydrodynamic properties of the three models. In stage two, the proposed approach in this thesis work is validated in regular wave analysis. In stage three, coupled analysis of the floater is executed, and cross-sectional loads on the pontoons are obtained. Further, the rigid body model used in the thesis is com-

---

pared with a flexible body model developed by NTNU Master's Student Mr. Yu Ma. A flexible body model is a multi-body representation of the FOWT modeled in SIMA, and loads of the flexible body model are obtained in SIMA.

The validation of the proposed approach resulted in reasonably consistent results. The resonance zone exhibited discrepancies attributed to the differences in non-linear damping properties in the WADAM, WASIM, and SIMA models. The proposed approach to obtaining the loads in this thesis is relevant to obtaining the loads on a structure parallel to the global axes in the numerical tools. The proposed approach cannot be used to obtain the loads on the structure which are not parallel to the global axes. Comparing the rigid body model with the flexible body model was consistent for the axial loads but displayed huge variations for bending moments. The discrepancies in the comparative study between rigid and flexible body models must be further investigated. If the flexible body and rigid body approach results are consistent, the flexible body approach will be a one-stop solution to estimate loads on a structural member in a coupled domain. The flexible body approach has no restriction regarding the orientation of structural members, unlike the rigid body approach, where the structural members must be parallel to the global axes.

# Contents

<b>Preface</b>	<b>1</b>
<b>Abstract</b>	<b>3</b>
<b>List of Tables</b>	<b>11</b>
<b>List of Figures</b>	<b>17</b>
<b>1 Introduction</b>	<b>1</b>
1.1 Offshore Wind Energy . . . . .	1
1.1.1 Offshore Wind Energy In Europe . . . . .	2
1.2 Offshore Wind Substructure . . . . .	2
1.2.1 Floating Wind Turbines . . . . .	4
1.3 Semi-Submersible Foundation . . . . .	5
1.3.1 Three-Legged Semi-Submersible Foundation . . . . .	6
1.3.2 Ring-Shaped Semi-Submersible Foundation . . . . .	6
1.3.3 V-Shaped Semi-Submersible Foundation . . . . .	6
1.3.4 Compact Semi-Submersible Foundation . . . . .	7
1.4 Research Aim and Motivation . . . . .	10



1.5	Related Works . . . . .	11
1.6	Proposed Approach . . . . .	12
1.6.1	Model Validation . . . . .	12
1.6.2	Validation Of Proposed Approach . . . . .	13
1.6.3	Execution . . . . .	13
1.7	Scope and Objective . . . . .	13
1.8	Structure Of The Report . . . . .	14
<b>2</b>	<b>Theoretical Background</b>	<b>17</b>
2.1	Rigid Body Mechanics . . . . .	17
2.2	Environmental Loads . . . . .	18
2.3	Hydrodynamics Loads . . . . .	18
2.3.1	Definition Of Waves . . . . .	18
2.3.2	The Hydrodynamic Problem In a Regular Wave . . . . .	19
	Excitation Loads . . . . .	20
	Radiation Loads . . . . .	21
	Panel Method . . . . .	22
	Restoring Loads . . . . .	22
2.3.3	Rigid Body Response . . . . .	24
	Transfer Function And Phase Lag . . . . .	25
2.4	Motion in Irregular Waves . . . . .	25
2.4.1	Wave Spectrum . . . . .	25
2.4.2	JONSWAP Wave Spectrun . . . . .	28
2.5	Aerodynamics Loads . . . . .	29
2.5.1	Blade Element Momentum Method (BEM) . . . . .	30
	Tower Shadow Effect . . . . .	31
	Fault Conditions . . . . .	31

---

2.5.2	Wind Spectrum . . . . .	31
	Kaimal Spectrum . . . . .	32
2.6	Sectional Loads . . . . .	32
2.7	Time-domain analysis . . . . .	32
2.7.1	Equations Of Motion . . . . .	33
	Solutions By Convolution Integral . . . . .	34
	Separation Of Motions . . . . .	36
2.8	Finite Element Modeling Of A Floating Wind Turbine . . . . .	37
<b>3</b>	<b>Numerical Tools</b>	<b>39</b>
3.1	DNV SESAM . . . . .	39
3.1.1	WADAM . . . . .	39
	Definition Of Model Types In WADAM . . . . .	40
	Hydro Model . . . . .	40
	Mass Model . . . . .	40
	Structural Modelling . . . . .	40
3.1.2	WASIM . . . . .	41
3.2	SIMA . . . . .	42
3.3	Coordinate Systems . . . . .	42
<b>4</b>	<b>Numerical Modeling</b>	<b>45</b>
4.1	Umaine VoltturnUS-S 15 MW . . . . .	45
4.1.1	Design Details . . . . .	45
	Mooring Line Properties . . . . .	45
	Mass Moment of Inertia Calculation for the Complete Structure . . . . .	46
4.2	Hydrodynamic Analysis Of The Reference SIMA Model . . . . .	48
4.2.1	Coordinate System . . . . .	48

4.2.2	Hydrodynamic Coefficients . . . . .	49
4.2.3	Rigid Body Decay Tests . . . . .	49
4.3	Modeling In Genie . . . . .	51
4.3.1	Panel Model . . . . .	51
4.3.2	Structural Model . . . . .	52
	Section Model . . . . .	53
4.4	Comparison Of Hydrodynamic Properties Of The Reference Model (SIMA), Panel Model (WADAM), and Section Model (WASIM) .	54
<b>5</b>	<b>Regular Wave Analysis</b>	<b>63</b>
5.1	Motion Response . . . . .	63
5.1.1	Wave Elevation Time Series . . . . .	63
5.1.2	Time Series Of The Rigid Body Response . . . . .	63
5.1.3	Comparison Of RAO Between SIMA, WASIM, and WADAM.	66
5.2	Sectional Load . . . . .	66
5.2.1	Definition Of The Cross-Section . . . . .	66
5.2.2	Time Series Of The Sectional Load . . . . .	69
5.2.3	Comparison Of Load Amplitude Between SIMA, WASIM, and WADAM. . . . .	70
<b>6</b>	<b>Coupled analysis</b>	<b>77</b>
6.1	Load Cases . . . . .	77
6.2	Modified Mass Model . . . . .	78
6.3	Sectional Loads . . . . .	78
<b>7</b>	<b>Flexible body vs. Rigid body</b>	<b>87</b>
7.1	Flexible Body . . . . .	87
7.2	Results and Discussions . . . . .	87

---

7.2.1	Axial Load . . . . .	87
7.2.2	Bending Moment, $M_y$ . . . . .	88
<b>8</b>	<b>Summary and Conclusion</b>	<b>99</b>
8.1	Summary . . . . .	99
8.2	Conclusion and Future Recommendations . . . . .	100
	<b>Appendices</b>	<b>107</b>
<b>A</b>		<b>109</b>
A.1	Wind turbine performance curve . . . . .	110
A.2	Linearized Boundary Value problem . . . . .	111
A.3	PQ Analysis . . . . .	113
<b>B</b>		<b>115</b>
B.1	Miscellaneous Results in Coupled Analysis . . . . .	115
B.1.1	Motion results . . . . .	115
B.1.2	Aerodynamic And Mooring Loads . . . . .	116



# List of Tables

4.1	Umaine VolturnUS-S 15MW FWT System Properties[1]. . . . .	47
4.4	Mass moment of inertia calculation. . . . .	47
4.2	Umaine VolturnUS-S 15MW FWT Mooring line Properties[1]. . .	48
4.3	Modified VCG calculation. . . . .	48
4.5	Hull Infinite-Frequency Added Mass in kg, kg-m or kg-m <sup>2</sup> [1]. . .	50
4.6	Hull hydrostatic stiffness in N/m, N/rad or N-m/rad [1]. . . . .	50
4.7	Natural Period in the six degrees of freedom [1]. . . . .	52
6.1	Load cases . . . . .	77



# List of Figures

1.1	Forecasted cumulative installed capacity until 2030 [2]. . . . .	3
1.2	2016 and 2030 offshore wind installations per sea basin [2]. . . . .	3
1.3	Offshore wind foundations [3]. . . . .	4
1.4	Floating wind turbine a) Spar (Hywind from Statoil) b) Semi-submersible (WindFloat from Principle Power), c) Semisubmersible(OO Star from Dr techn Olav Olsen) d) Barge (IDEOL) e) TLP (Glosten) f) TLB (IFE) [4] (figure 4.3). . . . .	5
1.5	Three-legged Dutch Tri-Floater FWT [5]. . . . .	7
1.6	Three-legged WindFloat FWT [5]. . . . .	7
1.7	Ring Shaped semi-submersible foundation [5]. . . . .	8
1.8	V-Shaped semi-submersible foundation [5]. . . . .	8
1.9	Compact semi-submersible foundation OC4-DeepCwind [6]. . . . .	9
1.10	Comparison of the hydrodynamic response of Compact and V-shaped semi-submersible substructure [6]. . . . .	10
2.1	Six degrees of freedom of a floating rigid body. . . . .	17
2.2	Definition of phase lag in the transfer functions[7]. . . . .	19
2.3	Hydrodynamic loads [8]. . . . .	20
2.4	Mooring system of the reference model. . . . .	23



2.5	Irregulars waves represented as a sum of the regular long crested waves [9]. . . . .	26
2.6	Wave spectrum [10]. . . . .	28
2.7	Annular element used in the BEM model [11]. . . . .	30
2.8	Sectional load calculation in WADAM and WASIM. [12]. . . . .	32
2.9	Forces on Floating wind turbine [13]. . . . .	33
2.10	Finite element model for a floating wind turbine[4]. . . . .	38
3.1	Model types in WADAM [12]. . . . .	40
3.2	Different hydro models in WADAM [12]. . . . .	41
3.3	Floating wind turbine analysis using SIMA[14]. . . . .	42
3.4	The coordinate system in WADAM and WASIM [12]. . . . .	43
3.5	The coordinate system in SIMA [15]. . . . .	43
4.1	General Arrangement of UMaine VoltturnUS-S 15 MW FWT[1]. . . . .	46
4.2	Mooring Arrangement of UMaine VoltturnUS-S 15 MW FWT [1]. . . . .	47
4.3	V.C.G of the reference FWT [1]. . . . .	49
4.4	Global coordinate system. . . . .	50
4.5	Results of free decay test in the six degrees of freedom. . . . .	51
4.6	Panel model for WADAM. . . . .	52
4.7	Structural model. . . . .	53
4.8	Mass properties and structural data. . . . .	53
4.9	Section model for WASIM. . . . .	54
4.10	Model validation . . . . .	55
4.11	Added mass in surge due to surge motion $[A_{11}]$ . . . . .	56
4.12	Added mass in heave due to heave motion $[A_{33}]$ . . . . .	56
4.13	Added mass in pitch due to pitch motion $[A_{55}]$ . . . . .	57
4.14	Potential in surge due to surge motion $[B_{11}]$ . . . . .	57

---

4.15	Potential damping in heave due to heave motion [B <sub>33</sub> ]. . . . .	58
4.16	Potential damping in pitch due to pitch motion [B <sub>55</sub> ]. . . . .	58
4.17	First order wave excitation transfer function in surge. . . . .	59
4.18	First order wave excitation transfer function in heave. . . . .	60
4.19	First order wave excitation transfer function in pitch. . . . .	61
5.1	Validation of proposed approach. . . . .	64
5.2	Wave elevation for a wave period of 21 seconds. . . . .	65
5.3	Unfiltered time series of heave response. . . . .	65
5.4	Filtered time-series of heave response. . . . .	66
5.5	Positive peaks in a time series. . . . .	67
5.6	Surge RAO comparison between SIMA, WASIM, and WADAM. . . . .	68
5.7	Heave RAO comparison between SIMA, WASIM, and WADAM. . . . .	68
5.8	Pitch RAO comparison between SIMA, WASIM, and WADAM. . . . .	69
5.9	Location of the three cross-sections defined. . . . .	70
5.10	Section plane overlaps with Pontoon 2 and Pontoon 3. . . . .	71
5.11	Unfiltered time series of load in section 1 - comparison between WASIM and WASIM+SIMA. . . . .	72
5.12	Filtered time-series of load in section 1 - comparison between WASIM and WASIM+SIMA. . . . .	73
5.13	Load amplitude in section 1 - comparison between SIMA, WASIM, and WADAM. . . . .	74
5.14	Load amplitude in section 2 - comparison between SIMA, WASIM, and WADAM. . . . .	75
5.15	Load amplitude in section 3 - comparison between SIMA, WASIM, and WADAM. . . . .	76
6.1	Coupled Analysis - Simultaneous wind and wave action. . . . .	78
6.2	Modified Mass Model . . . . .	79

---

6.3	Comparison of motion response in SIMA (existing mass model) and WASIM+SIMA (modified mass model) . . . . .	79
6.4	Comparison of tower base bending moment in SIMA (existing mass model) and WASIM+SIMA (modified mass model) . . . . .	80
6.5	Sectional Load in LC1 . . . . .	81
6.6	Sectional Load in LC2 . . . . .	81
6.7	Sectional Load in LC3 . . . . .	82
6.8	Sectional Load Spectrum in LC1 . . . . .	82
6.9	Sectional Load Spectrum in LC2 . . . . .	83
6.10	Sectional Load Spectrum in LC3 . . . . .	83
6.11	Sectional Load Statistics in LC1 . . . . .	84
6.12	Sectional Load Statistics in LC2 . . . . .	84
6.13	Sectional Load Statistics in LC3 . . . . .	85
7.1	Flexible Body [16] . . . . .	88
7.2	Axial Load in LC1 . . . . .	88
7.3	Axial Load in LC2 . . . . .	89
7.4	Axial Load in LC3 . . . . .	89
7.5	Axial Load Spectrum in LC1 . . . . .	90
7.6	Axial Load Spectrum in LC2 . . . . .	90
7.7	Axial Load Spectrum in LC3 . . . . .	91
7.8	Axial Load Statistics in LC1 . . . . .	91
7.9	Axial Load Statistics in LC2 . . . . .	92
7.10	Axial Load Statistics in LC3 . . . . .	92
7.11	Bending Moment, $M_y$ in LC1 . . . . .	93
7.12	Bending Moment, $M_y$ in LC2 . . . . .	94
7.13	Bending Moment, $M_y$ in LC3 . . . . .	94
7.14	Bending Moment Spectrum, $M_y$ in LC1 . . . . .	95

---

7.15	Bending Moment Spectrum, $M_y$ in LC2	95
7.16	Bending Moment Spectrum, $M_y$ in LC3	96
7.17	Bending Moment Statistics, $M_y$ in LC1	96
7.18	Bending Moment Statistics, $M_y$ in LC2	97
7.19	Bending Moment Statistics, $M_y$ in LC3	97
A.1	Wind turbine performance curves	110
A.2	Control surface in boundary value problem [17]	111
A.3	Hydrodynamic and Hydrostatic loads	112
A.4	PQ Analysis	113
A.5	Mooring Stiffness coefficients	113
B.1	Heave	115
B.2	Pitch	116
B.3	Tower Base Axial Loads	116
B.4	Tower Base Bending Moment	117
B.5	Mooring Loads	117



# Glossary

## Commonly applied symbols

$\eta$	Wave elevation
$\omega$	Wave frequency in rad/sec
$\phi$	Velocity Potential
$\rho$	Density of sea water
A	Added Mass
B	Damping Coefficient
BEM	Boundary Element Method
C	Restoring coefficient
COG	Center of Gravity
f	Wave frequency in Hz
$F_{ex}$	Excitation Force
$F_x$	Axial Force
$F_z$	Shear Force

---

FEM	Finite Element Method
FOWT	Floating Offshore Wind Turbine
FWT	Floating Wind Turbine
GW	Giga Watts
$H_s$	Significant Wave Height
Hz	Hertz
LC	Load Case
M	Mass
m	Meters
$M_y$	Bending moment about y axis
MW	Mega Watts
N	Newtons
RAO	Response Amplitude Operator
$T_p$	Time Period
$U_w$	Wind speed
x	Rigid body response

# Chapter 1

## Introduction

Mankind's energy production primarily causes global warming. In 2015, United Nations General Assembly (UN-GA) set up Sustainable Development Goals (SDG) to achieve a better and more sustainable future. The seventh goal of the 17 goals in SDG is about providing clean and affordable energy. The seventh goal has three target areas [18]:

1. 7.1 Access to energy
2. 7.2 Renewable energy
3. 7.3 Energy efficiency

By 2030, SDG 7.2 target is to substantially increase the share of renewable energy in the global energy mix. According to DNV Energy Transition Outlook (ETO) 2021, the contribution of fossil fuels is expected to drop from 80% to 50%, and the share of renewable energy is expected to increase from 15% to 45% [18]. Wind and Solar energy remain attractive renewable sources due to their low cycle emission. Wind energy is expected to contribute up to one-third of the total energy demand by 2050 [19].

### 1.1 Offshore Wind Energy

Onshore wind energy is not sufficient to meet the target 7.2 of SDG. Hence, the contributions from offshore wind turbines are important for achieving renewable energy targets. Offshore wind turbines have some advantages over onshore wind turbines. They are listed below [20]:



1. Wind resources are of better quality in the open sea. There are almost no obstacles in offshore sites, and wind speed is higher and steadier offshore. Hence fewer turbines are enough to produce the same amount of energy as onshore wind turbines.
2. Noise emission and visual impacts are significantly reduced since offshore wind turbines are installed far away from the human habitat.
3. Offshore wind turbines are generally bigger than onshore wind turbines and can harness more wind energy.

Some demerits of offshore wind turbines are [20]:

1. Engineering and construction costs of offshore wind turbines are very high. High cost is due to:
  - Robust structure needed to withstand the harsh and corrosive environment.
  - Marine installation is complex and requires expensive logistics.
  - Power transmission through submarine cables to shore.
2. Offshore wind farms must consider variables like marine life, shipping routes, and fisheries when designing their layout.

### 1.1.1 Offshore Wind Energy In Europe

The first offshore wind turbine was installed in Denmark in 1991. So far, Europe has installed 25 GW capacity of offshore wind turbines. By 2030, the European Union expects to have about 70 GW of installed offshore wind capacity in Europe [2]. Figure 1.1 gives the forecast of cumulative installed capacity until 2030. North sea is expected to increase its offshore wind installation from 10 MW to 48 MW by 2030. Following the North sea, the Baltic sea is expected to increase its capacity from 1.5 MW to 9 MW by 2030. Atlantic sea is expected to open its account and will have close to 8 MW installed by 2030 [2]. Figure 1.2 gives the forecast of installed capacity until 2030 per sea basin.

## 1.2 Offshore Wind Substructure

As of 2017, Monopile constitutes 81.7% of substructures of offshore wind turbines, followed by jacket/tripod with 9.8% [21]. To achieve the EU target of 70 GW by 2030, it is important to expand the offshore wind installations in deep waters and upscale the capacity of the wind turbines. Different types of offshore

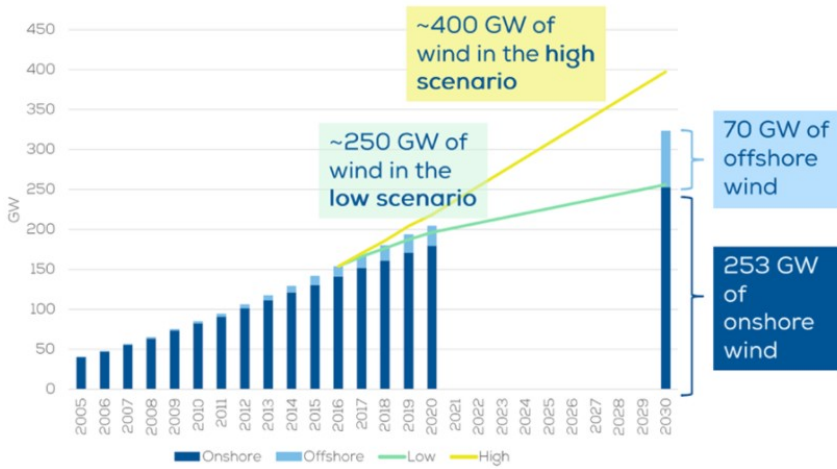


Figure 1.1: Forecasted cumulative installed capacity until 2030 [2].

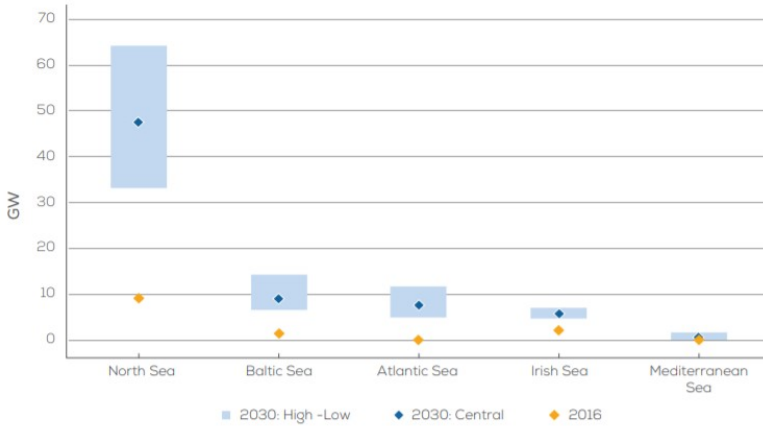
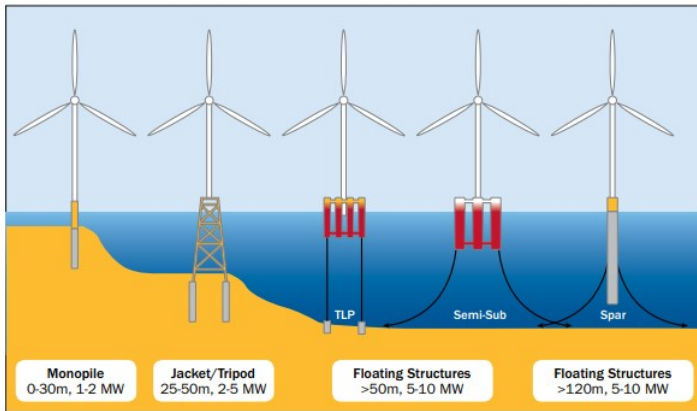


Figure 1.2: 2016 and 2030 offshore wind installations per sea basin [2].

wind foundations are shown in Figure 1.3. Fixed offshore substructures monopiles, jacket, tripod, or gravity-based structures are not economically feasible for water depths over 50 m [21].



**Figure 1.3:** Offshore wind foundations [3].

### 1.2.1 Floating Wind Turbines

Different types of floating offshore wind turbines are shown in the Figure 1.4. For deeper water, a floating substructure moored to the seabed is economical compared to a fixed bottom substructure [22]. Being further away from the coast reduces the impact of noise emissions [22]. The decommissioning process is simpler on a floating platform and can easily be towed to a different site. The installation procedures are also easier on a floating platform [5]. The floating structure is subject to large motions. This leads to transmission losses, and blade control complications; tall towers experience high inertial loads [22]. Following floating concepts are under consideration for deepwater applications:

1. Spar Buoy
2. Tension leg platform (TLP)
3. Tension leg buoy (TLB)
4. Barge
5. Semi submersible

Barge and Semi-submersible obtain their stability from the waterplane moment of inertia. Increasing the area further away from the neutral axis increases the waterplane moment of inertia. This allows for the efficient use of material. Columns have a small waterplane area. Therefore, they are exposed to less wave force than the barge. Small waterplane area reduces the wave forces in SPAR configuration,

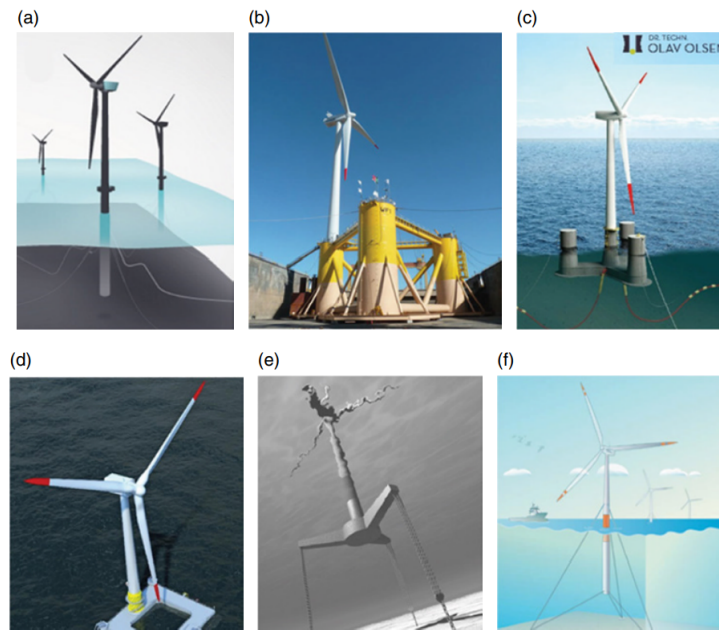


**Figure 1.4:** Floating wind turbine a) Spar (Hywind from Statoil) b) Semi-submersible (WindFloat from Principle Power), c) Semisubmersible (OO Star from Dr techn Olav Olsen) d) Barge (IDEOL) e) TLP (Glosten) f) TLB (IFE) [4] (figure 4.3).

and they obtain stability by placing their center of gravity far below the center of buoyancy. Mathieu instability is a concern in spar configuration since the natural frequencies of heave and pitch are similar [4]. Spar is a deep draft structure hence the turbine installation (connecting the tower) has to be on-site, and they cannot be pre-assembled onshore [4].

TLP and TLB are designed such that buoyancy forces exceed the weight. This is due to the tendons under tension providing the restoring force to TLP and TLB. In TLP, the tendons are vertical and restrict the platform in heave, pitch, and roll, while in TLB, the tendons are angled and help to restrict all six degrees of freedom [4]. An expensive mooring system is a disadvantage in TLPs and TLBs [4].

### 1.3 Semi-Submersible Foundation

This section is based on [5] and [6]. To be competitive in the renewable energy market, the offshore wind energy industry needs to be a cost-effective solution. Of all the configurations discussed in Section 1.2.1, the semi-submersible configuration is reliable and cost-effective [5]. The semi-submersible concept has low construction and installation cost. The wave cancellation effect in semi-submersible signi-

ificantly reduces the wave-induced motions [5]. Several semi-submersible designs have been studied in the past. The driftwind project (2002) has a three-legged semi-submersible design, and the WindFloat project (2011) has a three-legged semi-submersible design. Different semi-submersible designs are dealt in detail in this section. The reference model used in the thesis work has a semi-submersible substructure. The details of the reference model are given in Section 4.1. The different configurations in the semi-submersible design are [5] :

1. Three-legged semi-submersible foundation
2. Ring Shaped semi-submersible foundation
3. V-Shaped semi-submersible foundation
4. Compact semi-submersible foundation

### **1.3.1 Three-Legged Semi-Submersible Foundation**

Three hollow columns support the three-legged semi-submersible foundation. Dutch tri-floater has a three-legged semi-submersible foundation. The wind turbine is positioned at the center of the triangle connecting the three columns. Each column is 8 meters in diameter and comprises two layers of shell. Vertical stiffeners are attached to the external shell to prevent buckling. Each column is divided into two compartments. The bottom compartment is used as a water ballast tank. A foot-plate is attached to the base of the column to dampen the wave-induced vertical motions [5].

WindFloat also has a three-legged semi-submersible foundation. In WindFloat, the wind turbine is positioned on one of the columns. The horizontal water entrapment plate is attached to the base of the column. These plates displace a large volume of water and improve the hydrodynamic response of the structure. WindFloat has an active ballast system to control the wave-induced motions.

### **1.3.2 Ring-Shaped Semi-Submersible Foundation**

Quadran and Ideol developed a ring-shaped semi-submersible substructure design. This design provides sufficient space for the operation and maintenance activities. The moonpool acts as a damper to reduce the floater motions [5].

### **1.3.3 V-Shaped Semi-Submersible Foundation**

Karimirad and Michailides designed the V-shaped semi-submersible foundation for the Fukushima project. The V-shaped semi-submersible foundation consists of the main column and two side columns connected by pontoons. The wind turbine



**Figure 1.5:** Three-legged Dutch Tri-Floater FWT [5].



**Figure 1.6:** Three-legged WindFloat FWT [5].

is positioned on the main column. The V-shaped design is asymmetric, and a ballast system stabilizes it [6].

### 1.3.4 Compact Semi-Submersible Foundation

The compact semi-submersible design consists of one central column and three side columns. The wind turbine is positioned in the central column. The OC4-DeepCwind semi-submersible is an example of a compact semi-submersible foundation. It is designed by the National renewable energy laboratory (NREL). This



**Figure 1.7:** Ring Shaped semi-submersible foundation [5].



**Figure 1.8:** V-Shaped semi-submersible foundation [5].

design has several bracing, including horizontal and diagonal bracing connecting the columns.

A research paper by Lixian Zhang et al. [6] compares hydrodynamic response between V-shaped and Compact (OC4- Deep Cwind). The results are presented in the Figure 1.10. The first-order response of the OC4-DeepCwind in the surge is larger than the V-shaped semi-submersible foundation. The second-order response in the surge is similar for both substructures. The V-shaped semi-submersible substructure exhibited two peaks in the heave RAO in the wave frequency range (0.064 Hz - 0.12 Hz). The first-order response in heave is similar in OC4-DeepCWind and V-shaped substructure. In pitch motion, the V-shaped semi-submersible substructure exhibited two peaks at the low-frequency region corresponding to pitch and heave natural frequencies showing the coupling effect of these modes. OC4-



**Figure 1.9:** Compact semi-submersible foundation OC4-DeepCwind [6].

DeepCWind semi-submersible FWT has two parts in the pitch motion spectra. One is in the low-frequency region related to pitch natural frequency, and the other is the high-frequency region related to wave peak frequency [6].



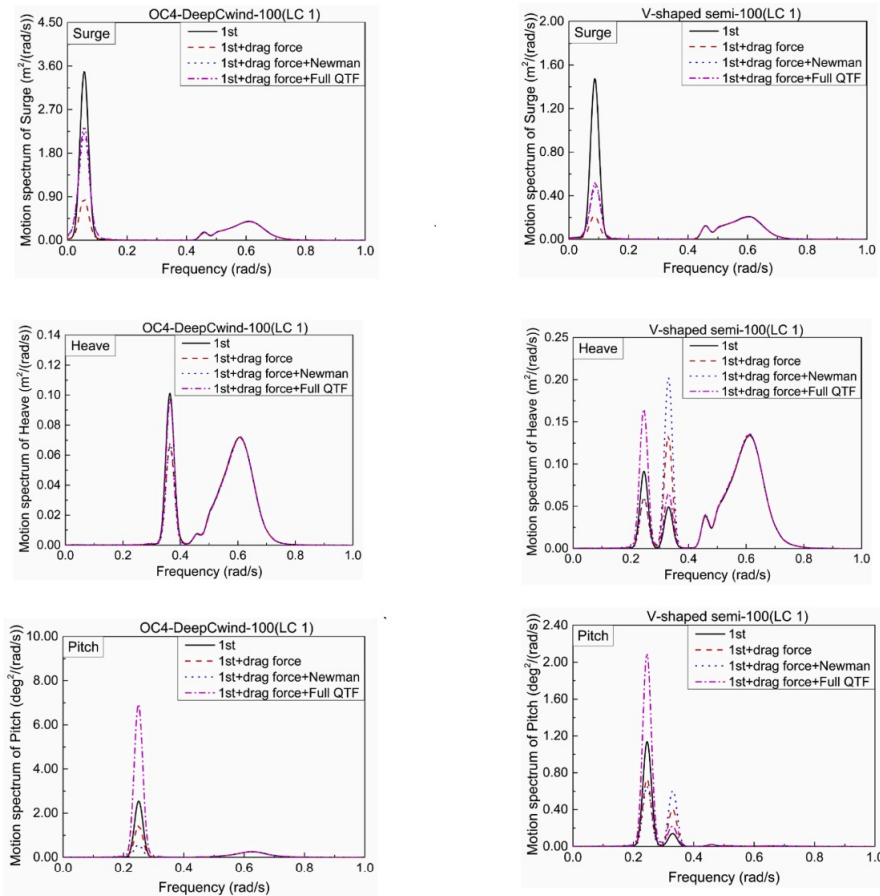


**Figure 1.10:** Comparison of the hydrodynamic response of Compact and V-shaped semi-submersible substructure [6].

## 1.4 Research Aim and Motivation

Traditionally floating offshore platforms use decoupled analysis [23]. In decoupled analysis, the effects of the mooring line are assumed to be quasi-static, and the nonlinear dynamic behavior of the mooring lines is ignored. Floating wind structures are subjected to a complicated aero-hydro-servo-elastic dynamic problem. The rotating turbine affects the floater's motion, which further affects the internal loads on the substructure. Hence, all the relevant coupling effects must be taken into consideration. It is also important to transfer the loads from the floater, mooring lines, and wind turbine to the structural model for structural analysis. Most

of the current numerical solutions cannot handle both coupled analysis and load transfer [23]. For example, most of the analyses assume the floater as a rigid body and perform coupled analysis using numerical tools like SIMA. Numerical tools like SIMA, which can handle coupled analysis, do not facilitate obtaining the cross-section load on a rigid body. The thesis addresses the challenge of handling coupled analysis and load transfer for a floating offshore wind structure and demonstrates a procedure to transfer loads to a floating wind turbine structure.

In this study, it is decided to use an existing reference concept that has established hydrodynamic properties. Hence, the IEA 15 MW turbine supported by the VolturnUS-S four-legged semi-submersible concept is studied [1].

## 1.5 Related Works

This section is based on [23], [24], [25], and [26]. Several papers deal with coupled dynamic analysis of offshore wind turbines. Very few papers have dealt with internal loads for a floating wind structure. In particular, a study by Kaija han et al. [23] deals with the time domain coupled analysis and load transfer for floating wind structures. One of the earliest studies by V. Leble et al. [24] discusses coupled analysis with a high fidelity method where a 10 MW FWT is supported by semi-submersible. The FWT is assumed to be a rigid body. The hydrodynamic loads were computed using Smoothed Particle Hydrodynamics (SPH), and the aerodynamic loads were computed using a Helicopter multi-block flow solver. The multi-body dynamics model was used to compute the rigid body motions. Mooring lines were modeled as springs and dampers. The applied thrust dominates the initial motion of the FWT. Combined thrust and wave action results in the pitching motion. The maximum pitch angle was observed to be 6.9 degrees.

A paper by J.M Jonkman et al. [25] aims to develop a comprehensive simulation tool capable of modeling fully coupled aero-hydro-elastic responses of a floating wind turbine. This is achieved by improving FAST ( Fatigue, Aerodynamics, Structures, and Turbulence), a publicly available code to determine the structural responses. The improvement is done by including the support platform kinematics and kinetics, support platform hydrodynamic loading, and mooring system dynamics. The hydrodynamic loading equation in the time domain is implemented in FAST and ADAMS (Autodynamic Dynamic Analysis of Mechanical Systems). Mooring line loads are included by interfacing FAST and ADAMS with LINES. LINES is a module in SWIM-MOTION-LINES (SML) a software suite by MIT. LINES module determines the nonlinear mooring line / tether / riser effects upon the platform [25].

The paper by Chenyu Luan et al. [26] and Kaija han et al. [23] emphasized time-

domain approaches to determine the loads on the floating wind turbine structures. These two papers served as a stepping stone for this thesis. The paper by Chenyu Luan et al. [26] proposes a method for modeling the inertia and external load and mapping the loads on to the finite element model of the hull. Contrary to other papers, in this study, the floating wind turbine is not considered as a single rigid body, instead it is considered to be a system of several components. The FEM model of the hull represents the global stiffness of the structural components. The external and inertial loads are modeled as distributed loads. Hydrodynamic loads are computed by integrating the pressure loads obtained by solving the linear hydrodynamic equation. Beam elements are used to represent the global stiffness of the structural components. The results indicate that low-frequency aerodynamic loads and fluctuation of buoyancy and weight are major contributors to the structural responses.

The paper by Kaija han et al. [23] proposes a method to perform time-domain coupled analysis and load transfer of a floating wind turbine structure. In this study, the hydrodynamic coefficients are sent to a time-domain solver for carrying out the coupled analysis, including both mooring lines and wind turbine forces. Then the responses, mooring line forces, wind turbine forces, and wave elevation used in the coupled analysis are sent to another time domain Rankine solver to transfer the loads. A converter code is written in Python to handle the inconvenience of transferring data between the two solvers with two different coordinate systems.

## 1.6 Proposed Approach

The proposed approach in this thesis work on load transfer from coupled analysis to structural design is described in Section 1.6.1 to Section 1.6.3. The task comprises of three stages:

1. Model validation
2. Proposed approach validation
3. Execution of coupled analysis

### 1.6.1 Model Validation

A reference SIMA model of the UMAINE VoltturnUS-S 15MW is given upfront. A panel model, a mass model (or structural model), and a section model are created in DNV Genie. A detailed structural model is given by Aker solutions. A hydrodynamic analysis of all the models is performed and the mass and various hydro-

dynamic properties are compared. Once the results of the models are consistent they are forwarded to regular wave analysis to validate the proposed approach.

### 1.6.2 Validation Of Proposed Approach

The proposed approach uses the numerical tools SIMA, WADAM, and WASIM to estimate the load on a section of the FWT in the coupled domain (simultaneous wind and wave load). First, the motion response is compared between the different numerical tools. In SIMA and WASIM, results are obtained in the time domain, and these are converted to the frequency domain. In WADAM, results are obtained in the frequency domain. The sectional loads are obtained in WADAM in the frequency domain and WASIM in the time domain. There is no provision to obtain the sectional load in SIMA. The motions obtained in the SIMA are given as prescribed motions in WASIM. WASIM obtains the sectional loads using these prescribed motions obtained from the SIMA. The technique of obtaining sectional load in WASIM using SIMA prescribed motions and forces are referred as WASIM+SIMA in this thesis work. The sectional loads from the three numerical tools (WADAM, WASIM, and WASIM+SIMA) are compared. If the results match the numerical tools well, they are forwarded to the execution stage.

### 1.6.3 Execution

Operating conditions like wind speed, significant wave height ( $H_s$ ), and peak period ( $T_p$ ) are selected in the execution stage. The coupled analysis is performed in SIMA for the given conditions. The aerodynamic loads are obtained at the tower base point, and the mooring loads are obtained at the fair lead points. In WASIM, the mass model has to be modified by removing the structure above the tower base to avoid duplication of the tower loads. The aerodynamic load, including the self-weight of the tower, is applied at the tower base as a point load in WASIM. Similarly, mooring loads are also applied as a point load in WASIM. In addition to these loads, wave elevations and motion responses are transferred from SIMA to WASIM. WASIM obtains the sectional loads using these prescribed motions and forces from SIMA.

## 1.7 Scope and Objective

As discussed in the previous sections, traditionally, the hull of a floating wind turbine has been considered a rigid body in aero-hydro-servo-elastic analysis. These analyses thus provide limited information about the global loads from wind, waves, inertia, and effects from the tower and mooring system. In the oil and gas industry, the loads are typically dominated by wave and inertia effects, and a frequency domain or design wave approach can be used. The applicability of such methods, and improved ways of estimating the global loads for input into a finite element model

of the hull, will be further examined in the thesis. A case study will be studied considering the 15MW IEA turbines supported by the VolturnUS-S semi-submersible. The scope of work is enumerated as follows:

1. Literature review into the wave and wind statistical description (spectra), wind and wave loads, floating offshore wind turbine dynamics, fatigue and ultimate strength, relevant guidelines and standards, and existing approaches for estimating loads in the hull.
2. Based on the established WADAM model and the provided mass model in Genie, develop a WASIM model of the chosen FWT and compare the responses in regular waves to the previously obtained results (extended to more frequencies) from WADAM and SIMA.
3. For a small number of environmental (wind and wave) conditions, obtain loads at the selected cross sections in the hull and tower by using the motion response from SIMA as input to WASIM.
4. In collaboration with fellow student Yu Ma, develop a SIMA model with the hull modelled using flexible beams. Extract loads at the same locations using the SIMA model, and compare to the WASIM results.
5. Conclusions and recommendations for further work

## 1.8 Structure Of The Report

1. In Chapter 2, Hydrodynamic and Aerodynamic theories are briefly discussed. It also briefly discusses how the rigid body response and internal loads are obtained.
2. In Chapter 3, A brief introduction to the SESAM package WADAM and WASIM are presented in this chapter. This chapter also provides an overview of the numerical tool SIMA.
3. In Chapter 4, Discusses on the the reference model used in the thesis work. The stage one of this thesis work where validation of the reference model and the comparison plots are presented in this chapter.
4. In Chapter 5, Stage two of the thesis work where analysis performed in regular wave are presented. The motion and sectional loads obtained in the regular wave analysis are presented in this chapter.

5. In Chapter 6, Final stage of the thesis work where sectional loads for selected environmental conditions are derived in a coupled domain ( simultaneous wind and wave loads). The results are presented for three different load cases.
6. In Chapter 7, Comparison between Flexible body method (multi-body representation of the OWT) and the Rigid body method are presented in this chapter.
7. In Chapter 8, Conclusion and recommended future works are discussed.



## Chapter 2

# Theoretical Background

### 2.1 Rigid Body Mechanics

A rigid body has six degrees of freedom. Three translational degrees of freedom (Surge, Sway, and Heave) and three rotational degrees of freedom (Roll, Pitch, and Yaw). The Figure 2.1 represents the six degrees of freedom of a floating rigid body. Floating rigid body dynamic equilibrium can be expressed as follows:

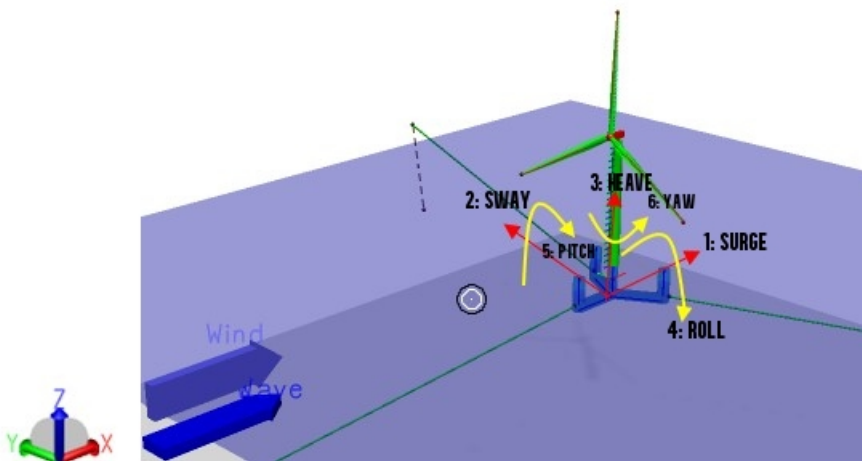


**Figure 2.1:** Six degrees of freedom of a floating rigid body.



$$(M + A)\ddot{x} + B\dot{x} + Cx = F_{ex} \quad (2.1)$$

$x$  is a  $6 \times 1$  vector representing the rigid body responses.  $F_{ex}$  is also a  $6 \times 1$  vector representing the excitation forces.  $M$  is a  $6 \times 6$  matrix representing the structural mass of the floating rigid body.  $A$  is also a  $6 \times 6$  matrix representing the hydrodynamic mass (also called added mass).  $B$  is a  $6 \times 6$  matrix that contains the damping coefficients.  $C$  is a  $6 \times 6$  matrix containing restoring coefficients. Heave, Roll, and Pitch have inherent hydrostatic stiffness due to the change in the buoyancy while Surge, Sway, and Yaw are restored by the stiffness of the mooring lines. The above dynamic equilibrium equation is established excluding the non-linear effects like the quadratic damping term in the Morison's equation.

## 2.2 Environmental Loads

Offshore wind turbines are exposed to the following loads [10]:

1. Wind loads
2. Wind-generated local wave loads
3. Swell loads generated by the distant storm
4. Surface current loads
5. Deepwater current loads
6. Ice Loads

Broadly we can classify the environment loads on an offshore wind turbine as hydrodynamic and aerodynamic loads. In this study, only the wind and wave loads are discussed. Current loads and Ice loads are not discussed in this study.

## 2.3 Hydrodynamics Loads

### 2.3.1 Definition Of Waves

The incoming wave is defined as follows [7]:

$$\eta(x, y, t) = A \cos[(k \cos \beta)x + (k \sin \beta)y - \omega t + \gamma] \quad (2.2)$$

The Equation (2.2) can be written in complex form as follows [7]:

$$\eta(x, y, t) = A \exp[i((k \cos \beta)x + (k \sin \beta)y - \omega t + \gamma)] \quad (2.3)$$

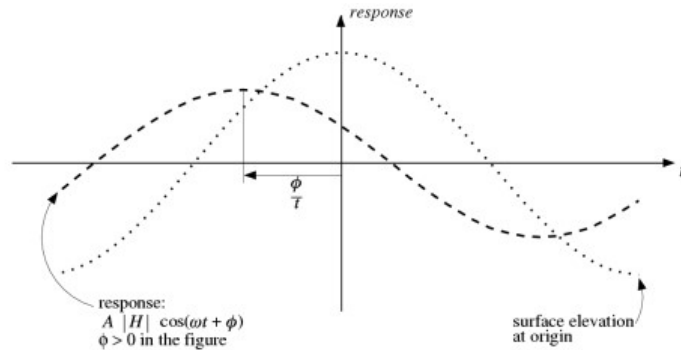


**Figure 2.2:** Definition of phase lag in the transfer functions[7].

In the Equation (2.2),  $k$  is the wave number,  $\beta$  is the wave direction (direction between the positive  $x$ -axis and direction of the wave propagation),  $\omega$  is the wave frequency,  $A$  is the wave amplitude,  $\phi$  is the phase angle,  $t$  is the time [7].

### 2.3.2 The Hydrodynamic Problem In a Regular Wave

This section is based on [8] and [17]. The hydrodynamic problem in regular wave is solved in WADAM and WASIM using potential flow theory [12]. A linear wave theory can describe the wave loads on an offshore structure to a large extent. Non-linear effects are important in severe sea states in describing the horizontal motion of a moored structure. Linear wave theory is applicable when the wave steepness is small. In linear theory, the response amplitude of the floating rigid body is linearly proportional to the wave amplitude. The linear theory also implies that wave kinematics are valid up to the mean water level only.

The Hydrodynamic problem in a regular wave comprises of two sub-problems [17]:

1. The forces and moments on the body in a regular wave when the body is restrained from oscillating. These are called wave excitation loads and are composed of Froude-Kriloff and Diffraction forces and moments.
2. The forces and moments on the body, when the body is forced to oscillate in wave excitation frequency in the absence of an incident wave. These are called radiation loads and are composed of added mass, damping, and restoring forces and moments.

In linear theory, sub-problem 1 and 2 can be added to obtain the total hydrodynamic loads as described in the Figure 2.3 [17].

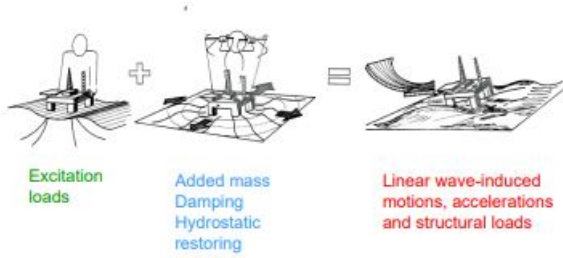


**Figure 2.3:** Hydrodynamic loads [8].

The velocity potential for this problem is the sum of the contribution from the radiated waves ( $\phi_R$ ) and diffracted waves ( $\phi_D$ ) [8].

$$\phi(x, y, z, t) = \phi_R(x, y, z, t) + \phi_D(x, y, z, t) \quad (2.4)$$

The linearized Bernoulli equation can obtain the total pressure. The first term in the Equation (2.5) represents the linear dynamic pressure, and the second term in the Equation (2.5) represents the hydrostatic pressure [8].

$$p = -\rho \left( \frac{\partial \phi}{\partial t} + gz \right) \quad (2.5)$$

The linear hydrodynamic loads can be obtained by integrating the pressure over the wetted surface area ( $S_B$ ). The first term in the Equation (2.6) represents the hydrodynamic load which is obtained by integrating the linear dynamic pressure over the mean wetted surface area ( $S_{B0}$ ). The second term in the Equation (2.6) represents the hydrostatic load which is obtained by integrating the hydrostatic pressure over the instantaneous wetted surface area ( $S_B$ ) [8].

$$F = \int_{S_{B0}} \rho \frac{\partial \phi}{\partial t} n ds + \int_{S_B} \rho g z n ds \quad (2.6)$$

$n$  in the Equation (2.6) is the unit normal to the body boundary.

### Excitation Loads

In the problem associated with excitation loads, the body is assumed to be fixed, interacting with the incident wave. The diffracted velocity potential for this problem is the sum of the contribution from the incident wave ( $\phi_I$ ) and the diffracted waves ( $\phi_D$ ) [8].

$$\phi(x, y, z, t) = \phi_I(x, y, z, t) + \phi_D(x, y, z, t) \quad (2.7)$$

1. Froude-Kriloff loads are caused when a flow due to  $\phi_I$  penetrates a body at normal velocity  $\partial\phi/\partial n$ . It is assumed the body is transparent, and the fluid can pass through it [8].
2. The body presence causes a flow which corresponds to  $\phi_D$ . Diffraction loads are the result of restoring the body's impermeability [8].

Excitation load is obtained by integrating the diffracted wave dynamic pressure along the mean wetted hull surface [8]:

$$F_{exc,k}(t) = - \int_{S_{0B}} \rho \frac{\partial\phi_I}{\partial t} n_k ds - \int_{S_{0B}} \rho \frac{\partial\phi_D}{\partial t} n_k ds \quad (2.8)$$

$n$  in the Equation (2.8) is the unit normal to the body boundary.  $k$  in the Equation (2.8) ranges from 1 to 6 for the six degrees of freedom.

### Radiation Loads

In the problem associated with radiation loads, body is forced to oscillate in six degrees of freedom in the absence of an incident wave [8].

$$F_{rad,k}(t) = - \int_{S_{0B}} \rho \frac{\partial\phi_R}{\partial t} n_k dS \quad k = 1..6 \quad (2.9)$$

$$\phi_R = i\omega \sum_{j=1}^6 x_j \phi_j \quad (2.10)$$

Radiation velocity potential  $\phi_R$  is a linear combination of the components in the six degrees of freedom.  $x_j$  and  $\phi_j$  in the Equation (2.10) are the response amplitude and unit-amplitude radiation potential in each degree of freedom [27].

1. When a body oscillates, it generates waves (radiated waves) associated with radiation velocity potential and is subjected to hydrodynamic loads called added mass and damping [8].
2. Added mass is proportional to the acceleration, and Damping is proportional to the velocity [8].

$$F_{rad,k}(t) = \sum_{j=1}^6 \{-A_{kj}\ddot{x}_j - B_{kj}\dot{x}_j\}, k = 1..6 \quad (2.11)$$

Where,

$$A_{kj}(\omega) = \Re \left[ \rho \int_{S_{0B}} \varphi_j n_k dS \right] \quad (2.12)$$

$$B_{kj}(\omega) = -\omega \Im \left[ \rho \int_{S_{0B}} \varphi_j n_k dS \right] \quad (2.13)$$

### Panel Method

We can apply the concepts discussed so far in the panel methods, solve equations, and derive the forces and moments. Summary of panel method and its application is described below [28]:

1. Derive integral equations for velocity potentials on the body boundary using Green's theorem
2. The body surface should be divided into N panels
3. In each panel, the dipole moments and sources are assumed to be constants
4. The total potential is evaluated at the centroid of each panel.
5. Solve the system of equations and compute the required forces and moments.

### Restoring Loads

Hydrostatic pressure contributes to restoring loads in the vertical motions. The change in hydrostatic pressure due to the change in buoyancy in the vertical motion results in restoring forces and moments.

$$\frac{dp}{dz} = -\rho g \quad (2.14)$$

The Equation (2.15) to Equation (2.19) describes the hydrostatic coefficients for a floating body[17]:

$$C_{33} = \rho g A_{wp} \quad (2.15)$$

$$C_{35} = -\rho g \iint_{A_{wp}} x dx dy \quad (2.16)$$

$$C_{44} = \rho g V_D (z_B - z_G) + \rho g \iint_{A_{wp}} y^2 dx dy = \rho g V_D \overline{GM}_T \quad (2.17)$$

$$C_{53} = C_{35} \quad (2.18)$$

$$C_{55} = \rho g V_D (z_B - z_G) + \rho g \iint_{A_{wp}} x^2 dx dy = \rho g V_D \overline{GM}_L \quad (2.19)$$

$C_{ij}$  is the restoring force in  $i$  due to unit displacement in  $j$ , where  $i$  and  $j$  ranges from 1 to 6 representing the six degrees of freedom.  $A_{wp}$  is waterplane area,  $V_D$  is displaced volume,  $z_B$  and  $z_G$  are the vertical center of buoyancy and vertical center of gravity.  $\overline{GM}_T$  and  $\overline{GM}_L$  are transverse and longitudinal metacentric height respectively.

Mooring stiffness contributes to the restoring force and moments in the horizontal motions. The Figure 4.2 describes the mooring system of the reference model. The Equation (2.21) to Equation (2.24) describes mooring stiffness coefficients for a floating body[17]: The linear restoring coefficient of mooring system can be

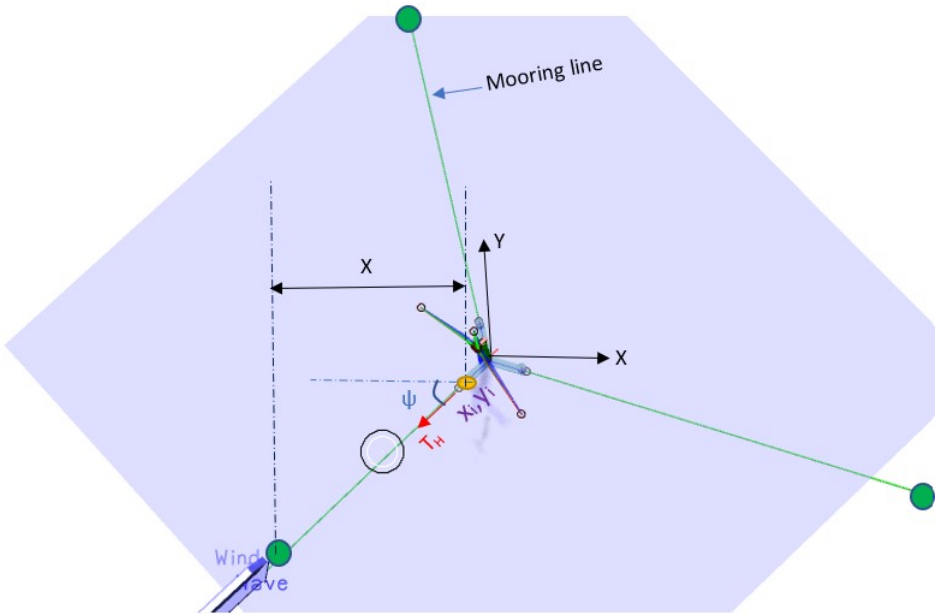


**Figure 2.4:** Mooring system of the reference model.

expressed as :

$$k = \frac{dT_H}{dX} \quad (2.20)$$

$T_H$  is the horizontal force from the anchor line, and  $X$  is the horizontal distance from the anchor point on the vessel and the anchor on the seabed.

$$C_{11} = \sum_{i=1}^n k_i \cos^2 \psi_i \quad (2.21)$$

$$C_{22} = \sum_{i=1}^n k_i \sin^2 \psi_i \quad (2.22)$$

$$C_{66} = \sum_{i=1}^n k_i (x_i \sin \psi_i - y_i \cos \psi_i)^2 \quad (2.23)$$

$$C_{26} = C_{62} = \sum_{i=1}^n k_i (x_i \sin \psi_i - y_i \cos \psi_i) \sin \psi_i \quad (2.24)$$

$i$  is the anchor line number,  $x_i$  and  $y_i$  are x and y coordinates of the attachment point of the anchor line to the vessel,  $\psi_i$  is the angle between the anchor line and the x-axis.

### 2.3.3 Rigid Body Response

The Equation (2.25) is the equation of motion for the rigid body assuming linear damping and linear wave loads, where  $\mathbf{x}$  represents the rigid body response,  $\mathbf{M}$  is a  $6 \times 6$  matrix representing the structural mass of the floating rigid body.  $\mathbf{A}(\omega)$  is also a  $6 \times 6$  matrix representing the frequency dependent added mass.  $\mathbf{B}(\omega)$  is a  $6 \times 6$  matrix that representing the frequency dependent damping coefficients.  $\mathbf{C}$  is a  $6 \times 6$  matrix containing restoring coefficients[8].

$$(\mathbf{M} + \mathbf{A}(\omega))\ddot{\mathbf{x}} + \mathbf{B}(\omega)\dot{\mathbf{x}} + \mathbf{C}\mathbf{x} = \mathbf{F}_{ex} \quad (2.25)$$

$$(-\omega^2(\mathbf{M} + \mathbf{A}(\omega)) + i\omega\mathbf{B}(\omega) + \mathbf{C}) \begin{bmatrix} x_{1a} \\ x_{2a} \\ x_{3a} \\ x_{4a} \\ x_{5a} \\ x_{6a} \end{bmatrix} = \begin{bmatrix} f_{1a}(\omega) \\ f_{2a}(\omega) \\ f_{3a}(\omega) \\ f_{4a}(\omega) \\ f_{5a}(\omega) \\ f_{6a}(\omega) \end{bmatrix} \quad (2.26)$$

$$\mathbf{x}_a = \mathbf{D}^{-1} \mathbf{f}_a \quad (2.27)$$

Where matrix  $D$  is  $(-\omega^2(M + A(\omega)) + i\omega B(\omega) + C)$ .  $x_{1a}$  to  $x_{6a}$  represents the response amplitude in the six degrees of freedom.  $f_{1a(\omega)}$  to  $f_{6a(\omega)}$  represents the excitation force amplitude in the six degrees of freedom.

### Transfer Function And Phase Lag

The time dependent response variable  $x(\omega, \beta, t)$  can be expressed in terms of a transfer function  $H((\omega, \beta))$  as shown in the Equation (2.28) [12].

$$x(\omega, \beta, t) = A \operatorname{Re} \left[ |H((\omega, \beta))| e^{i(\omega t + \phi)} \right] \quad (2.28)$$

In the Equation (2.28)  $A$  is the wave amplitude,  $\omega$  is the wave frequency,  $\beta$  is the wave direction (direction between the positive x-axis and direction of the wave propagation) and  $t$  denotes the instantaneous time period,  $|H((\omega, \beta))|$  is the amplitude of the transfer function,  $\phi$  is the phase angle between the incident wave and the time dependent response [12].

The transfer function and phase angle can be expressed as follows [12]:

$$H = H_{\operatorname{Re}} + iH_{\operatorname{Im}} \quad (2.29)$$

$$\phi = \operatorname{atan} \frac{H_{\operatorname{Im}}}{H_{\operatorname{Re}}} \quad (2.30)$$

In the Equation (2.29) and Equation (2.30)  $\operatorname{Re}$  and  $\operatorname{Im}$  indicates real and imaginary parts. The definition of phase between response and incident wave is given in the Figure 2.2. The transfer function is referred as Response Amplitude Operator (RAO) in the thesis work

## 2.4 Motion in Irregular Waves

This section is based on [9], [29] and [30].

### 2.4.1 Wave Spectrum

In the previous sections, it is assumed that the waves are periodic. In reality, waves are random or irregular. This section describes the motion of a floating body in an irregular sea. It is assumed sea surface is constructed by a series of long crested waves. Irregular waves can be represented as a sum of the regular long crested waves [9].

The following assumptions are made in the irregular wave analysis [9]:



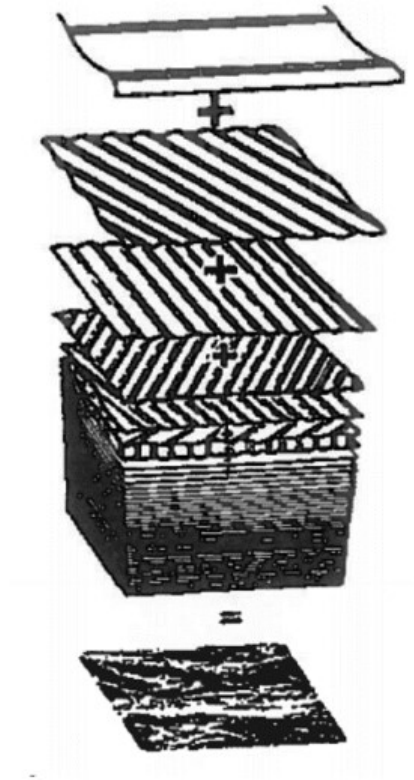


**Figure 2.5:** Irregular waves represented as a sum of the regular long crested waves [9].

1. The wave process is stationary within a short-term interval (20 minutes to 3 hours). Hence the mean and the variance of the process is constant.
2. Wave elevation is normally distributed.
3. The wave process is ergodic, i.e., a particular time series represents the entire process. The expected value and the variance can be obtained by time-averaging of one time series.

The Equation (2.31) represents the wave surface elevation,

$$\zeta(x, t) = \sum_{n=1}^N \zeta_{An} \cos(\omega_n t - k_n x + \varepsilon_n) \quad (2.31)$$

In the Equation (2.31),  $\zeta_{An}$  is the wave amplitude,  $\omega$  is the wave frequency, and  $k$  is the wave number.  $t$  is the instantaneous time,  $x$  is the instantaneous position

in the space,  $N$  represents the total number of wave components, and  $\varepsilon$  represents the phase angle, a stochastic variable uniformly distributed between 0 and  $2\pi$  [9].

At a particular location ( $x = 0$ ) in space, the Equation (2.31) becomes:

$$\zeta(t) = \sum_{n=1}^N \zeta_{An} \cos(\omega_n t + \varepsilon_n) \quad (2.32)$$

$$\frac{E}{\rho g} = \sum_{n=1}^N \frac{1}{2} \zeta_{An}^2(\omega_n) \quad (2.33)$$

In the Equation (2.33),  $E$  represents the energy per unit area of the linear wave.  $\rho$  is the density of the seawater, and  $g$  is the acceleration due to gravity.

An energy density spectrum can represent the random ocean wave. The spectrum describes the energy content of an ocean wave and its distribution over a frequency range of the random wave.

$$\frac{1}{2} \zeta_{An}^2 = S(\omega_n) \Delta\omega \quad (2.34)$$

In the Equation (2.34),  $S(\omega_n)$  represents the spectrum of  $\zeta(t)$ . Combining Equation (2.33) and Equation (2.34),

$$\frac{E}{\rho g} = \sum_{n=1}^N \frac{1}{2} \zeta_{An}^2 = \sum_{n=1}^N S(\omega_n) \Delta\omega \quad (2.35)$$

If we assume that  $N \rightarrow \infty$  such that  $\Delta\omega \rightarrow 0$ , the equation 2.35 can be rewritten as:

$$\frac{E}{\rho g} = \frac{1}{2} \sum \zeta_{An}^2 = \int_0^{\infty} S(\omega) d\omega \quad (2.36)$$

From Equation (2.34),

$$\zeta_{An} = \sqrt{2S(\omega_n) \Delta\omega} \quad (2.37)$$

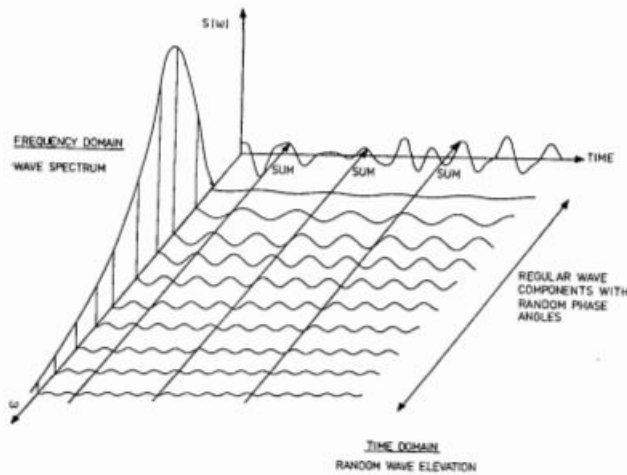


**Figure 2.6:** Wave spectrum [10].

Inserting the Equation (2.37) in the Equation (2.32),

$$\zeta(t) = \sum_{n=1}^N \sqrt{2S(\omega_n) \Delta\omega} \cos(\omega_n t + \varepsilon_n) \quad (2.38)$$

Variance( $\sigma^2$ ) of the wave elevation is given by:

$$\sigma^2 = \int_0^{\infty} S(\omega) d\omega \quad (2.39)$$

## 2.4.2 JONSWAP Wave Spectrum

DNVGL-ST-0437 [31] recommends the JONSWAP wave spectrum to represent the energy spectrum of wind-generated waves. For floating wind turbine, which can be excited by swells of 20 to 25 seconds, can be represented by two JONSWAP spectrums combined to represent wind-generated waves and swells [30].

JONSWAP spectrum was developed by analyzing the data during the Joint North Sea Wave Observation Project. The research details are presented in the literature by Hasselmann et al [29] in 1973. JONSWAP spectrum is the peak-enhanced Pierson-Moskowitz (P-M) spectrum. In P-M spectrum, fully developed sea is assumed. Hasselmann et al, found that the wave spectrum is never fully developed. A multiplicative factor was introduced to the Pierson-Moskowitz spectrum to improve the fit to their measurements. The JONSWAP spectrum is thus a Pierson-Moskowitz spectrum multiplied by an extra peak enhancement factor [29].

P-M spectrum is given by,

$$S(\omega) = \frac{A}{\omega^5} \exp \left[ -\frac{B}{\omega^4} \right] \quad (2.40)$$

Where  $A = 0.0081g^2$ ,  $B = 0.74 \left(\frac{g}{V}\right)^4$ .  $g$  is the acceleration due to gravity and  $V$  is the wind speed [9].

In JONSWAP spectrum peak frequency ( $\omega_p$ ) is used instead of wind speed  $V$  [9].  $A = \alpha g^2$  ( $\alpha = 0.0081$  for the PM spectrum),  $B = \frac{5}{4}\omega_p^4$ .

JONSWAP spectrum is given by,

$$S(\omega) = \frac{\alpha g^2}{\omega^5} \exp \left[ -\frac{5}{4} \left(\frac{\omega_p}{\omega}\right)^4 \right] \gamma^r \quad (2.41)$$

$$r = \exp \left[ -\frac{(\omega - \omega_p)^2}{2\sigma^2\omega_p^2} \right]$$

$\gamma$  is the peak enhancement factor.

$$\sigma = \begin{cases} \sigma_a & \text{for } \omega \leq \omega_p \\ \sigma_b & \text{for } \omega > \omega_p \end{cases}$$

Mean value for the each parameter in the Equation (2.41) are as follows [9]:

$$\begin{aligned} \bar{\gamma} &= 3.3 \\ \sigma_a &= 0.07 \quad \text{and} \quad \sigma_b = 0.09 \\ \alpha &= 0.076 \left(\frac{gx}{V^2}\right)^{-0.22} \\ \omega_p &= 7.0\pi \left(\frac{g}{V}\right) \left(\frac{gx}{V^2}\right)^{-0.33} \end{aligned} \quad (2.42)$$

$x$  is the fetch (the distance over which the wind blows over the sea with constant velocity).  $V$  is the wind speed, and  $g$  is the acceleration due to gravity.

## 2.5 Aerodynamics Loads

This section is based on [4], [32], and [11]. Tower, Rotor-Nacelle Assembly (RNA) are the components above the water surface of an offshore wind turbine. These components are exposed to aerodynamic loads. During operation, aerodynamic loads on the rotor contribute significantly to rigid body motion and structural responses. The Blade Element Momentum method (BEM) and Generalized Dynamic Wake (GDW) are the two commonly used tools to describe the aerodynamic

loads on the rotor [4]. The numerical tool SIMA uses BEM to describe the aerodynamic loads on the rotor [15]. The substructure design of the OWT is influenced by the magnitude and frequency of the loads induced by the rotor. The excitation frequency of a wind turbine is expressed as a function of rotor rotational frequency.  $1p$  frequency corresponds to the rotor rotational frequency, and  $3p$  corresponds to three times the rotor rotational frequency. The  $3p$  effects are critical for the excitation of the lowest modes of the bottom-fixed structures [4].

### 2.5.1 Blade Element Momentum Method (BEM)

The BEM is based on the conservation of momentum combined with blade element theory. In blade element theory, the blades are assumed to be discretized into small elements which are independent of the other elements. Each blade element act as a two-dimensional airfoil and the forces can be calculated based on local flow conditions. The total force is the summation of all the elemental forces along the span of the blade. The momentum theory assumes the airflow passing through the rotor plane causes a loss of momentum at the rotor plane. Axial and tangential induced velocities can be calculated from the loss of momentum. An iterative process is set up to obtain the aerodynamic forces and induced velocities near the rotor [32]. In BEM, it is assumed that  $N$  annular elements discretize the stream tube. The forces are constant at each of the annular elements, and hence the rotor is assumed to consist of an infinite number of blades [11].

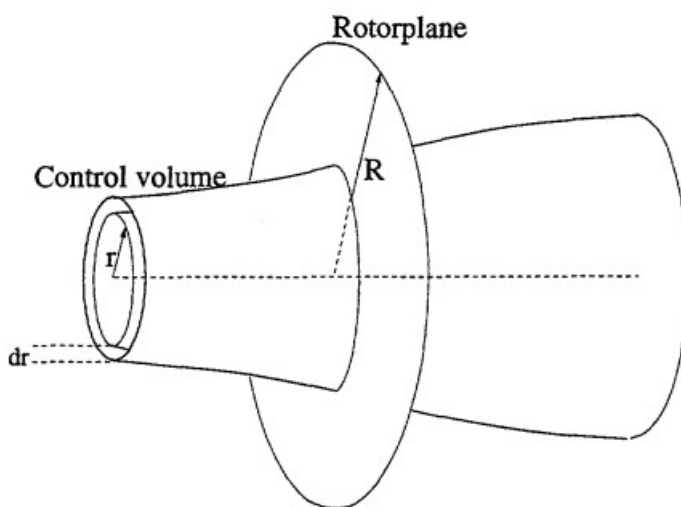


**Figure 2.7:** Annular element used in the BEM model [11].

To account for the finite number of blades, Prandtl's correction is used. The momentum theory is not valid for the large induction factors ( $>0.4$ ). To compensate for these limitations, Glauret developed a correction to the rotor thrust coefficient. The effect of dynamic wake and dynamic stall is also significant in aerodynamic modeling. The wind seen locally at a point on a blade varies due to incoming wind turbulence, yaw misalignment, wind shear, etc. This causes the angle of attack to dynamically change during the revolution. There will be a time delay in the aerodynamic loads due to the change in angle of attack. This effect is called a dynamic stall. The BEM model uses the Stig Øye model, which gives unsteady lift by filtering the trailing edge separation [11]. Dynamic wake is due to the response to a large flow field of turbulence or change in rotor operation (example: Change in pitch, rotor speed, etc.). There is a time lag in the induced velocities to balance the aerodynamic loads. The dynamic wake effect is more pronounced in heavily loaded rotors. The BEM model uses the Stig Øye model to filter the induced velocities [11].

### Tower Shadow Effect

The tower obstructs the wind flow, which results in the wind speed deficit behind the tower. The blades of the wind turbine will experience this speed deficit once per revolution. This results in a drop in the power and also leads to structural vibrations [33].

### Fault Conditions

Fault conditions induce aerodynamic loads to the OWT substructures. Blade pitch failure, where one of the blade pitching mechanisms is faulted, will result in an imbalance load on the turbine. The wind turbines that are equipped with a supervisory control system will detect the fault and will initiate a shutdown [4]. The shutdown process will result in negative thrust force, causing a significant transient response of the OWT [4].

## 2.5.2 Wind Spectrum

The wind profile used for all the wind spectra is described by [15] :

$$\bar{u}(z) = \bar{u}_r \left( \frac{z}{z_r} \right)^\alpha \quad (2.43)$$

$z$  is the height above the water plane.

$z_r$  is the reference height, usually 10 m.

$\bar{u}_r$  is the average velocity at the reference height.

$\alpha$  is the height coefficient ranges between 0.10 to 0.14.

$\bar{u}$  is the average velocity at the height  $z$ .

## Kaimal Spectrum

DNV recommends the Kaimal spectrum to represent the energy spectrum of the wind [34]. Kaimal spectrum is given as :

$$S_{uu}(f) = \frac{\sigma_U^2 \left( \frac{4L_k}{U} \right)}{\left( 1 + \frac{6fL_k}{U} \right)^{\frac{5}{3}}} \quad (2.44)$$

$\sigma_U$  is the standard deviation of the wind speed,  $f$  is the wind frequency,  $\bar{U}$  is the mean wind speed,  $L_k = 5.67z$  for  $z < 60$  m and,  $L_k = 340.2$  m for  $z \geq 60$  m where  $z$  denotes the height above the water plane.

## 2.6 Sectional Loads

This section is based on [12]. In the sectional load calculation in WADAM or WASIM, sectional planes where the load needs to be calculated need to be defined. WADAM and WASIM both calculate the sectional load by integration of the distributed loads on the specified sides of the defined planes. Sectional planes are specified in the input coordinate system which is normal for the global coordinate system. Figure 2.8 describes a submerged beam with a sectional plane at  $x_{inp} = 0$  [12]. The sectional load is obtained by integration of net load ( $F - ma$ ) where  $F$  is the force and  $m$  is the mass and  $a$  is the acceleration due to gravity. The loads computed on the positive side and the negative side of the cut sectional plane will be equal with a phase difference of 180 degrees [12].

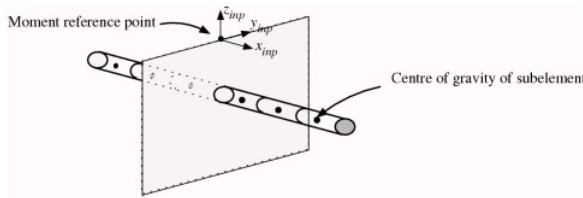


**Figure 2.8:** Sectional load calculation in WADAM and WASIM. [12].

Panel models include the exciting forces at the centroid of each panel. The inertia forces are included with respect to a center of gravity calculated for the part of the model that is on the specified side of the sectional plane [12].

## 2.7 Time-domain analysis

This section is based on [4] and [15]. Wind turbines are subjected to aero-hydro-servo-elastic loads. Hydrodynamic loads cause structural deformation. On the

other hand, hydrodynamic loads depend on the structural response. The interaction between the hydrodynamic loads and the elastic response of the body is called hydro-elasticity. Similarly, aerodynamic loads cause structural deformation in blades and towers. This interaction is called aero-elasticity. When an aerodynamic model is coupled with the hydro-elastic model, a aero-hydro-elastic model is obtained. When control logic is implemented in the aero-hydro-elastic model, we obtain the aero-hydro-servo-elastic model [27]. Frequency domain analysis re-

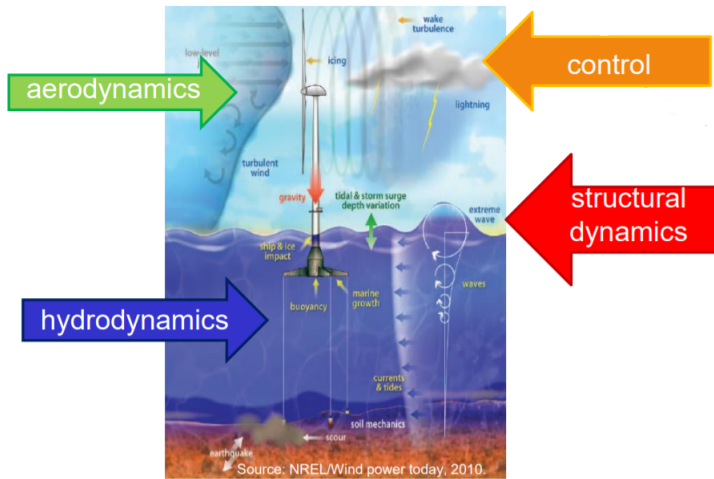


**Figure 2.9:** Forces on Floating wind turbine [13].

quires linearization of the loads and responses. To account for the non-linearity due to wind turbine control, large platform motions, large deflection of blades, and non-linear damping, the time domain analysis is preferred [4].

### 2.7.1 Equations Of Motion

Equation of motion in time domain can be written as follows [15]:

$$M\ddot{x} + C\dot{x} + D_1\dot{x} + D_2f(\dot{x}) + K(x)x = q(t, x, \dot{x}) \quad (2.45)$$

$$M = m + A(\omega)$$

$$A(\omega) = A_\infty + a(\omega)$$

$$A_\infty = A(\omega = \infty)$$

$M$  is the frequency-dependent mass matrix, and  $m$  is the body mass matrix.  $a(\omega)$  is the frequency-dependent added mass matrix.  $A_\infty$  is the added mass at the infinite



frequency.  $A(\omega)$  is the total frequency-dependent added mass.  $C$  is the potential damping matrix which is also dependent on the frequency.  $D_1$  is the linear damping matrix, and  $D_2$  is the quadratic damping matrix.  $f$  is a vector function where each element is given by  $f_i = \dot{x}_i |\dot{x}_i|$ .  $\dot{x}_i$  is the element velocity.  $K$  is the restoring matrix which consists of the hydrostatic as well as the mooring stiffness.

$$\mathbf{q}(t, \mathbf{x}, \dot{\mathbf{x}}) = \mathbf{q}_{WI} + \mathbf{q}_{WA}^{(1)} + \mathbf{q}_{WA}^{(2)} + \mathbf{q}_{CU} + \mathbf{q}_{ext} \quad (2.46)$$

The excitation force vector  $\mathbf{q}$  comprises of wind drag force  $\mathbf{q}_{WI}$ , first order and the second order wave excitation force ( $\mathbf{q}_{WA}^{(1)}$  &  $\mathbf{q}_{WA}^{(2)}$ ), current drag force  $\mathbf{q}_{CU}$ .  $\mathbf{q}_{ext}$  includes any other forces such as wave drift damping, forces from station-keeping etc.

Two methods can be used to solve the equation [15]:

1. Solution by convolution integral
2. Separation of motions

### Solutions By Convolution Integral

We bring the linear and quadratic damping terms in the Equation (2.45) to the right hand side and rewrite the equation as:

$$\mathbf{m} + \mathbf{A}(\omega)\ddot{\mathbf{x}} + \mathbf{C}(\omega)\dot{\mathbf{x}} + \mathbf{K}\mathbf{x} = \mathbf{f}'(t) \quad (2.47)$$

$$\mathbf{f}'(t) = \mathbf{q} - \mathbf{D}_2\mathbf{f}(\dot{\mathbf{x}}) - \mathbf{D}_1\dot{\mathbf{x}} \quad (2.48)$$

Frequency dependent terms are kept in the left hand side and remaining terms are placed in the right hand side:

$$\mathbf{A}(\omega)\ddot{\mathbf{x}} + \mathbf{C}(\omega)\dot{\mathbf{x}} = \mathbf{f}(t) = \mathbf{f}'(t) - \mathbf{K}\mathbf{x} - \mathbf{m}\ddot{\mathbf{x}} \quad (2.49)$$

In frequency domain, the equation is written as:

$$(-\omega^2\mathbf{A}(\omega) + i\omega\mathbf{C}(\omega))\mathbf{X}(\omega) = \mathbf{F}(\omega) \quad (2.50)$$

or

$$(i\omega\mathbf{A}(\omega) + \mathbf{C}(\omega))i\omega\mathbf{X}(\omega) = \mathbf{F}(\omega) \quad (2.51)$$

$\mathbf{X}(\omega)$  is the response. Using the relation,

$$\begin{aligned} \mathbf{A}(\omega) &= A_\infty + \mathbf{a}(\omega) \\ \mathbf{B}(\omega) &= \mathbf{C}_\infty + \mathbf{c}(\omega) \end{aligned} \quad (2.52)$$

Where,  $C_\infty = C(\omega = \infty) = 0$

Applying the relation established in Equation (2.52) in Equation (2.50):

$$-\omega^2 \mathbf{A}_\infty \mathbf{X}(\omega) + (i\omega \mathbf{a}(\omega) + \mathbf{c}(\omega)) i\omega \mathbf{X}(\omega) = \mathbf{F}(\omega) \quad (2.53)$$

Using inverse Fourier transform gives:

$$\mathbf{A}_\infty \ddot{\mathbf{x}}(t) + \int_{-\infty}^{\infty} \mathbf{h}(t - \tau) \dot{\mathbf{x}}(\tau) d\tau = \mathbf{f}(t) \quad (2.54)$$

$\mathbf{h}(t - \tau) = 0$  for,  $t < 0$  (before start of the experiment). Similarly,  $\mathbf{h}(t - \tau) = 0$  for  $\tau > t$  (after the experiment). Hence, Equation (2.54) can be re-written as:

$$\mathbf{A}_\infty \ddot{\mathbf{x}}(t) + \int_0^t \mathbf{h}(t - \tau) \dot{\mathbf{x}}(\tau) d\tau = \mathbf{f}(t) \quad (2.55)$$

Substituting the Equation (2.55) in Equation (2.49) and Substituting the Equation (2.48) in Equation (2.49) we get,

$$(\mathbf{m} + \mathbf{A}_\infty) \ddot{\mathbf{x}} + \mathbf{D}_1 \dot{\mathbf{x}} + \mathbf{D}_2 \mathbf{f}(\dot{\mathbf{x}}) + \mathbf{K} \mathbf{x} + \int_0^t \mathbf{h}(t - \tau) \dot{\mathbf{x}}(\tau) d\tau = \mathbf{q}(t, \mathbf{x}, \dot{\mathbf{x}}) \quad (2.56)$$

$\mathbf{h}(\tau)$ , the retardation function, is computed as:

$$\mathbf{h}(\tau) = \frac{1}{2\pi} \int_{-\infty}^{\infty} \mathbf{c}(\omega) + i\omega \mathbf{a}(\omega) e^{i\omega\tau} d\omega = \frac{1}{2\pi} \int_{-\infty}^{\infty} \mathbf{H}(\omega) e^{i\omega\tau} d\omega \quad (2.57)$$

(or)

$$\mathbf{H}(\omega) = \int_{-\infty}^{\infty} \mathbf{h}(\tau) e^{-i\omega\tau} d\tau = \mathbf{c}(\omega) + i\omega \mathbf{a}(\omega) \quad (2.58)$$

$\mathbf{c}(\omega) = \mathbf{c}(-\omega)$  and  $\mathbf{a}(\omega) = \mathbf{a}(-\omega)$ ,

$$\mathbf{h}(\tau) = \frac{1}{\pi} \int_0^{\infty} (\mathbf{c}(\omega) \cos(\omega\tau) - \omega \mathbf{a}(\omega) \sin(\omega\tau)) d\omega \quad (2.59)$$

From causality,  $\mathbf{h}(\tau) = 0$  for  $\tau < 0$ ; the process can not have any memory effect of the future. This means that the two parts in the integral, Eq. (4.15) must be opposite for  $\tau < 0$  and identical for  $\tau > 0$ , or mathematically:

$$\mathbf{h}(\tau) = \frac{2}{\pi} \int_0^{\infty} \mathbf{c}(\omega) \cos(\omega\tau) d\omega = -\frac{2}{\pi} \int_0^{\infty} \omega \mathbf{a}(\omega) \sin(\omega\tau) d\omega \quad (2.60)$$

The frequency dependent added mass and damping can be found using the retardation function  $\mathbf{h}(\tau)$ :

$$\mathbf{a}(\omega) = -\frac{1}{\omega} \int_0^{\infty} \mathbf{h}(\tau) \sin(\omega\tau) d\tau \quad (2.61)$$

$$\mathbf{c}(\omega) = - \int_0^{\infty} \mathbf{h}(\tau) \cos(\omega\tau) d\tau \quad (2.62)$$

The relation between frequency-dependent added mass and damping term in the Equation (2.61) and Equation (2.62) is known as Kramers-Krönig relation.

for  $\tau = 0$ , Equation (2.59) becomes,

$$h(0) = \frac{1}{\pi} \int_0^{\infty} c(\omega) d\omega \quad (2.63)$$

or, if  $c$  is not known, we know that  $c(\omega = 0) = 0$ , which gives

$$\int_0^{\infty} h(\tau) d\tau = 0 \quad (2.64)$$

## Separation Of Motions

The position vector  $\mathbf{x}$  can be decomposed as low-frequency motion ( $\mathbf{x}_{LF}$ ) and high-frequency motion ( $\mathbf{x}_{HF}$ )

$$\mathbf{x} = \mathbf{x}_{LF} + \mathbf{x}_{HF} \quad (2.65)$$

Here low-frequency motions are solved in the time domain, and high-frequency motions are solved in the frequency domain.

Time Domain:

$$\mathbf{m} + \mathbf{A}(\omega = 0) \ddot{\mathbf{x}}_{LF} + \mathbf{D}_1 \dot{\mathbf{x}}_{LF} + \mathbf{D}_2 \mathbf{f}(\dot{\mathbf{x}}) + \mathbf{K} \mathbf{x}_{LF} = \mathbf{q}^{(2)} = \mathbf{q}_{WI} + \mathbf{q}_{WA}^{(2)} + \mathbf{q}_{CU} + \mathbf{q}_{ext} \quad (2.66)$$

Frequency Domain:

$$\mathbf{m} + \mathbf{A}(\omega)\ddot{\mathbf{x}}_{HF} + \mathbf{D}_1 + \mathbf{C}(\omega)\dot{\mathbf{x}}_{HF} + \mathbf{K}\mathbf{x}_{HF} = \mathbf{q}_{WA}^{(1)}(\omega) \quad (2.67)$$

$$\mathbf{X}_{HF}(\omega) = (-\omega^2(\mathbf{m} + \mathbf{A}(\omega)) + i\omega\mathbf{D}_1 + \mathbf{C}(\omega) + \mathbf{K})^{-1} \mathbf{H}_1(\omega)\bar{\zeta}(\omega) \quad (2.68)$$

$\mathbf{X}_{HF}(\omega)$  is the high-frequency response,  $\mathbf{H}_1(\omega)$  is the first-order transfer function and  $\bar{\zeta}(\omega)$  is the complex harmonic wave component.

## 2.8 Finite Element Modeling Of A Floating Wind Turbine

This section is based on [4]. The global finite element equation for an offshore wind turbine with nodal displacement  $\mathbf{D}$  can be expressed as in the Equation (2.69) [4].

$$M_g\vec{\mathbf{D}} + B_g\vec{\mathbf{D}} + R^{int} = R^{ext} \quad (2.69)$$

$M_g$  represents the mass matrix, and  $B_g$  represents the damping matrix.  $R^{int}$  and  $R^{ext}$  represents the internal and external forces. Internal forces are typically the product of the stiffness matrix and displacement vector. External forces include the hydrodynamic and aerodynamic loads [4].

In OWT towers and blades are usually modeled as a beam element, while mooring lines are modeled as a bar element. A rigid element is usually used to model the hull. The choice of the model is a trade of between fidelity and efficiency. The structural model is also influenced by how aerodynamic or hydrodynamic loads are applied. Rigid body models can only handle integrated forces and moments, while beam models can handle distributed line loads, and shell or solid models can handle distributed pressure loads. The Figure 2.10 gives an overview of the structural modeling of an offshore wind turbine and the different loads acting on the various parts of the offshore wind turbine [4]. In Chapter 7, sectional loads obtained from rigid body model and the flexible body model (multi-body representation of the OWT) are compared and the results are presented.

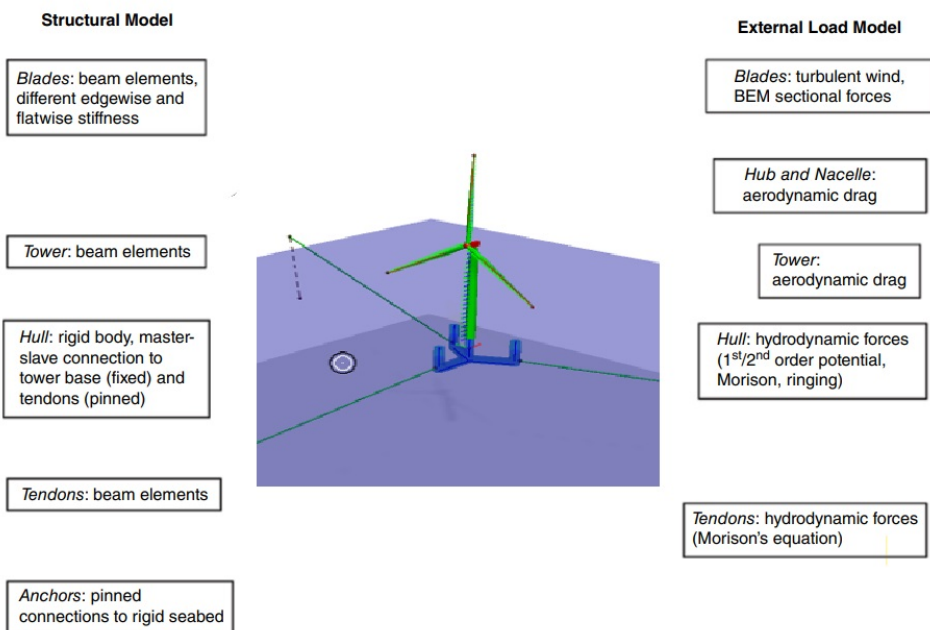


**Figure 2.10:** Finite element model for a floating wind turbine[4].

# Chapter 3

## Numerical Tools

This section is based on [12], [7] and [35]. DNV Sesam and SIMA are the two software packages used in this thesis work.

### 3.1 DNV SESAM

Sesam is a software package for the structural and hydrodynamic analysis of ships and offshore structures. Sesam has various modules, some of them used in the thesis are:

- The GeniE software is used to model, analyze, and code check beam, plate, and shell structures, such as offshore platforms and ships.
- HydroD for the hydrodynamic and hydrostatic analysis of any fixed or floating structures. HydroD has two sub-modules WADAM and WASIM.

#### 3.1.1 WADAM

WADAM is an acronym for Wave Analysis by Diffraction and Morison Theory. It is a program for calculating wave-structure interactions for fixed and floating structures [12].

Sesam's Wadam program is an integral component of the Sesam suite. It is used to calculate wave loads using the models created by Genie. A panel model and structural model are imported to WADAM as .FEM File [12]. In this thesis work, WADAM module in HydroD version 5.4 is used.

A Hydrodynamic Results Interface File (G-file) can store the results of the WADAM's global response analysis for postprocessing in Postrep [12].

## Definition Of Model Types In WADAM

In Figure 3.1 different types of WADAM models are given. There are three main model types:

1. Hydro model
2. Mass model
3. Structural model

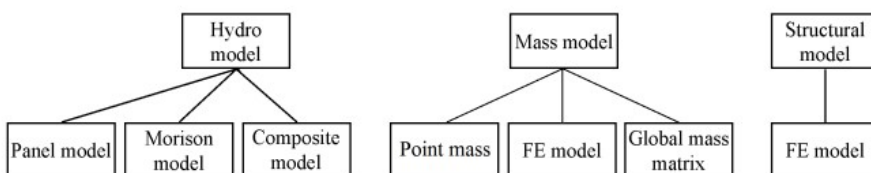


**Figure 3.1:** Model types in WADAM [12].

### Hydro Model

In the Figure 3.2 different types of hydro models are given. In this thesis, we use a panel model for hydrodynamic analysis in WADAM. The hydrodynamic loads and responses are calculated using the potential theory, which is discussed in the Section 2.3. The panel model consists of a quadrilateral or triangular panels representing the wet surface of the floater [12].

### Mass Model

The global mass information is required in WADAM to record the weight-buoyancy imbalance for the hydrodynamic analysis of floaters [12]. There are two methods to establish a global mass matrices:

1. Direct input of mass properties.
2. Assembling the global mass matrix from the mass file.

In this thesis work, mass properties are defined from the .FEM file.

### Structural Modelling

The structural model is built from an arbitrary large super element hierarchy [12]. For shell, element loads are transferred to FEM sides which are identified as wet

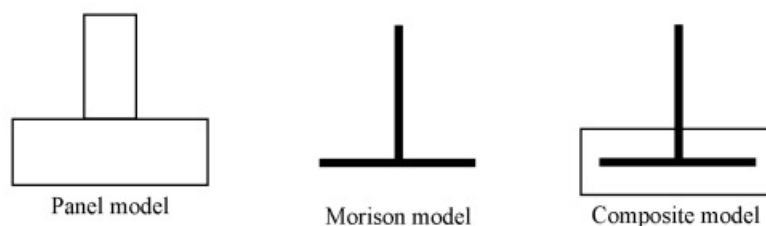


**Figure 3.2:** Different hydro models in WADAM [12].

[12]. A wet surface property is assigned to the plates below the waterline. A dummy hydro pressure load is defined in GeniE to identify the wet element sides [12].

### 3.1.2 WASIM

WASIM is a numerical tool for computing the global and local loading on a floating body or a moving vessel. In WASIM, the simulations are performed in the time domain [7]. The mass model and structural model are the same as that in the WADAM. In WASIM, section model (or PLN model) is used for the underwater meshing. This is different from the meshing done in the WADAM. The section model in WASIM is discussed briefly in Section 4.3.2. WASIM module in the HydroD version 4.10 is used in this thesis work. Wasim has the following executable elements [7]:

1. Wasim\_mesh: Mesh generation on the hull and free surface.
2. Wasim\_Setup: Sets up the matrices for solving the hydrodynamic problem.
3. Wasim\_Solve: Performs time domain simulations
4. Wasim\_Fourier: Transforms time domain results to the frequency domain.
5. Wasim\_Stru: Transfer the load from the panel model to the FEM model.



## 3.2 SIMA

SIMA is a numerical tool developed by SINTEF Ocean for simulation and analysis of marine operations. The Figure 3.3 describes the application of the numerical tool SIMA for a floating wind turbine. SIMA comprises four modules SIMO, RIFLEX, an Aerodynamic module, and a control module. SIMO is a time domain simulation program used to study the motions of a multibody system [35]. RIFLEX module is used to analyze flexible slender structures like mooring lines, turbine blades, towers, etc) using the non-linear Finite Element Method (FEM) [36]. The aerodynamic module in the SIMA calculates the aerodynamic loads on blades and towers using Boundary Element Method (BEM). TurbSim or IEC Turbulence simulator are used to create a turbulent wind field. The control module is a programmable java interface which communicates with RIFLEX to implement the control mechanism. In this thesis work, SIMA version 4.1.0 is used.

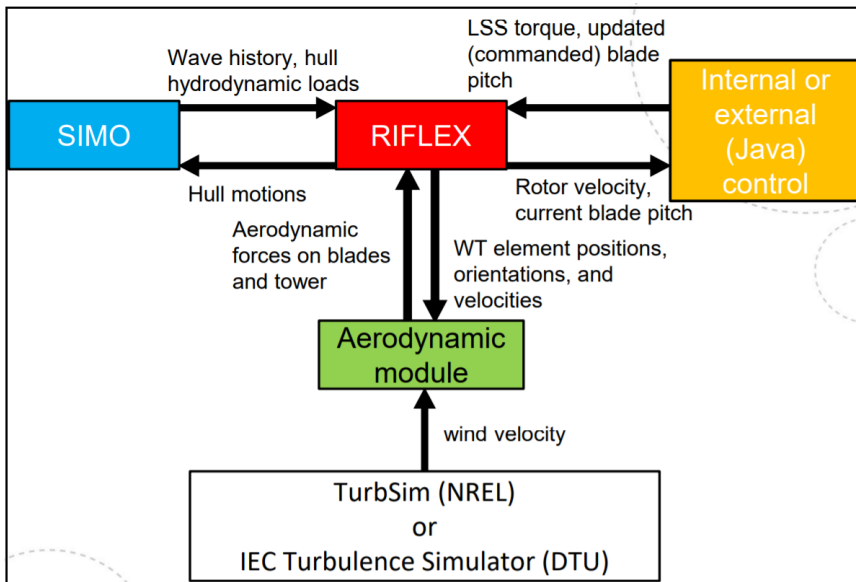
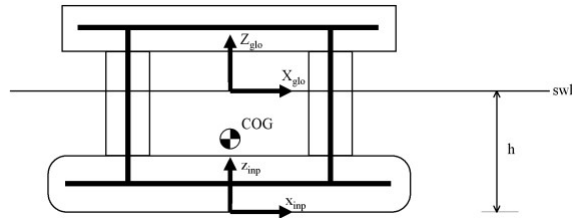


Figure 3.3: Floating wind turbine analysis using SIMA[14].

## 3.3 Coordinate Systems

This section is based on [12] and [15]. The Figure 3.4 and the Figure 3.5 describes the coordinate systems in WADAM/WASIM and SIMA. WADAM and WASIM has two coordinate systems namely, global coordinate system and input coordinate system. The global coordinate system is right handed and it is denoted by



**Figure 3.4:** The coordinate system in WADAM and WASIM [12].

$(X_{glo}, Y_{glo}, Z_{glo})$ . The origin of the global coordinate is at the still water. The input coordinates is denoted by  $(x_{inp}, y_{inp}, z_{inp})$ . Hydro model and the structural model are defined in input coordinate system [12]. In SIMA, the Global (Earth-Fixed) coordinate system (XG) and Body-Fixed (XB) coordinate system are used. Similar to WADAM and WASIM, the xy-plane coincides with the still water plane in SIMA. The environmental parameter like wave directions is referred with respect to the earth-fixed coordinate system. The body-fixed coordinate system follows the body motion and it is used to describe the position of the elements of the body [15].

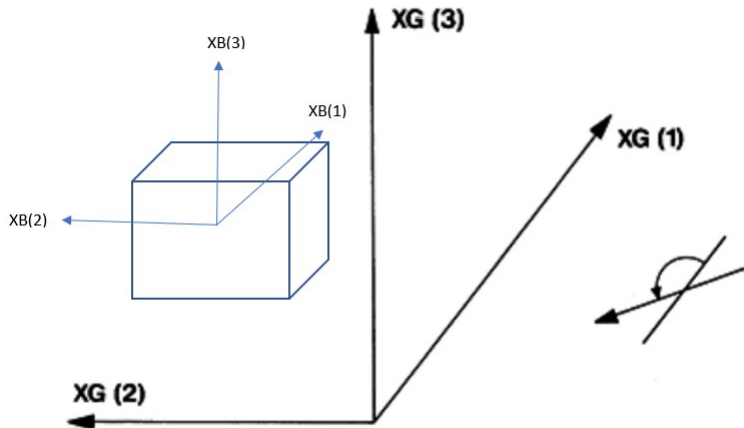


**Figure 3.5:** The coordinate system in SIMA [15].



# Chapter 4

## Numerical Modeling

### 4.1 Umaine VoltturnUS-S 15 MW

This section is based on [1]. In this project, we use the reference model VoltturnUS-S 15 MW semi-submersible FWT designed by the University of Maine. As there is an increase in demand for wind turbines with larger capacity, the University of Maine came up with a reference design for a 15 MW FWT with a semi-submersible substructure [4]. This design has a compact semi-submersible substructure similar to OC4-DeepCwind discussed in the Section 1.3.4 except that the reference design has three pontoons connecting the four columns. The OC4-DeepCwind discussed in the Section 1.3.4 has several bracings connecting the columns, while the reference design has just three horizontal bracings connecting the tower base and the columns.

#### 4.1.1 Design Details

Voltturn US-S 15 MW FWT is a four-column semi-submersible floating platform. The total mass of the platform is 17,854 t, of which 3,914 t is structural steel, 2,540 t is fixed iron-ore-concrete ballast, evenly distributed and placed at the base of the three radial columns. Seawater ballast of 11,300 t floods the three submerged pontoons to achieve the desired draft [1]. Table 4.1 describes various system properties of the reference FWT. In Table 4.1,  $I_{xx}$ ,  $I_{yy}$  and  $I_{zz}$  are the rotational inertia about the center of gravity of the floater for the roll, pitch, and yaw, respectively.

#### Mooring Line Properties

The Figure 4.2 represents the mooring arrangement in the reference model. The mooring system configuration consists of three chains of 850 meters each. Each

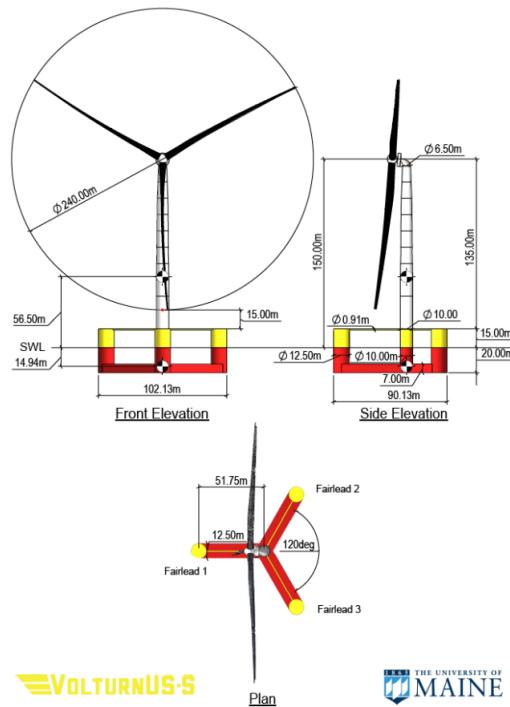


**Figure 4.1:** General Arrangement of UMaine VoltturnUS-S 15 MW FWT[1].

line is attached to an outer column at a depth of 14 meters below the SWL at the fairlead. In the x-y plane, the lines span 120 degrees to anchors located at a depth of 200 meters and 837.60 meters away from the tower's centerline. The line uses a studless R3 chain with a nominal bar diameter of about 185 mm [1]. The mooring line properties are given in the Table 4.2.

### Mass Moment of Inertia Calculation for the Complete Structure

The IEA report gives the vertical center of gravity (v.c.g) of the substructure. The modified v.c.g is calculated for the complete structure (including the tower and the RNA). This is given in the Table 4.3. Figure 4.3 shows the location of the v.c.g in the reference FWT. Similarly, the modified mass moment of inertia (m.o.i) is calculated. The results for the modified roll and pitch m.o.i is given in the Table 4.4.

Parameter	Units	Value
Turbine Rating	MW	15
Hub Height	m	150
Excursion (Length, Width, Height)	m	90.1, 102.1, 290.0
Platform Type		Semi-submersible
Freeboard	m	15
Draft	m	20
Vertical Center of Buoyancy from SWL	m	-14.94
Ixx (Floater only)	kg – m <sup>2</sup>	1.251E + 10
Iyy (Floater only)	kg – m <sup>2</sup>	1.251E + 10
Izz (Floater only)	kg – m <sup>2</sup>	2.367E + 10
Total System Mass	t	20,093
Platform Mass	t	17,839
Tower Mass	t	1,263
Rotor-nacelle assembly (RNA) mass	t	991
Water Depth	m	200
Mooring System		Three-line chain catenary

**Table 4.1:** Umaine VoltturnUS-S 15MW FWT System Properties[1].

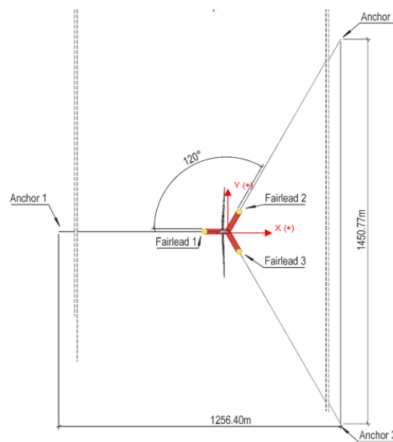


**Figure 4.2:** Mooring Arrangement of UMaine VoltturnUS-S 15 MW FWT [1].

	Mass (kg)	Distance from the Hull CG (m)	Mass moment of inertia (kg-m <sup>2</sup> )
Hull			12500000000.00
Tower	1263000.00	71.44	6445939756.80
RNA	991000	164.94	26960356767.60
		$\Sigma$	<b>4.59E+10</b>
		<b>Radius of Gyration, <math>r_{yy}</math></b>	<b>47.90 m</b>

**Table 4.4:** Mass moment of inertia calculation.

Parameter	Units	Value
Mooring System Type	–	Chain Catenary
Line Type	–	R3 Studless Mooring Chain
Line Breaking Strength	kN	22,286
Number of Lines	–	3
Anchor Depth	m	200
Fairlead Depth	m	14
Anchor Radial Spacing	m	837.6
Fairlead Radial Spacing	m	58
Nominal Chain Diameter	mm	185
Dry Line Linear Density	kg/m	685
Extensional Stiffness	MN	3270
Line Unstretched Length	m	850
Fairlead Pretension	kN	2,437
Fairlead Angle from SWL	<i>degrees</i>	56.4

**Table 4.2:** Umaine VoltturnUS-S 15MW FWT Mooring line Properties[1].

	Mass (t)	C.O.G (from SWL) (m)	Moment of weights (t-m)
Hull	17854	-14.94	-266738.76
Tower	1263	56.50	71359.50
RNA	991	150.00	148650.00
$\Sigma$	20108		-46729.26
		$\Sigma \frac{\text{Moments of weights}}{\text{Mass}}$	<b>-2.32 m from SWL</b>

**Table 4.3:** Modified VCG calculation.

Note: In the above calculation, own m.o.i for tower and RNA are ignored. Hull mass moment of inertia is given in the reference document by IEA [1].

## 4.2 Hydrodynamic Analysis Of The Reference SIMA Model

The reference SIMA model was given upfront by Professor Erin Bachynski-Polić of Department of Marine Technology, NTNU. In this section, the hydrodynamic properties of the reference model are presented. This includes added mass, damping, first-order wave excitation, rigid body natural frequencies.

### 4.2.1 Coordinate System

Figure 4.4 defines the global coordinate system. The x-y plane coincides with the calm water. The wave propagation direction and wind direction are defined

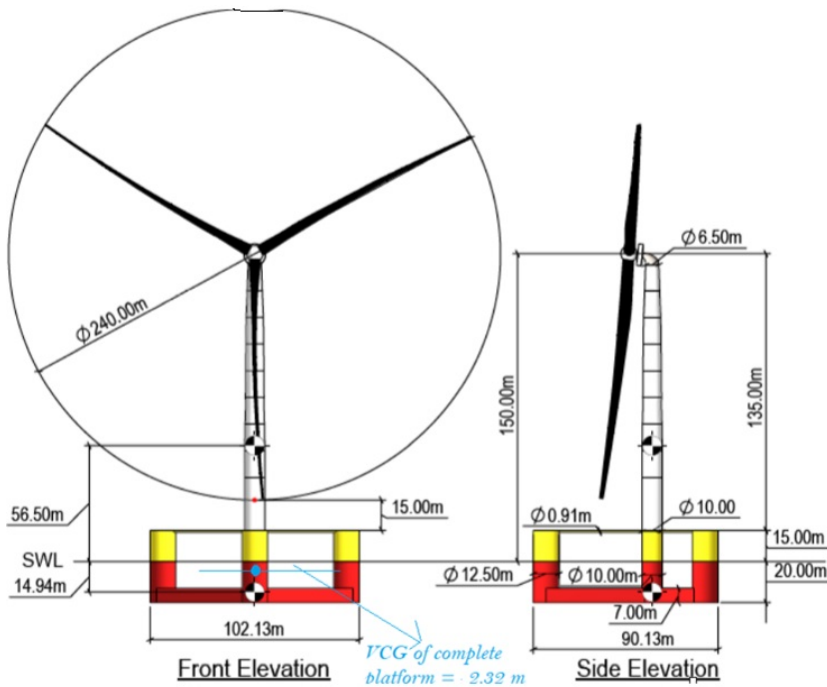


Figure 4.3: V.C.G of the reference FWT [1].

based on the global coordinate system [15]. The coordinate system follows a right-handed cartesian coordinate system where anti-clockwise rotations are positive [15].

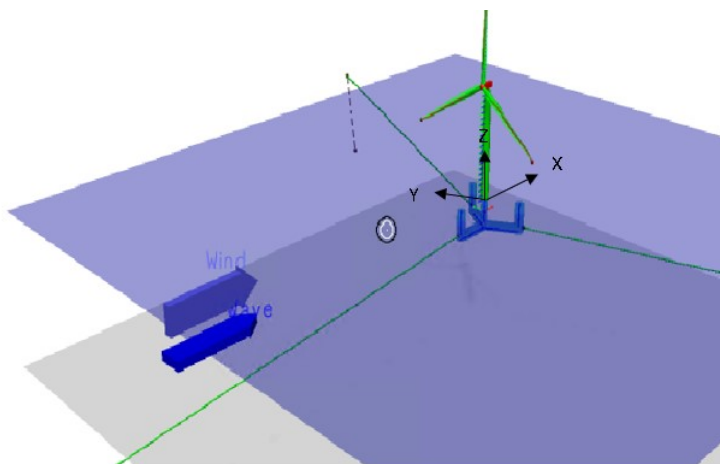
#### 4.2.2 Hydrodynamic Coefficients

Table 4.5 and Table 4.6 are the added mass and hydrostatic stiffness matrix. The hydrodynamic added mass and damping coefficients of the reference model are presented in the Figure 4.11 to Figure 4.16. The symmetry in the surge-sway plane results in identical added mass and damping values for roll-pitch and surge-sway [1]. In the Figure 4.17 to Figure 4.19 first-order wave excitation transfer functions are presented. Due to the aforementioned symmetry, the results for sway, roll, and yaw are not presented. The results are provided for zero-degree wave heading [1].

#### 4.2.3 Rigid Body Decay Tests

The free decay test is performed to obtain the natural period of the floater. In the free decay test, the blades of the wind turbine were oriented such that the reference model experienced minimum aerodynamic drag. The initial displacement is





**Figure 4.4:** Global coordinate system.

$$\begin{bmatrix} 9.640 \text{ E}+06 & 0 & 0 & 0 & -1.010 \text{ E}+08 & 0 \\ 0 & 9.640 \text{ E}+06 & 0 & 1.010 \text{ E}+08 & 0 & 0 \\ 0 & 0 & 2.480 \text{ E}+07 & 0 & 0 & 0 \\ 0 & 0 & 0 & 1.160 \text{ E}+10 & 0 & 0 \\ -1.010 \text{ E}+08 & 0 & 0 & 0 & 1.160 \text{ E}+10 & 0 \\ 0 & 0 & 0 & 0 & 0 & 2.010 \text{ E}+10 \end{bmatrix}$$

**Table 4.5:** Hull Infinite-Frequency Added Mass in kg, kg-m or kg-m<sup>2</sup> [1].

$$\begin{bmatrix} 0 & 0 & 0 & 0 & 0 & 0 \\ 0 & 0 & 0 & 0 & 0 & 0 \\ 0 & 0 & 4.470\text{E} + 06 & 0 & 0 & 0 \\ 0 & 0 & 0 & 2.190\text{E} + 09 & 0 & 0 \\ 0 & 0 & 0 & 0 & 2.190\text{E} + 09 & 0 \\ 0 & 0 & 0 & 0 & 0 & 0 \end{bmatrix}$$

**Table 4.6:** Hull hydrostatic stiffness in N/m, N/rad or N-m/rad [1].

achieved by applying a ramp force, followed by a constant force, which is then released. The results of the decay test are presented in Figure 4.5 and the natural period in the six degrees of freedom are given in Table 4.7.

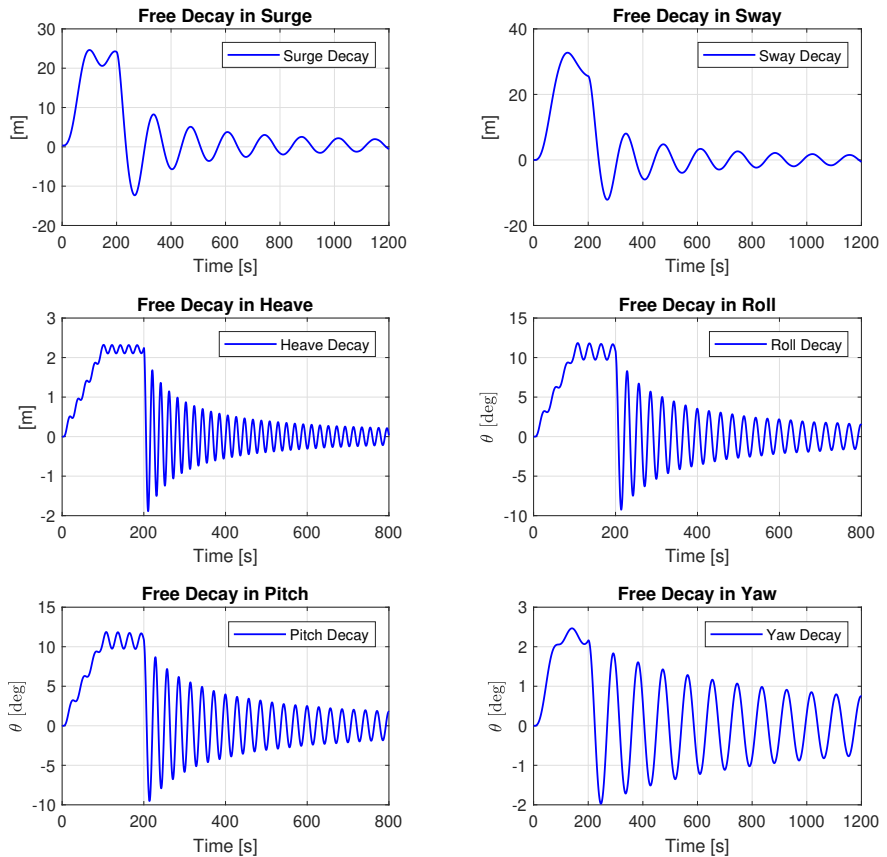


**Figure 4.5:** Results of free decay test in the six degrees of freedom.

## 4.3 Modeling In Genie

### 4.3.1 Panel Model

The reference model has been modeled in the DNV module Genie. The panels are created in Genie to describe the wetted surface area to perform the hydrodynamic analysis. The model is oriented in the same way as the reference SIMA model. There is a total of 8079 panels below the waterline of the model. The surface area of the panels is  $1 \text{ m}^2$ . DNV-RP-0286 recommends 7 to 10 panels per wavelength

Rigid-Body Mode	Period (secs)
Surge	143
Sway	143
Heave	21
Roll	28
Pitch	28
Yaw	91

**Table 4.7:** Natural Period in the six degrees of freedom [1].

[37]. The typical wave period ranges between 5 to 25 seconds. The corresponding wavelength is 39 m to 981 m. Therefore the minimum number of panels required is 6867. DNV-RP-C205 recommends diagonal length of the panel mesh should be less than  $1/6^{th}$  of the smallest wave length [38]. The diagonal length of the panel mesh is 1.41 m is less than the  $1/6^{th}$  of the smallest wavelength of 39 m ( $1/6^{th}$  of 39 = 6.5 m). The panel model created is exported to DNV module HydroD as .FEM file to perform hydrodynamic analysis in WADAM. The panel model exported to HydroD is given in the Figure 4.6.

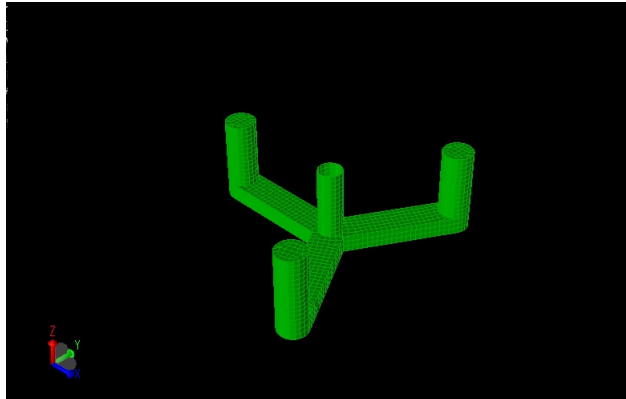


**Figure 4.6:** Panel model for WADAM.

### 4.3.2 Structural Model

Floaters can be either modeled as a rigid body or multi-body. The floater can be modeled as a rigid body, assuming elastic deformation of the floater does not significantly influence the global displacements of the FWT [37]. If the elastic deformations of the floater are important, then finite element or multi-body representation of the floater is recommended [37]. In this thesis, we start with modeling

the floater as a rigid body, and later in Chapter 7 multi-body representation is introduced. The results of the rigid body model and the multi-body models are compared. The structural model is given in the Figure 4.7. The structural data and mass properties of the structural model given in the Figure 4.8 are taken from the .LIS file in the WADAM analysis. The structural data and mass properties in the Figure 4.8 match well with the reference model mass properties given in the Table 4.1, Table 4.3 and Table 4.4.

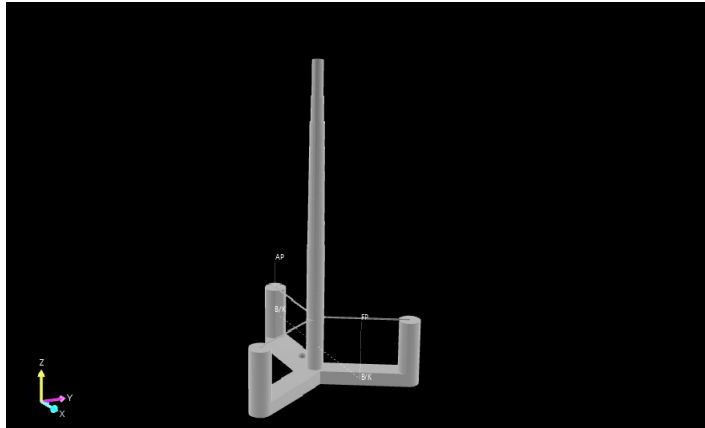


Figure 4.7: Structural model.

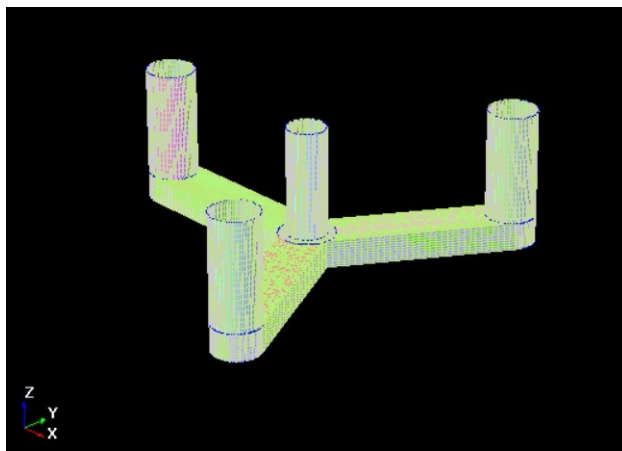
MASS PROPERTIES AND STRUCTURAL DATA:			
-----			
MASS OF THE STRUCTURE	M	= 2.08079E+07	[M]
WEIGHT OF THE STRUCTURE	M*G	= 2.04056E+08	[M*L/T**2]
CENTRE OF GRAVITY		XG	= 9.17705E-02 [L]
		YG	= 1.00607E-01 [L]
		ZG	= -2.67383E+00 [L]
ROLL RADIUS OF GYRATION	XRAD	= 4.59409E+01	[L]
PITCH RADIUS OF GYRATION	YRAD	= 4.58907E+01	[L]
YAW RADIUS OF GYRATION	ZRAD	= 3.25806E+01	[L]
ROLL-PITCH CENTRIFUGAL MOMENT	XYRAD	= 2.82472E+00	[L**2]
ROLL-YAW CENTRIFUGAL MOMENT	XZRAD	= 7.38319E+00	[L**2]
PITCH-YAW CENTRIFUGAL MOMENT	YZRAD	= 9.26398E+00	[L**2]

Figure 4.8: Mass properties and structural data.

### Section Model

For WASIM analysis section model (also called as PLN model) is required. This is different from the panel model (.FEM) used in the WADAM analysis. WASIM

is a time domain formulation requiring a Rankine panel model solution [39]. For WASIM, the floater is created in Genie using curves. The surfaces (or patches) are created in HydroD. Once the patches are created, section meshes are generated in HydroD. The structural model is the same for WASIM and WADAM [39].



**Figure 4.9:** Section model for WASIM.

#### **4.4 Comparison Of Hydrodynamic Properties Of The Reference Model (SIMA), Panel Model (WADAM), and Section Model (WASIM)**

The three stages of this thesis work is discussed in the Section 1.6. First of the three stages in the thesis work is on Model Validation. The Figure 4.10 illustrates the work flow in the Model Validation. In Model Validation, The hydrodynamic properties of the panel model and section model are compared with the SIMA reference model. The added mass of surge, heave, and pitch are compared. The comparison plot is presented in Figure 4.11 to Figure 4.13. In Figure 4.14 to Figure 4.16 potential damping comparison is presented for the surge, heave, and pitch. In the Figure 4.17 to Figure 4.19 comparison of the excitation transfer function is presented for surge, heave, and pitch. The hydrodynamic properties of the three models are reasonably consistent and match well, and can be used for further analysis in the thesis as given in Figure 4.10.

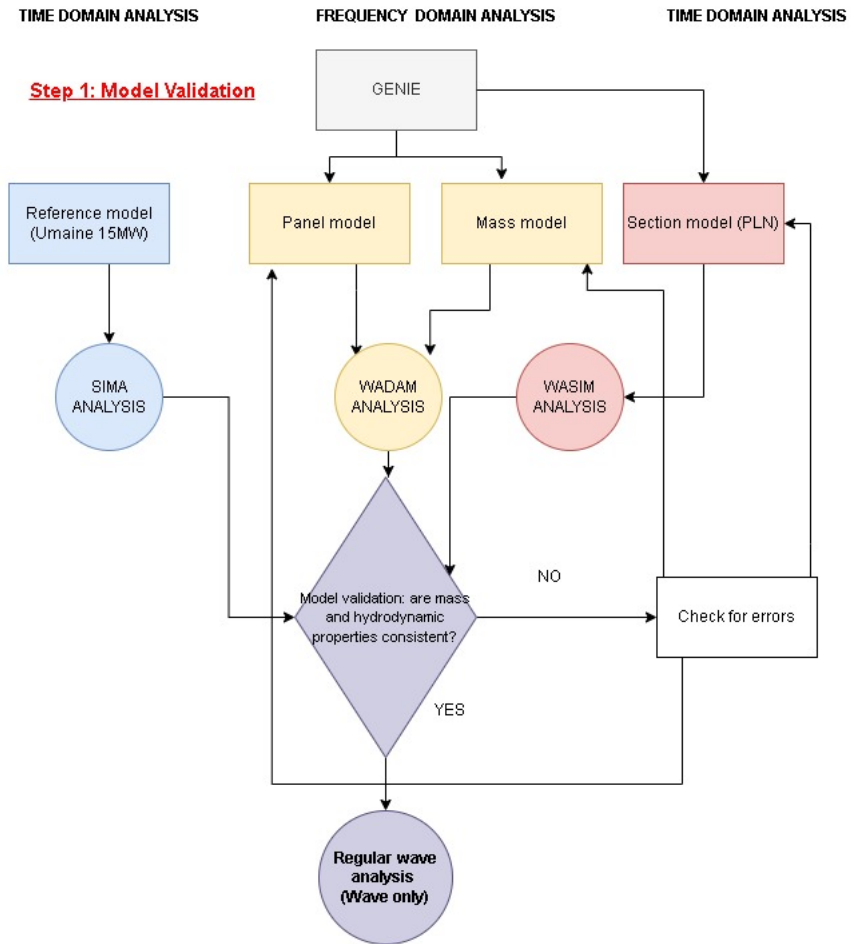
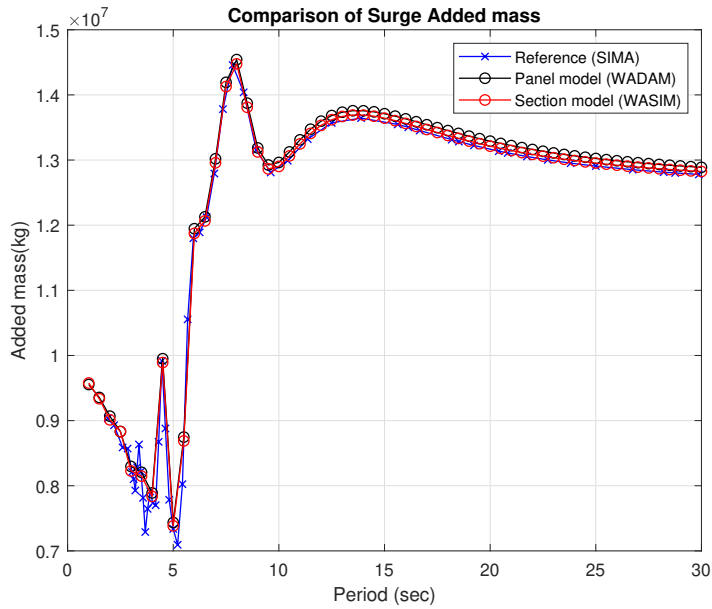
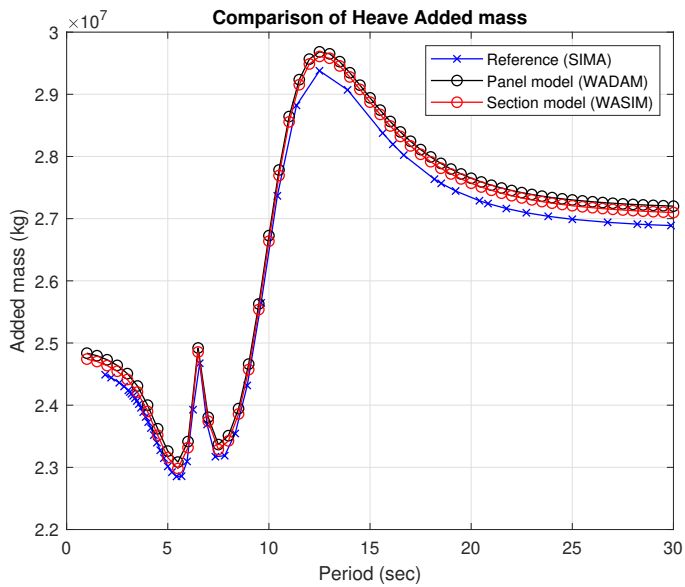


Figure 4.10: Model validation



**Figure 4.11:** Added mass in surge due to surge motion  $[A_{11}]$ .



**Figure 4.12:** Added mass in heave due to heave motion  $[A_{33}]$ .

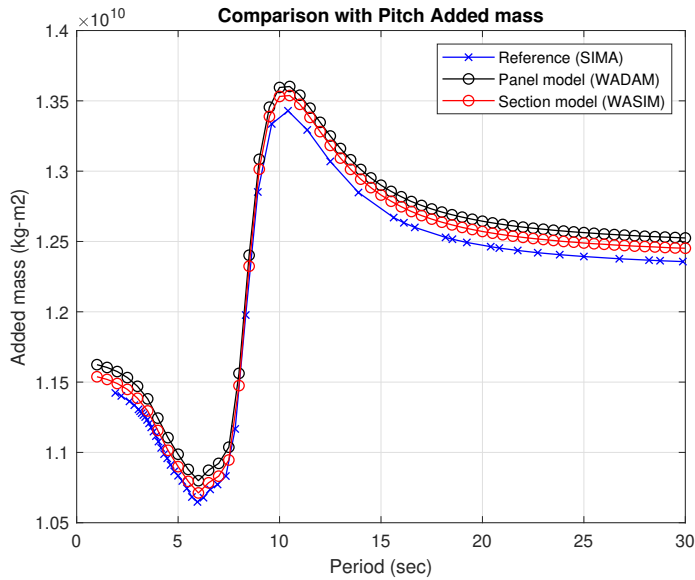


Figure 4.13: Added mass in pitch due to pitch motion [A<sub>55</sub>].

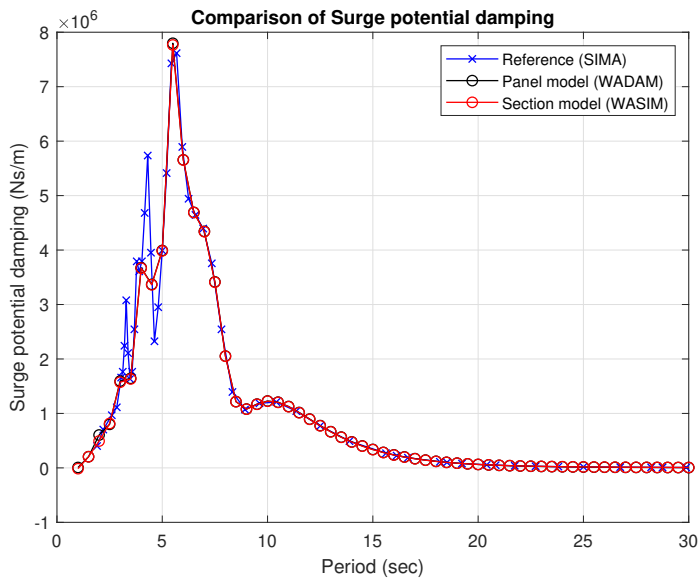
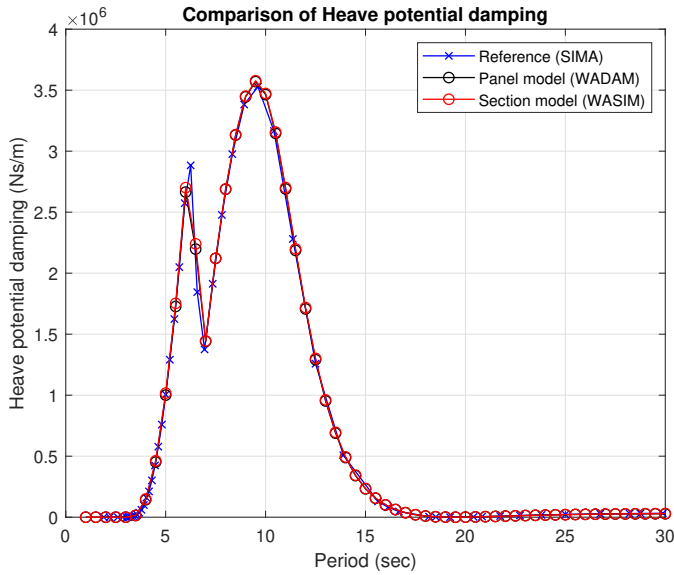
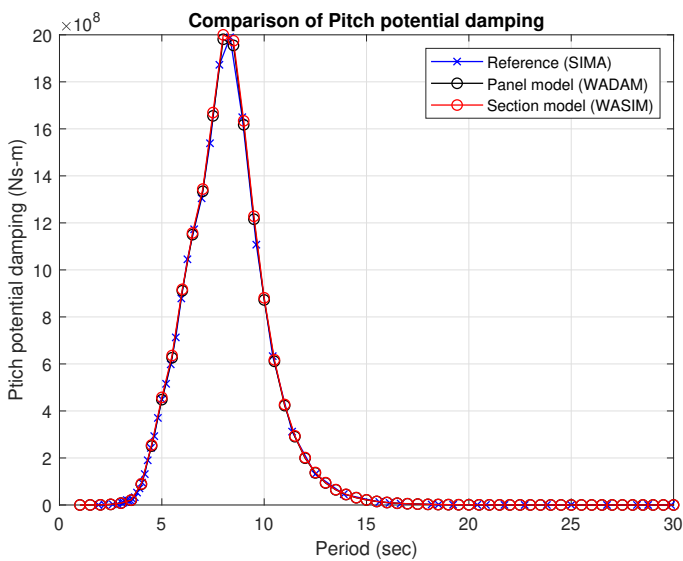


Figure 4.14: Potential in surge due to surge motion [B<sub>11</sub>].





**Figure 4.15:** Potential damping in heave due to heave motion [B<sub>33</sub>].



**Figure 4.16:** Potential damping in pitch due to pitch motion [B<sub>55</sub>].

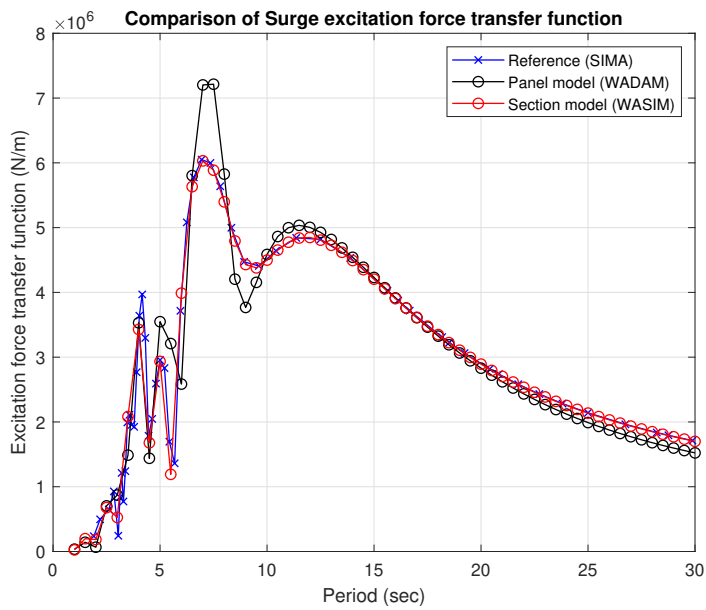


Figure 4.17: First order wave excitation transfer function in surge.

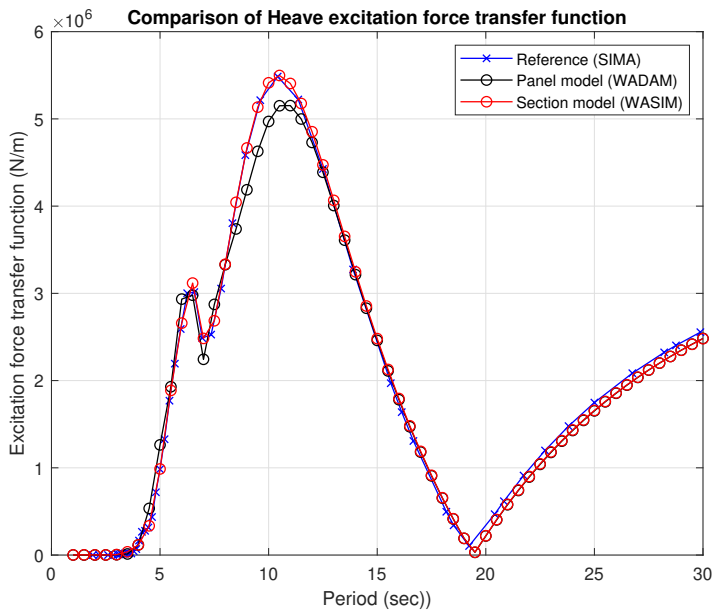


Figure 4.18: First order wave excitation transfer function in heave.

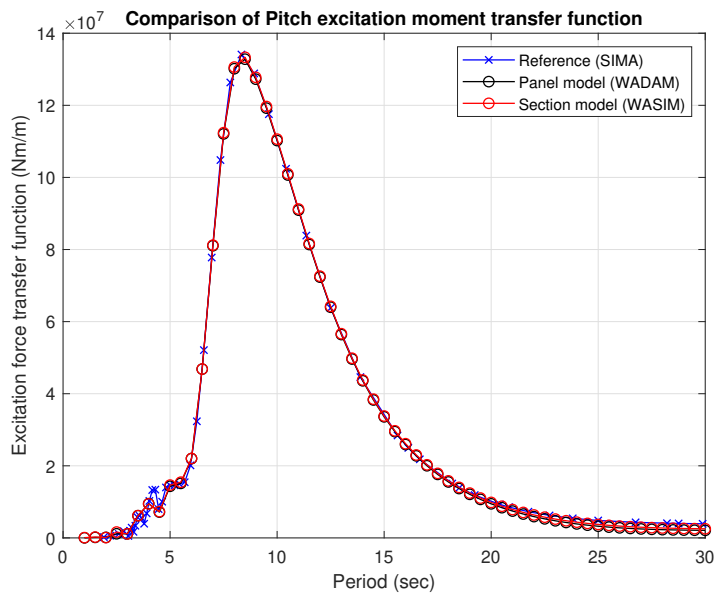


Figure 4.19: First order wave excitation transfer function in pitch.



# Chapter 5

## Regular Wave Analysis

Three stages in the thesis work were discussed in the Section 1.6. In Section 4.4, model validation results were presented. Model validation was satisfactory. In this chapter, stage two of the three stages are discussed. Stage two is described in Figure 5.1. In stage two, as discussed in Section 1.6.2, the proposed approach is validated in a regular wave analysis. In regular wave analysis, the FWT is investigated under a regular wave of period 5 to 30 seconds and, wind load is assumed to be minimal, and it is ignored.

### 5.1 Motion Response

In this section, we compare the motion response in a zero-degree wave heading obtained from the numerical tool SIMA, WADAM, and WASIM. Zero-degree wave heading is along the negative x-axis as described in Figure 4.4. WADAM analysis is performed in the frequency domain. SIMA and WASIM analyses are performed in the time domain. The time domain results are filtered and converted to the frequency domain. In the following section, sample results are presented for a wave excitation at a heave natural period of 21 seconds.

#### 5.1.1 Wave Elevation Time Series

The wave elevations from 5 to 30 seconds were input to the numerical tools. The Figure 5.2 presents the wave elevations for a wave period of 21 seconds.

#### 5.1.2 Time Series Of The Rigid Body Response

The numerical tool SIMA and WASIM performs the simulation based on the input signal (wave elevation) and provides the time series of the rigid body response. The unfiltered heave response time series for 21 second wave period is presented

**Step 2: Proposed approach validation**

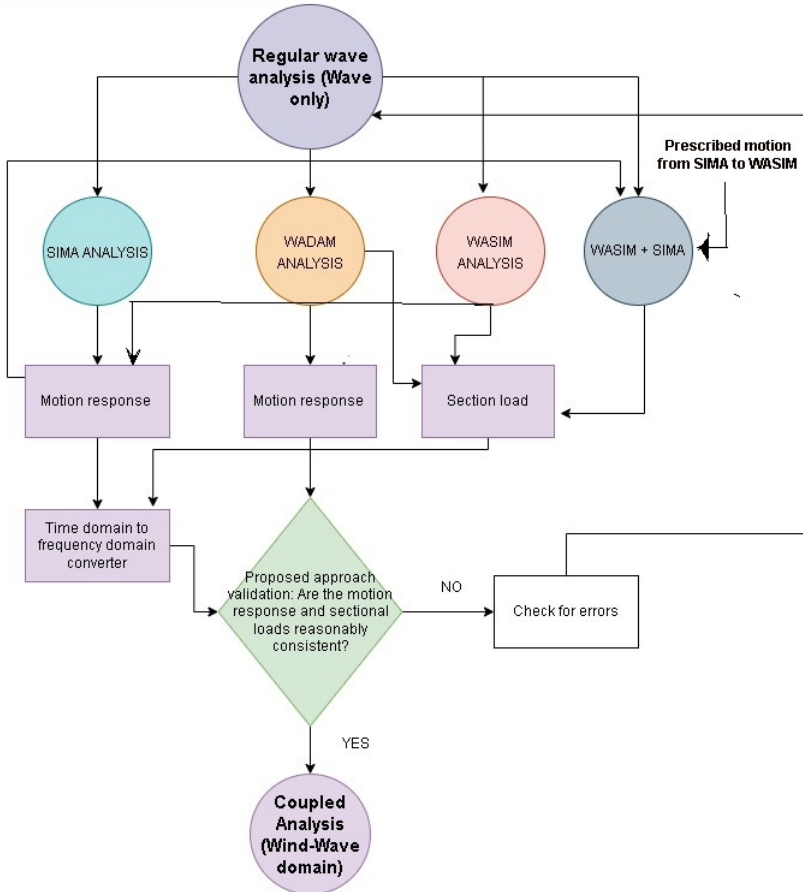


**Figure 5.1:** Validation of proposed approach.

in Figure 5.3. The time series presented in Figure 5.3 is detrended by subtracting from its mean value and then it is filtered using the band-pass filter function. The band-pass filter function is used to tune the time series to a desired frequencies and blocking lower and higher frequencies. The filtered time series is presented in Figure 5.4. As described in Figure 5.5 average of the positive peak of the response in a time series is assumed to represent the response for that particular wave period (or frequency).

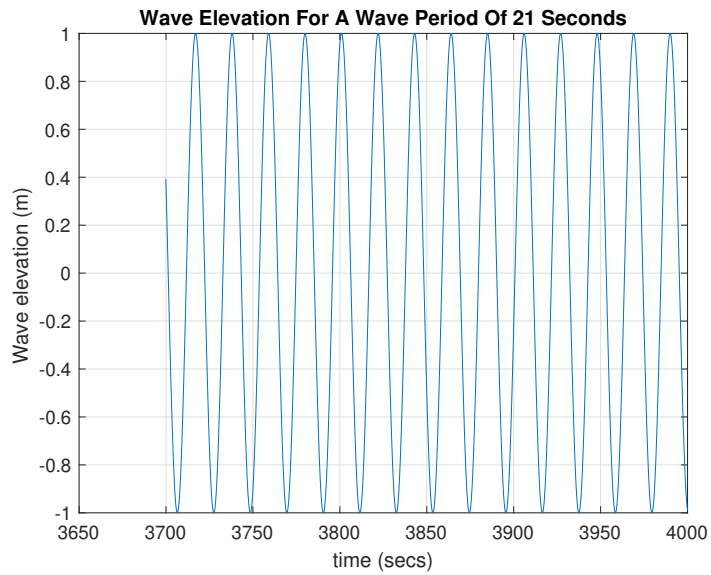


**Figure 5.2:** Wave elevation for a wave period of 21 seconds.

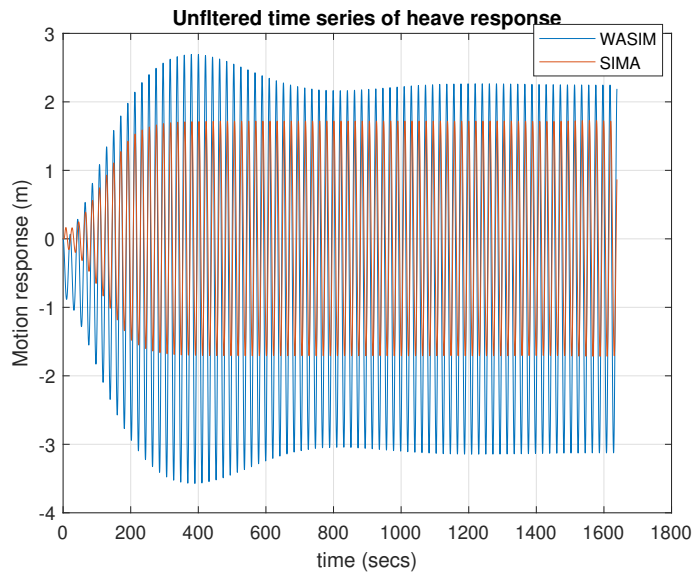


**Figure 5.3:** Unfiltered time series of heave response.



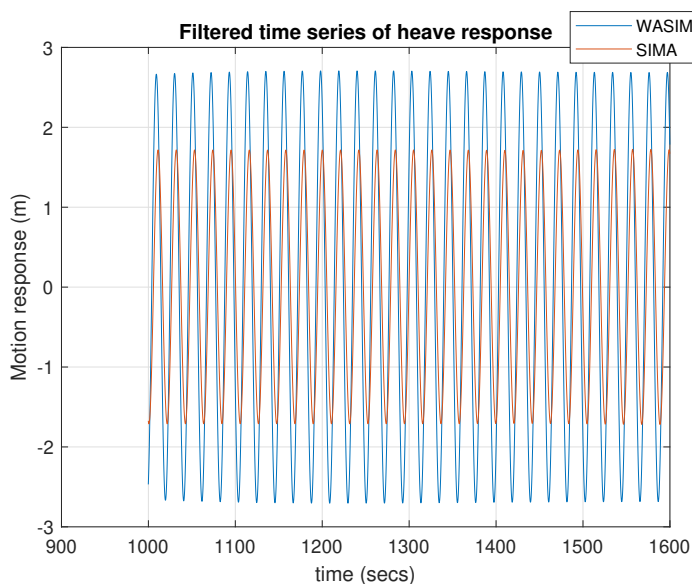


**Figure 5.4:** Filtered time-series of heave response.

### 5.1.3 Comparison Of RAO Between SIMA, WASIM, and WADAM.

The comparative plots between the numerical tools for surge, heave, and pitch RAO is presented in the Figure 5.6 to Figure 5.8. The comparison plots indicate the three motions are consistent across the numerical tools SIMA, WASIM, and WADAM except for the resonance frequency. The difference in the response at resonance is due to the damping term. The damping factor is different in the three numerical tools. Non-linear damping is not accounted for in WADAM. Hence, WADAM results has very high peak values, while the results of SIMA and WASIM are relatively closer. SIMA accounts for the non-linear damping due to the presence of mooring lines while WASIM do not account for the non-linear damping due to the mooring lines. Hence WASIM displays higher value at the peak frequency compared to SIMA. Other minor variation in the plot is attributed to the numerical error in filtering the time series.

## 5.2 Sectional Load

### 5.2.1 Definition Of The Cross-Section

The Figure 5.9 illustrates the location of the three cross-sections where the sectional loads are obtained in the FWT. In this thesis work, we are interested in the

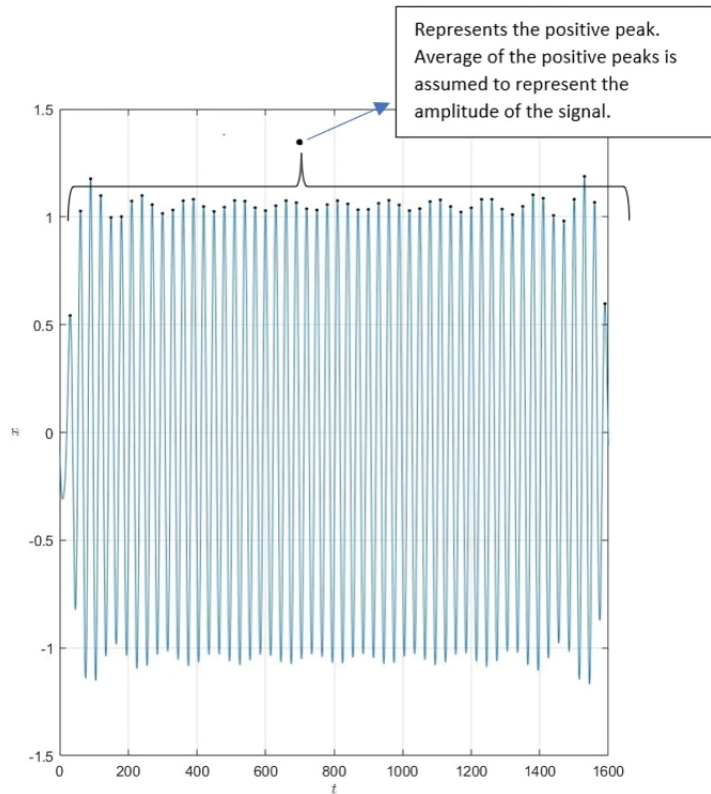


**Figure 5.5:** Positive peaks in a time series.

load at a cross-section of the pontoon. The other interesting point of interest is the tower of the FWT. Tower base bending moment can be obtained directly in SIMA. When a FWT is subjected to simultaneous turbulent wind and wave loads, loads at the pontoon are critical to establish. Hence, in this thesis work, only loads at a cross-section of the pontoon are computed. The three cross-sections are located at :

1. Section 1 : (-8, 0, 0m) close to the centre column (Column 2).
2. Section 2 : (-25, 0, 0 m) mid point of the pontoon ( Pontoon 1) connecting the centre column (Column 2) and the side column ( Column 1).
3. Section 3 : (-44, 0, 0 m) close to the side column (Column 1).

The sections are defined at Pontoon 1, which is oriented along the negative x-axis.

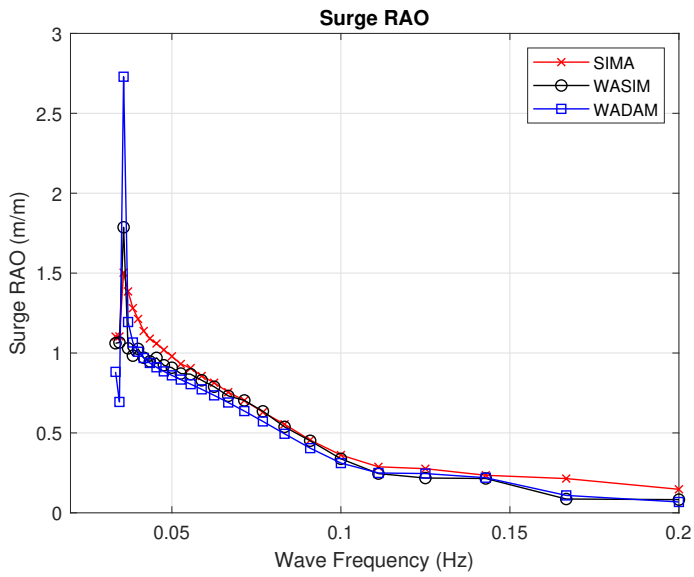


**Figure 5.6:** Surge RAO comparison between SIMA, WASIM, and WADAM.

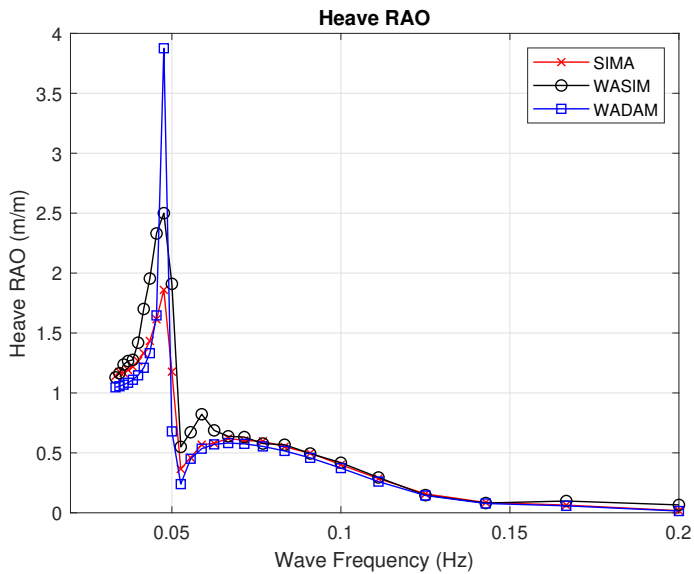


**Figure 5.7:** Heave RAO comparison between SIMA, WASIM, and WADAM.

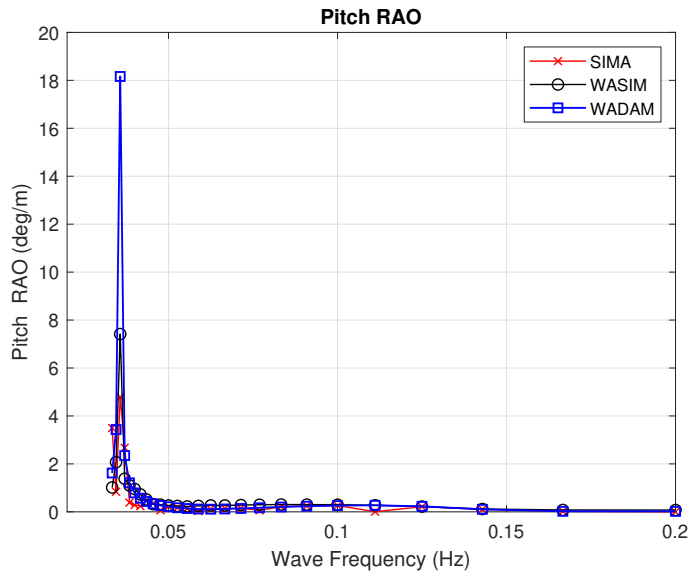


**Figure 5.8:** Pitch RAO comparison between SIMA, WASIM, and WADAM.

The numerical tools used in this thesis work do not support obtaining the sectional loads at the other two pontoons (Pontoon 2 and Pontoon 3). In the case of the other two pontoons, when you define a cross-section of one pontoon, it will overlap with the other pontoon as illustrated in Figure 5.10. Hence, it is not possible to obtain the sectional load from Pontoon 2 and Pontoon 3. This is a limitation in the proposed approach in this thesis work.

### 5.2.2 Time Series Of The Sectional Load

Similar to the motion RAO, the load time series at the defined cross-sections are obtained for the wave period from 5 to 30 seconds. WASIM allows to define the cross-section of the rigid body and computes the load in the defined cross-section. SIMA does not support obtaining the loads at the cross-sections of the rigid body. As illustrated in the Figure 5.1, the motion obtained from SIMA in the simulation is exported to WASIM as prescribed motions. WASIM performs the analysis based on the motions imported from SIMA and computes the load at the defined cross-section. The combined use of WASIM and SIMA is represented as "WASIM+SIMA". Similar to the motion RAO, the unfiltered time series of the load for a 21-second wave period is presented in the Figure 5.11. The time series presented in Figure 5.11 similar to motion RAO is detrended by subtracting from its mean value and filtered using a band-pass filter method. The filtered time series

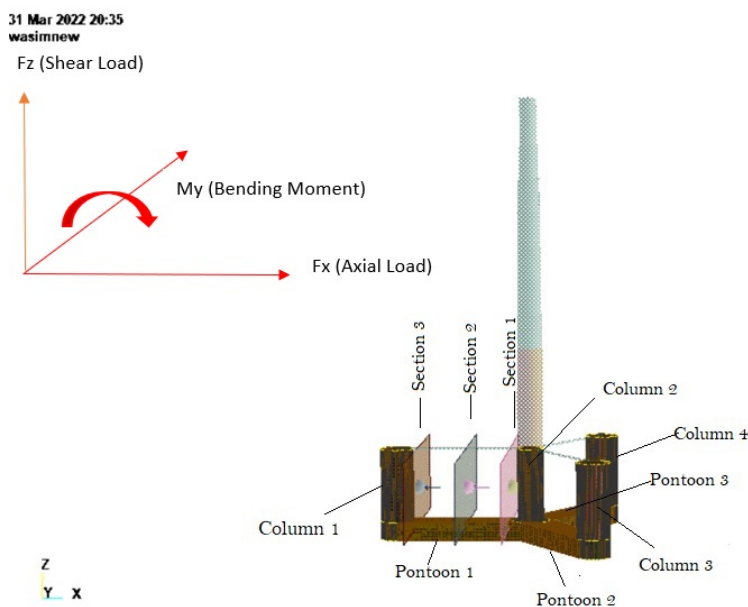


**Figure 5.9:** Location of the three cross-sections defined.

of the load is presented in the Figure 5.12. The filtered and detrended time series in the Figure 5.12 shows that the load obtained from standalone WASIM and the loads obtained from SIMA motions prescribed in WASIM are consistent.

### 5.2.3 Comparison Of Load Amplitude Between SIMA, WASIM, and WADAM.

The comparative plots between the numerical tools for the normalized load (Load per unit wave amplitude) in the three cross-sections are presented in the Figure 5.13 to Figure 5.15. The comparison plots indicate that the load at the three cross-sections across the numerical tools WASIM+SIMA, WASIM, and WADAM are reasonably consistent. Like motion RAO, WADAM results indicate higher peak values, but the WASIM and WASIM+SIMA results are relatively closer. The WASIM and WASIM+SIMA are used to compute the loads at the cross-section in the coupled analysis in the stage three of the thesis work. Since WASIM and WASIM+SIMA are consistent, the analysis is forwarded to stage three to conduct the computation of sectional load in the coupled analysis (simultaneous action of turbulent wind and irregular wave).

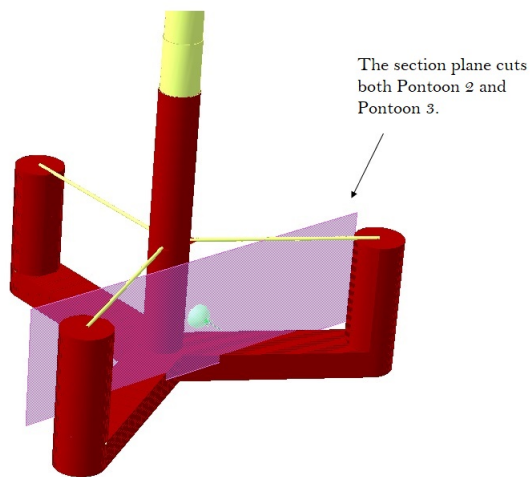


**Figure 5.10:** Section plane overlaps with Pontoon 2 and Pontoon 3.

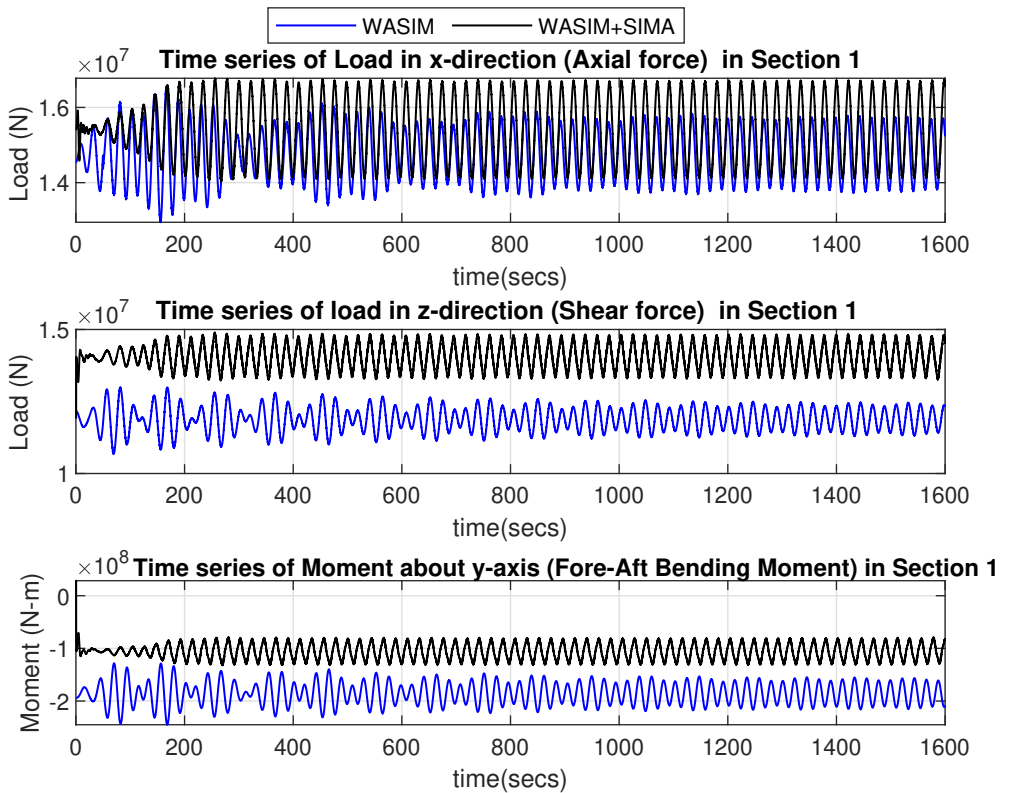


**Figure 5.11:** Unfiltered time series of load in section 1 - comparison between WASIM and WASIM+SIMA.

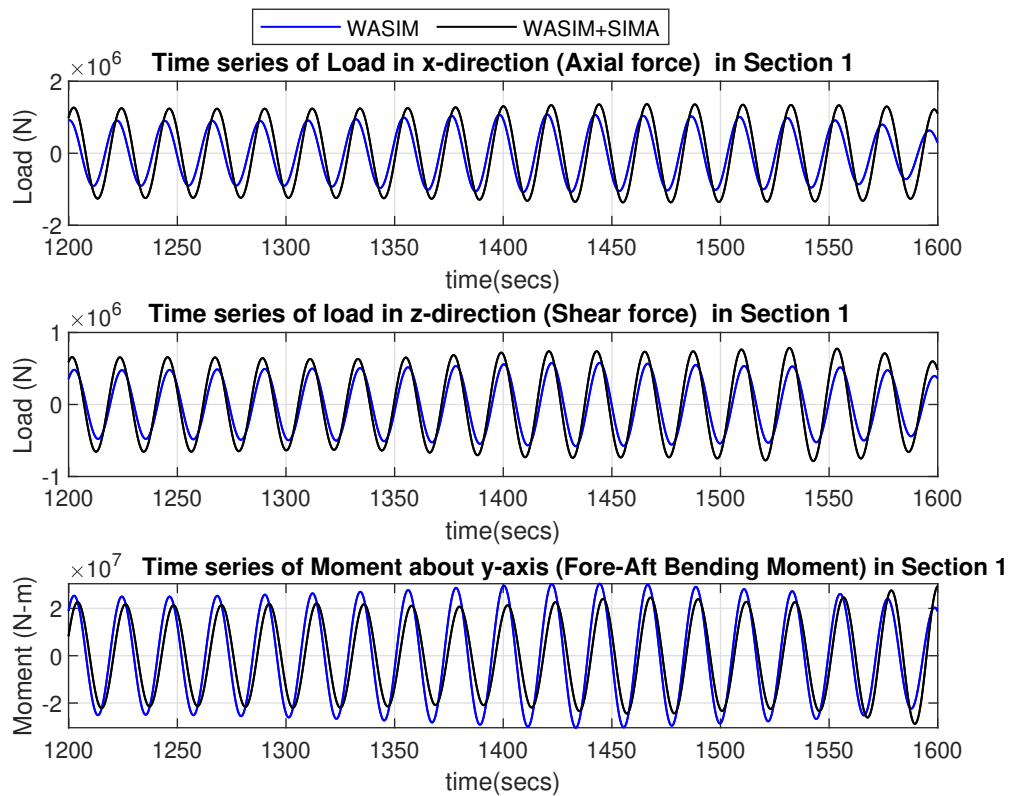


**Figure 5.12:** Filtered time-series of load in section 1 - comparison between WASIM and WASIM+SIMA.



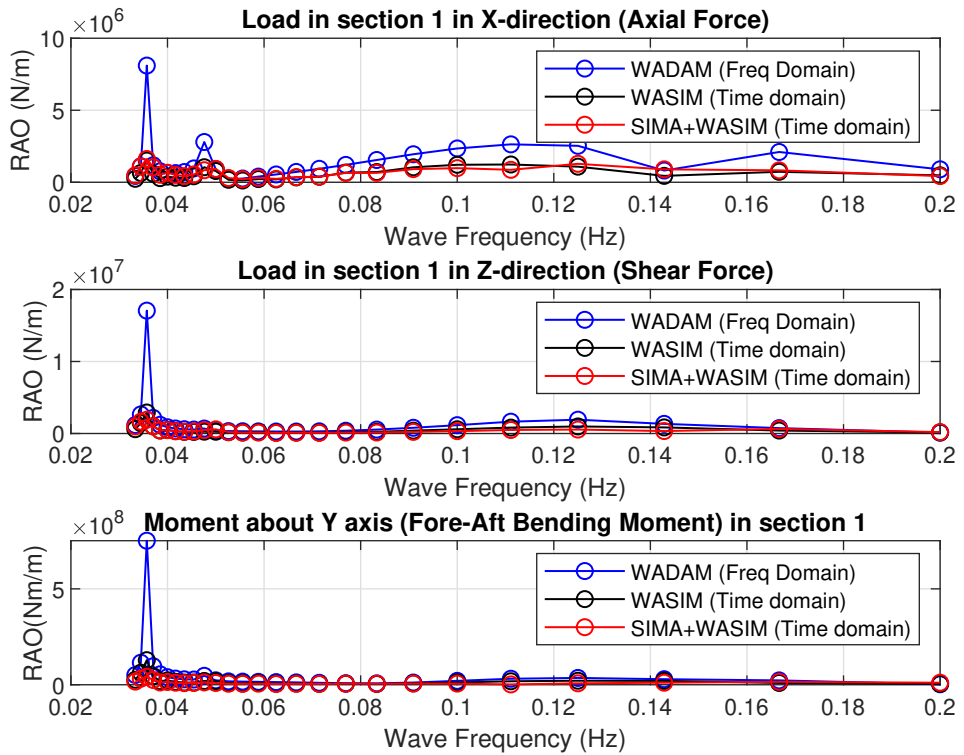


**Figure 5.13:** Load amplitude in section 1 - comparison between SIMA, WASIM, and WADAM.

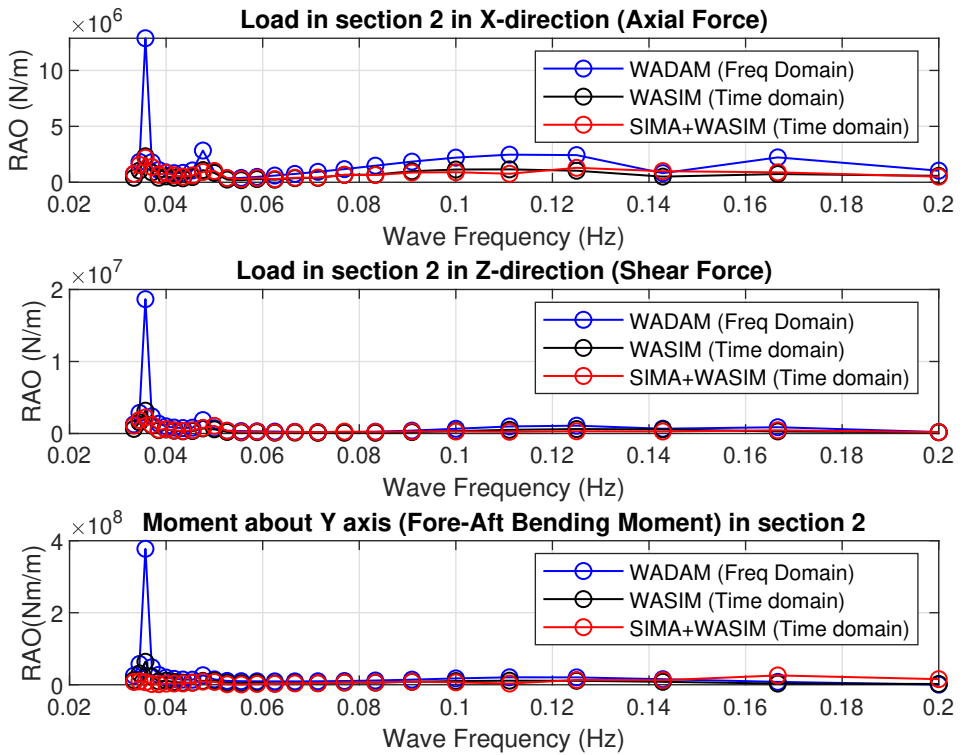


**Figure 5.14:** Load amplitude in section 2 - comparison between SIMA, WASIM, and WADAM.

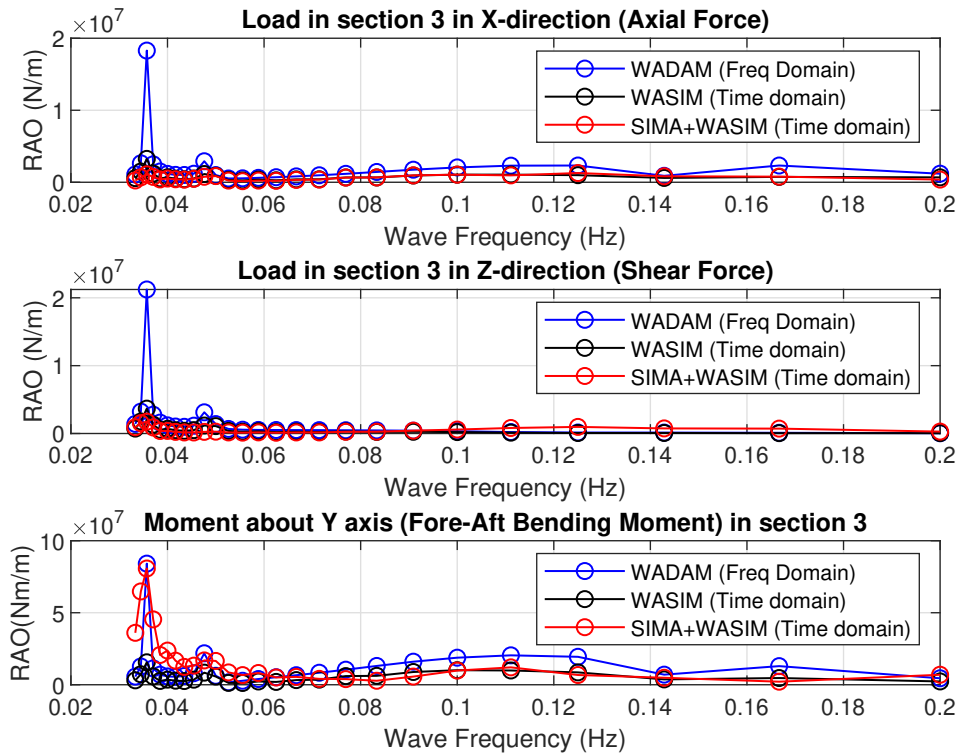


**Figure 5.15:** Load amplitude in section 3 - comparison between SIMA, WASIM, and WADAM.

# Chapter 6

## Coupled analysis

Three stages in the thesis work were discussed in Section 1.6. In Section 4.4, model validation results were presented. Model validation was satisfactory. In Chapter 5, stage two validation of the proposed approach were presented. In Section 5.2.3 results of the stage two were presented, and they were found satisfactory. In this chapter, stage three (final stage) is discussed. Figure 6.1 describes stage three, which deals with the execution of the coupled analysis. In coupled analysis, there is a simultaneous action of wind and wave hence there is a load due to the operating wind turbine, and there is a load on the substructure of the OWT due to wave loads. Stage three is briefly discussed in Section 1.6.3.

### 6.1 Load Cases

Three representative Load Cases (LC) were selected to perform the coupled analysis. The load cases are given in Table 6.1.  $U_W$  is wind speed,  $H_s$  is the significant wave height,  $T_p$  is the peak wave period.

	$U_w$ [m/s]	$H_s$ [m]	$T_p$ [s]
LC1	6	1.75	9.5
LC2	12	2.75	10.5
LC3	18	4.25	11.5

**Table 6.1:** Load cases

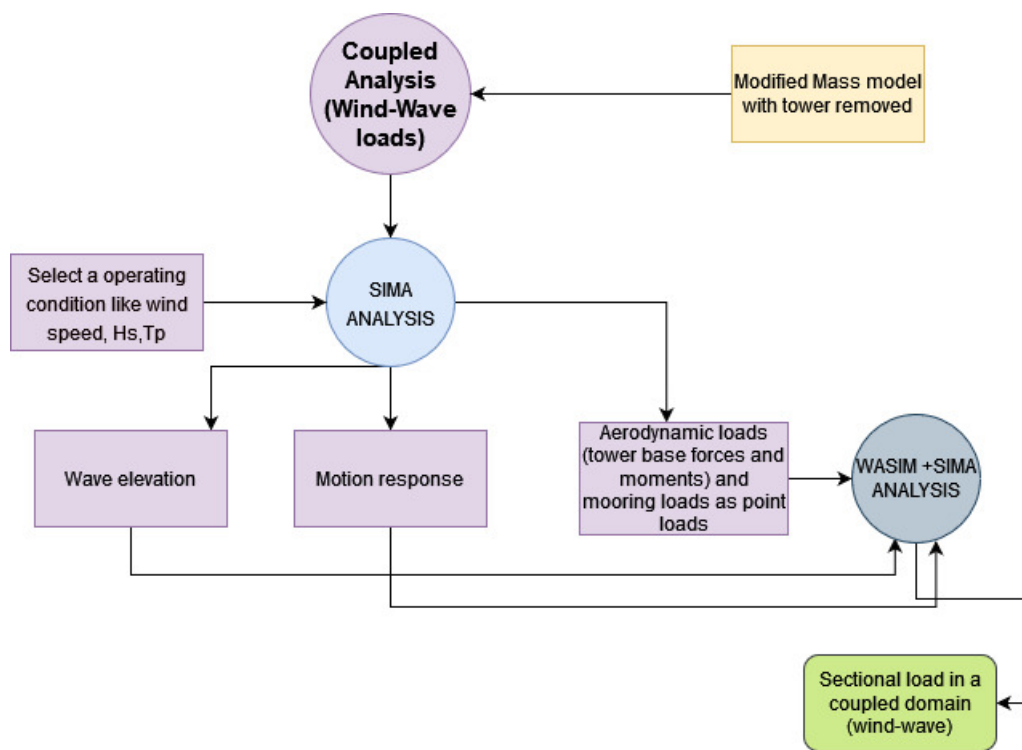


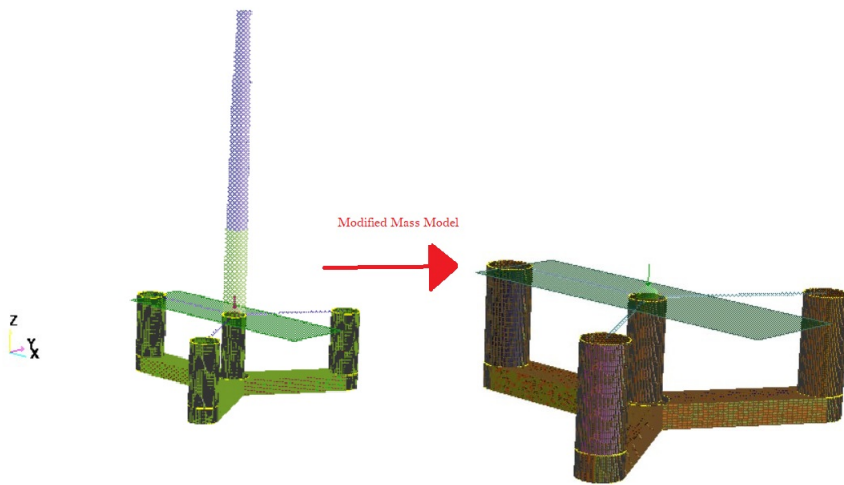
Figure 6.1: Coupled Analysis - Simultaneous wind and wave action.

## 6.2 Modified Mass Model

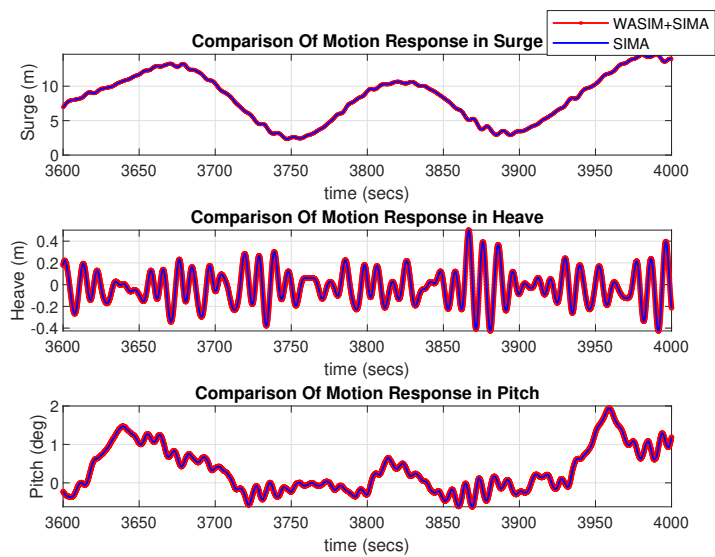
The existing mass model used in the regular wave analysis in Chapter 5 is modified in the coupled analysis. The modified mass model is presented in Figure 6.2. This is to avoid duplication of tower loads in the coupled analysis. The coupled analysis in SIMA is performed with the existing model, and WASIM+SIMA analysis (WASIM analysis using SIMA prescribed motions and forces) is performed with the modified mass model. The results of SIMA and the results of WASIM+SIMA are compared to ensure consistency of both the models. Figure 6.3 and Figure 6.4 presents the comparison for motions and tower base bending moment for LC1 in SIMA and WASIM+SIMA. The motion results in Figure 6.3 and the tower base bending moment in Figure 6.4 are consistent in both the model.

## 6.3 Sectional Loads

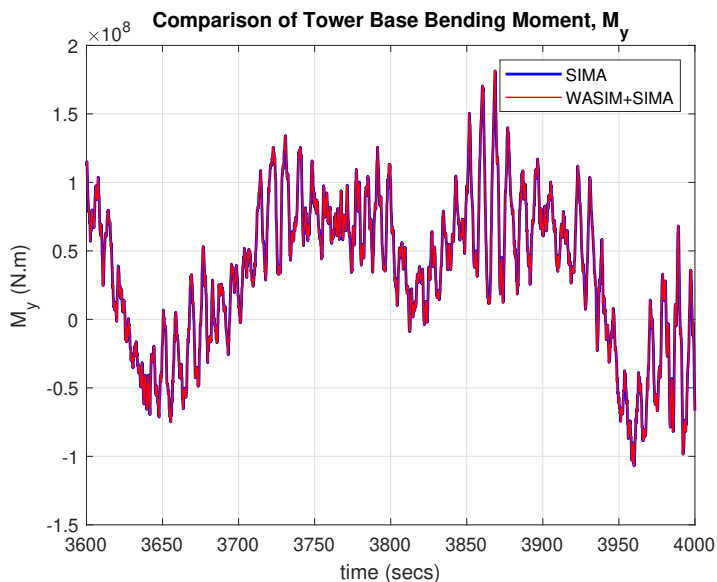
Figure 6.5 to Figure 6.7 presents the time series of the sectional load in Load Case 1, Load Case 2, and Load Case 3 respectively. The time series is transferred to



**Figure 6.2:** Modified Mass Model

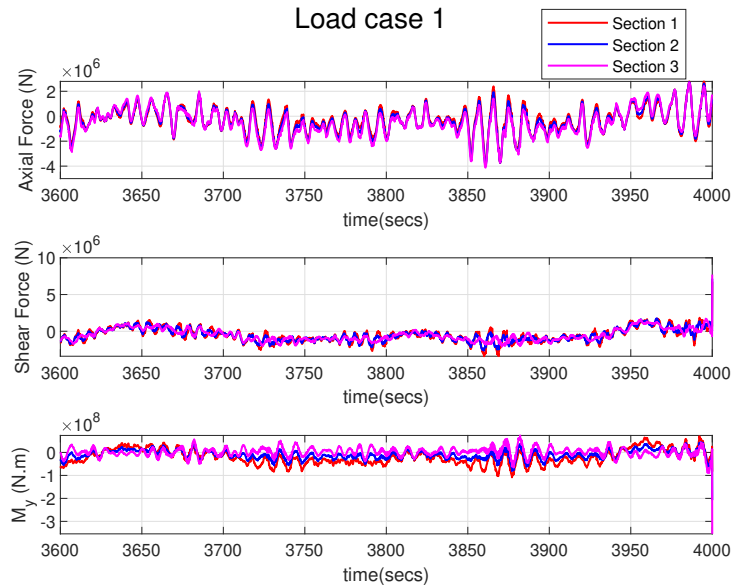
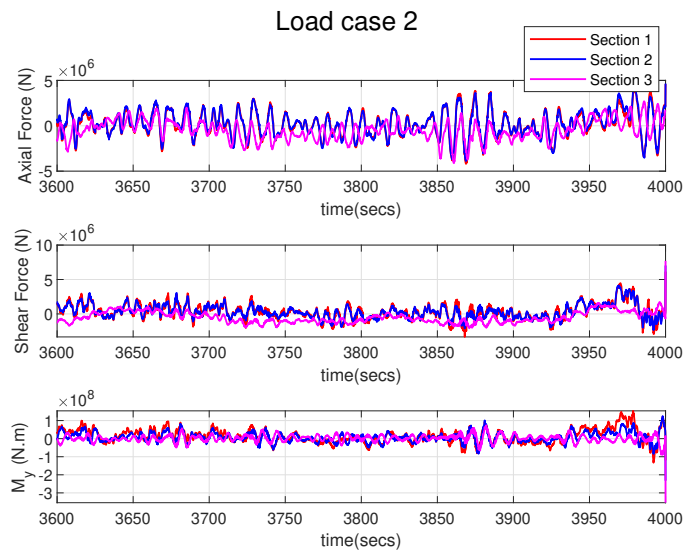


**Figure 6.3:** Comparison of motion response in SIMA (existing mass model) and WASIM+SIMA (modified mass model)



**Figure 6.4:** Comparison of tower base bending moment in SIMA (existing mass model) and WASIM+SIMA (modified mass model)

frequency domain using Fourier transformation and presented as a spectrum in Figure 6.8 to Figure 6.10. The spectrum plot indicates higher loads at pitch resonance (0.03 Hz). In LC1, Axial loads ( $F_x$ ) are higher at section 3 at pitch resonance. This effect is reduced in LC3, and all the three sections experience similar axial loads in LC3. The Shear Force ( $F_z$ ) is similar in LC1 in the three sections, while in LC2, section 2 and section 3 experience lower loads at pitch resonance. The high-frequency response is significant in load case three. The second peak occurs at 0.55 Hz in Axial, Shear, and Bending Moment in LC3. The bending moment ( $M_y$ ) is high at section 1 at pitch resonance. However, Section 3 experiences higher bending moment at higher frequencies, especially at LC3. Figure 6.11 to Figure 6.13 presents the statistical values mean and standard deviation for the loads at the three sections for the three load cases. The mean value of Bending Moment,  $M_y$  increases along the length of the pontoon, with Section 3 having the highest mean bending moment. The standard deviation of Bending Moment decreases along the pontoon length, indicating dispersed values in Section 1 and relatively lesser dispersed values in Section 3. The mean values of Shear Force and Bending Moment do not show significant variation along the pontoon length.

**Figure 6.5:** Sectional Load in LC1**Figure 6.6:** Sectional Load in LC2



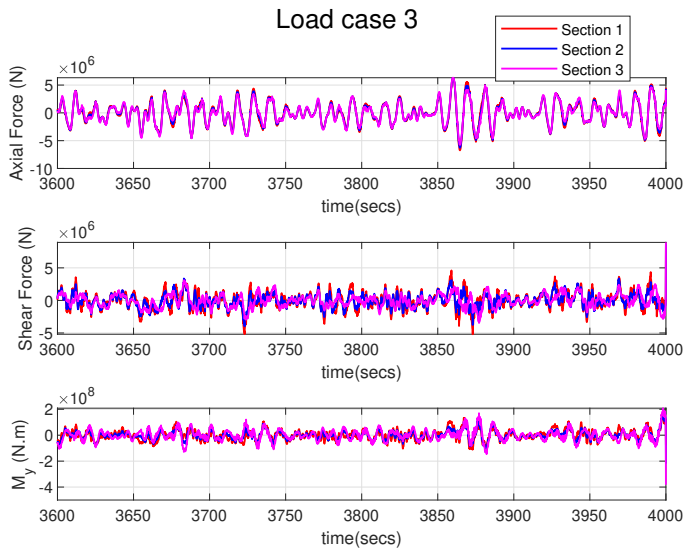


**Figure 6.7:** Sectional Load in LC3

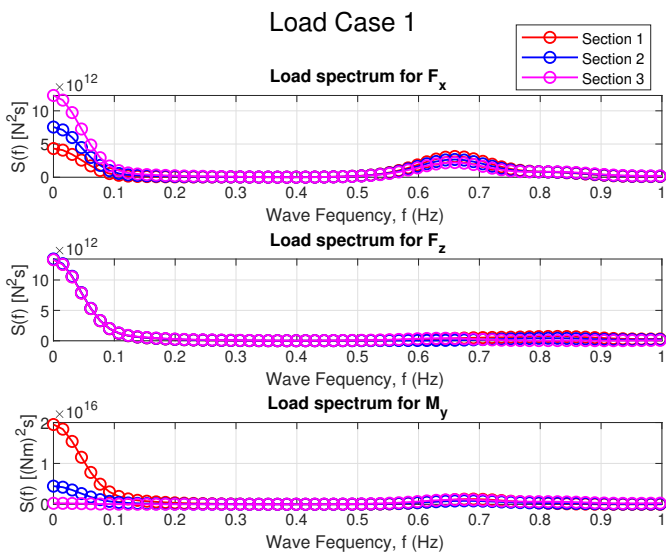


**Figure 6.8:** Sectional Load Spectrum in LC1

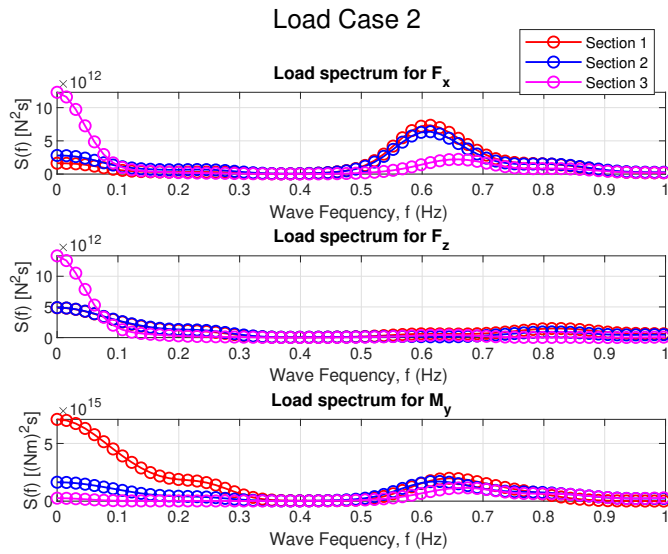


**Figure 6.9:** Sectional Load Spectrum in LC2

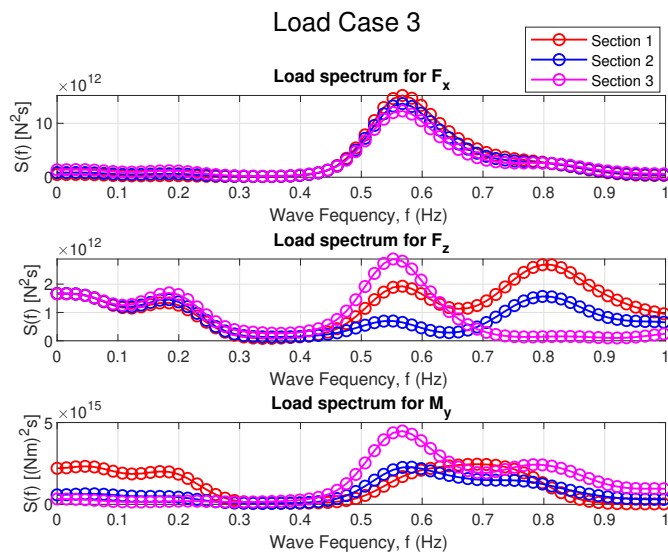


**Figure 6.10:** Sectional Load Spectrum in LC3

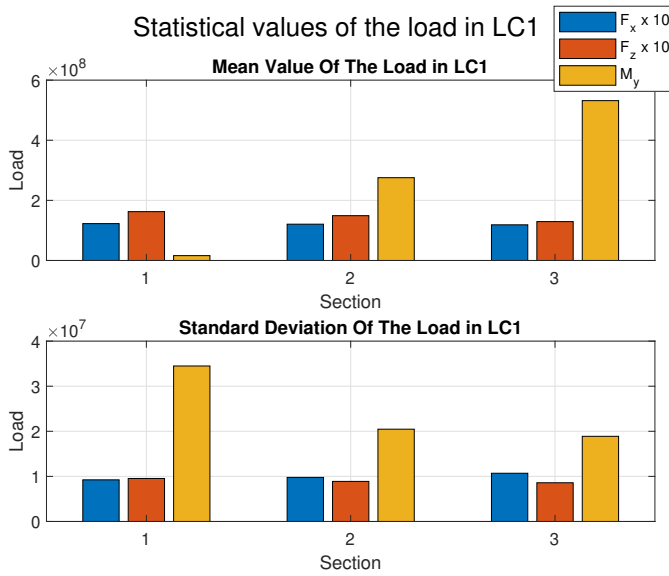


**Figure 6.11:** Sectional Load Statistics in LC1

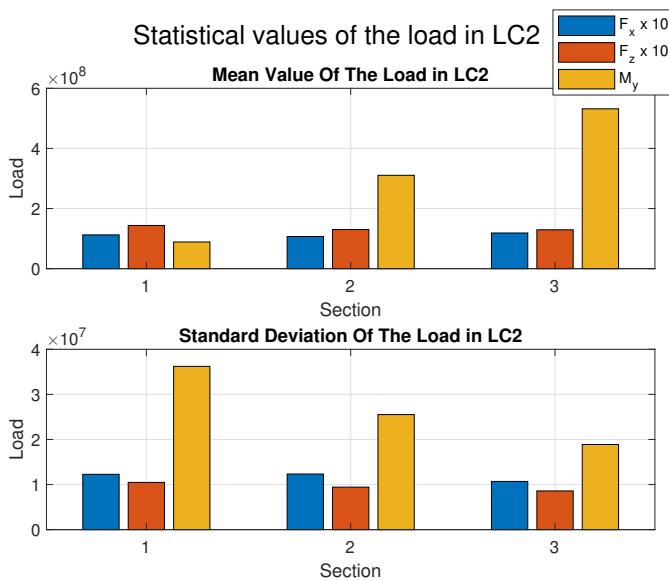


**Figure 6.12:** Sectional Load Statistics in LC2

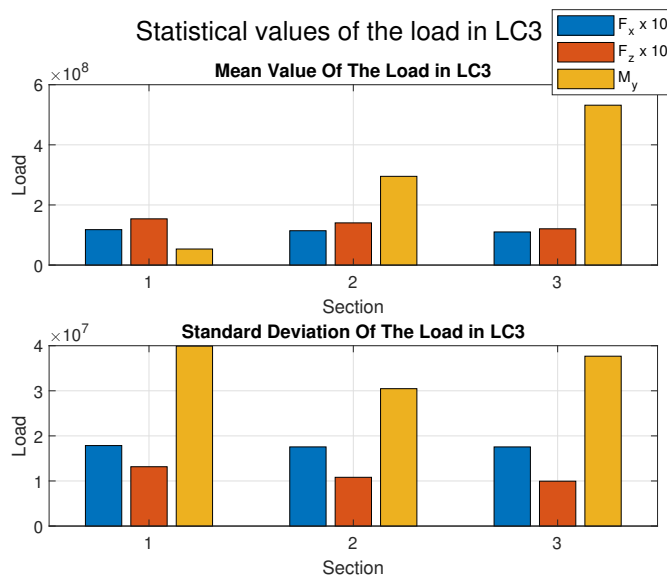


**Figure 6.13:** Sectional Load Statistics in LC3



# Chapter 7

## Flexible body vs. Rigid body

In this chapter, rigid body results presented in Chapter 6 is compared with a flexible body model.

### 7.1 Flexible Body

The flexible body model in this chapter was developed by a Master's student of NTNU, Mr. Yu Ma, for his master thesis "Novel Modeling and Fatigue Analysis for Early-phase Design of a 15-MW FOWT" [16]. The flexible body model is a multi-body representation of the FOWT. The flexible model was developed by discretizing the floater into sub-bodies. The sub-bodies were connected using beam elements in SIMO/RIFLEX [16]. Figure 7.1 presents the flexible body model.

### 7.2 Results and Discussions

#### 7.2.1 Axial Load

Figure 7.2 to Figure 7.4 presents the Axial Load time series comparison between Rigid Body and Flexible Body models for the three load cases. Figure 7.5 to Figure 7.7 presents the comparison in terms of a spectrum. In LC1 and LC2, there is a significant variation in the low-frequency range. This could be due to the influence of pitch resonance. In LC3, there is negligible variation between the rigid body and flexible body results. There is a significant variation in the second peak around 0.65 Hz in section 3 in LC2. Figure 7.8 to Figure 7.10 presents the Statistical values mean and standard deviation of the axial loads in the three load cases. There is no significant variation between the mean and standard deviation values in the three load cases. This indicates that both models show reasonably consistent results concerning axial loads.

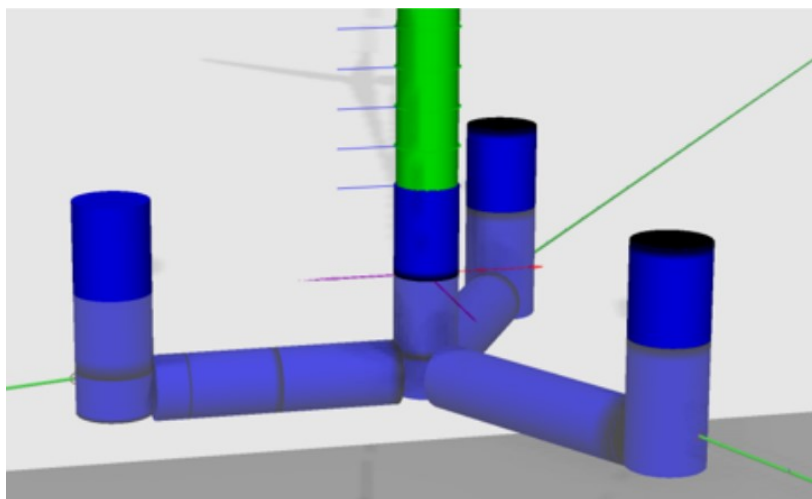


**Figure 7.1:** Flexible Body [16]

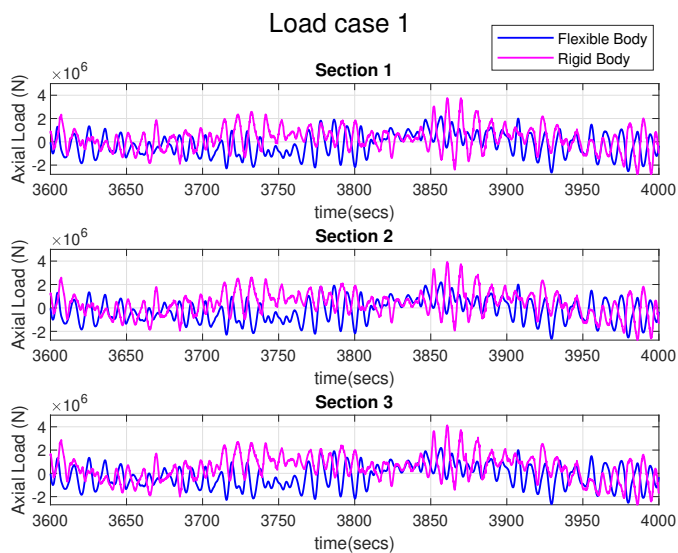


**Figure 7.2:** Axial Load in LC1

## 7.2.2 Bending Moment, $M_y$

Figure 7.11 to Figure 7.13 presents the time series of the bending moment. Figure 7.14 to Figure 7.16 presents the bending moment spectrum. Unlike the axial

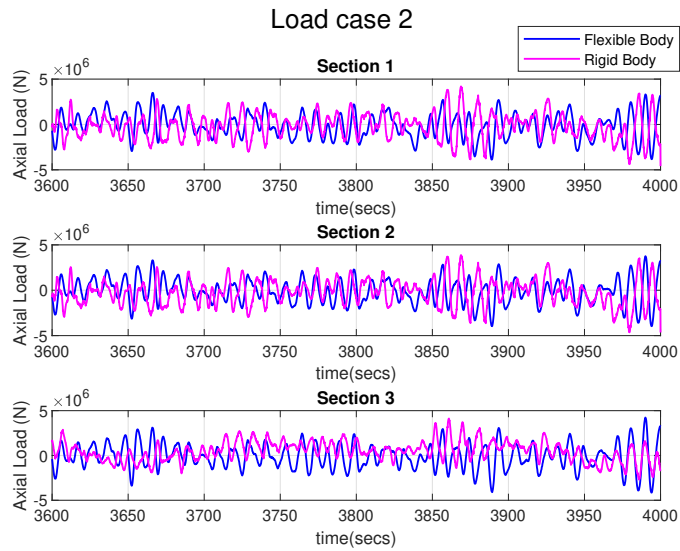


**Figure 7.3:** Axial Load in LC2

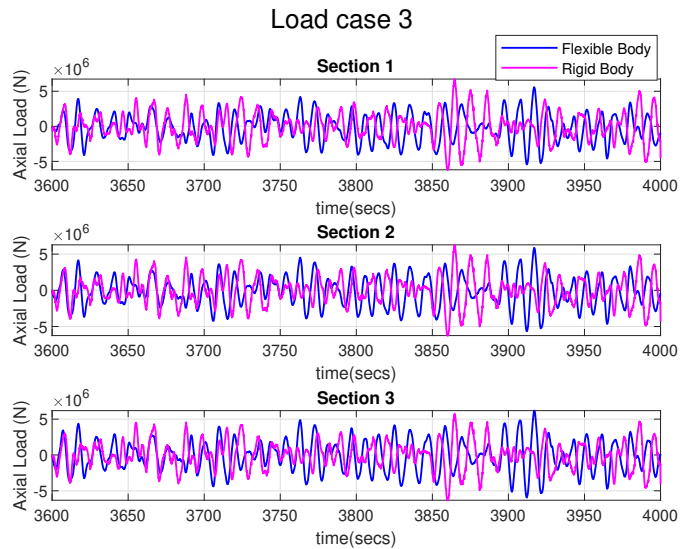


**Figure 7.4:** Axial Load in LC3



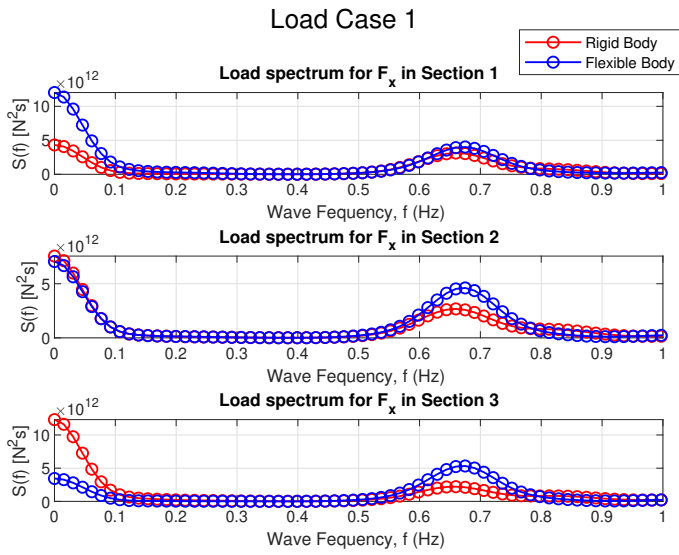


**Figure 7.5:** Axial Load Spectrum in LC1

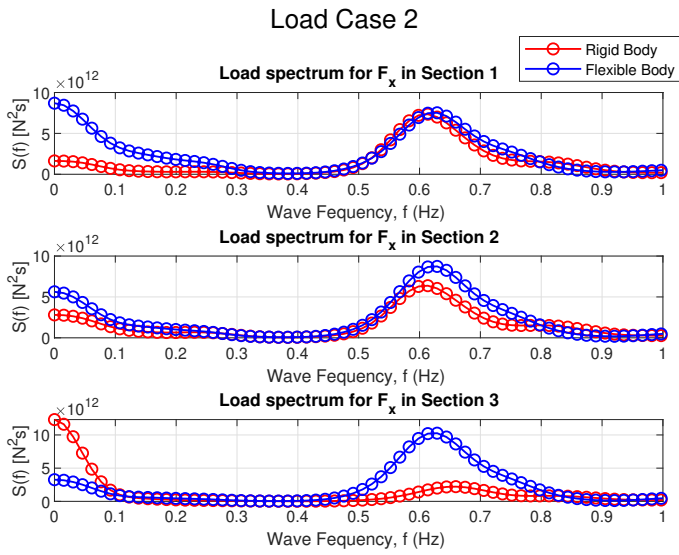


**Figure 7.6:** Axial Load Spectrum in LC2

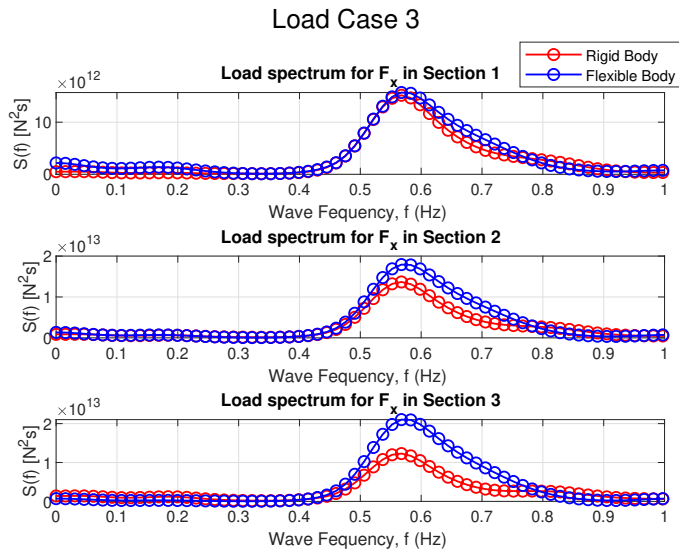


**Figure 7.7:** Axial Load Spectrum in LC3

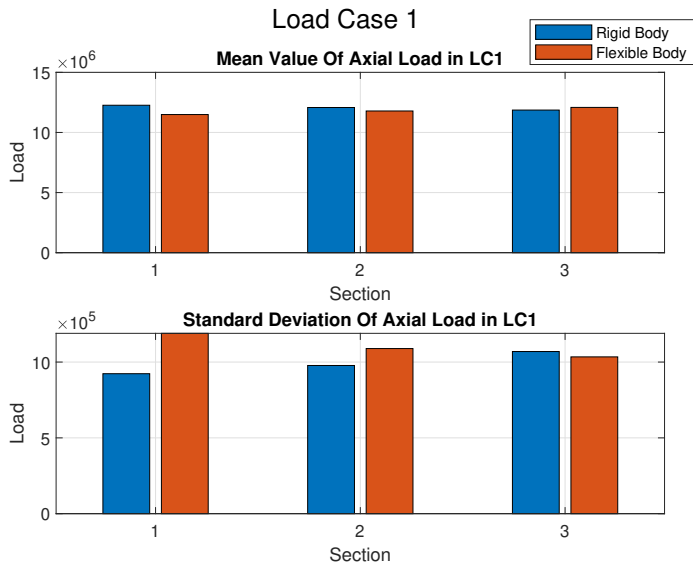


**Figure 7.8:** Axial Load Statistics in LC1

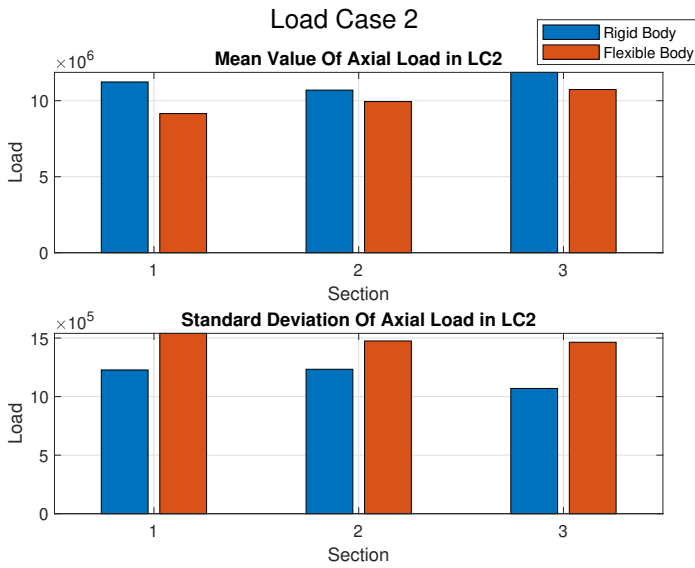


**Figure 7.9:** Axial Load Statistics in LC2

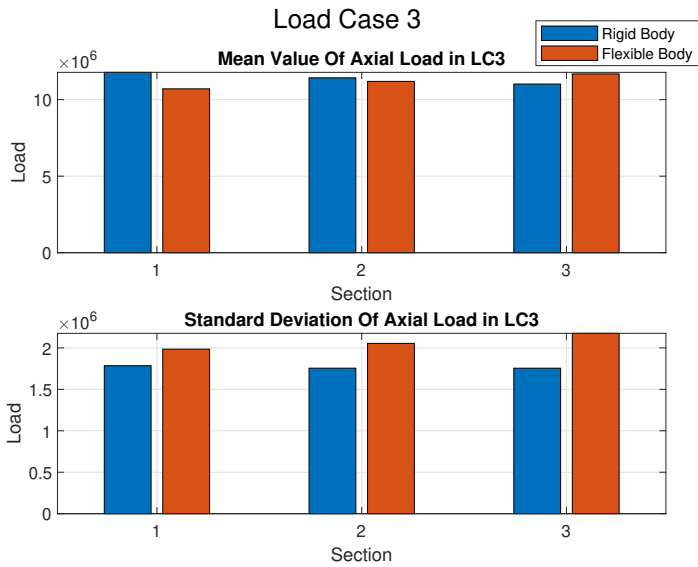


**Figure 7.10:** Axial Load Statistics in LC3

load results presented in Section 7.2.1, the bending moment results show a significant difference between the rigid and the flexible body results. This is also visible in the statistical comparison presented in Figure 7.17 to Figure 7.19. The spectrum plot shows a huge difference in pitch resonance. The rigid and flexible body models are expected to have similar motion responses. But in this case, there is an influence of pitch motion in the flexible body. Two reasons that could have caused these huge differences are :

1. Pitch motion characteristics of the rigid and flexible body models are different.
2. Flexible body model undergoes significant deformation causing this huge difference.

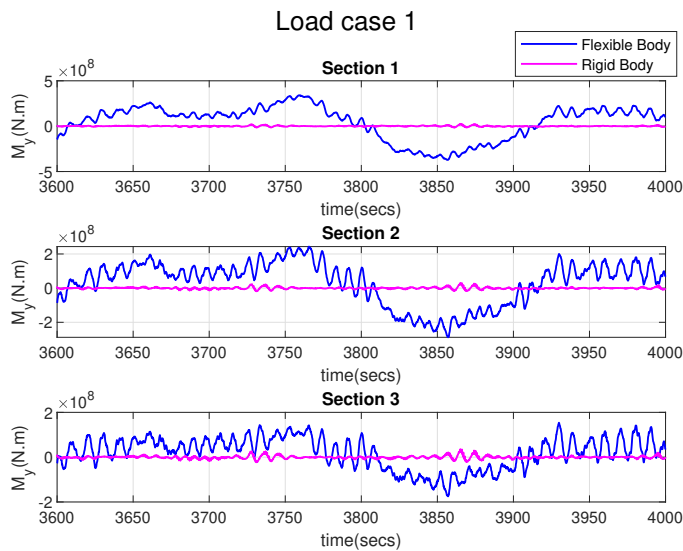


**Figure 7.11:** Bending Moment,  $M_y$  in LC1

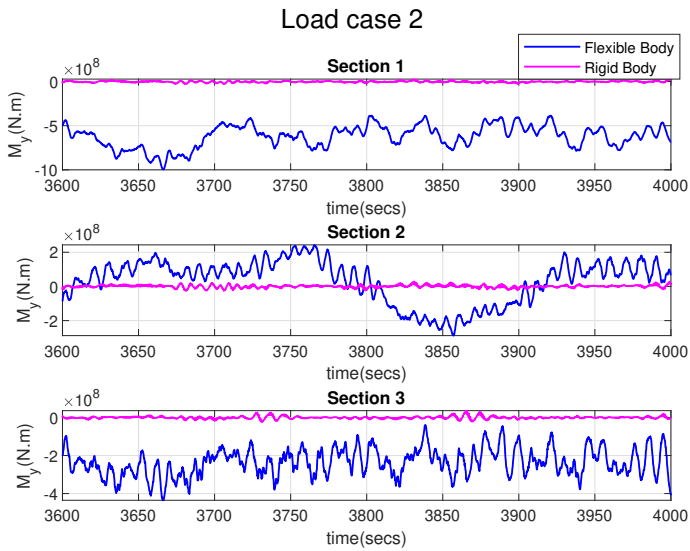


**Figure 7.12:** Bending Moment,  $M_y$  in LC2

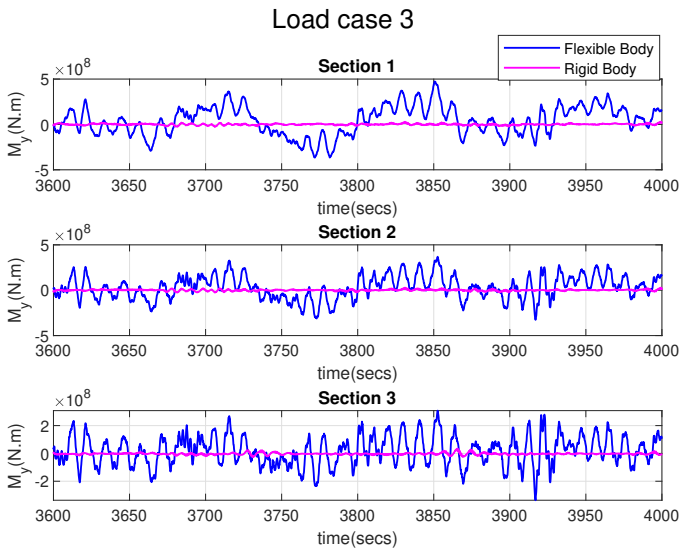


**Figure 7.13:** Bending Moment,  $M_y$  in LC3

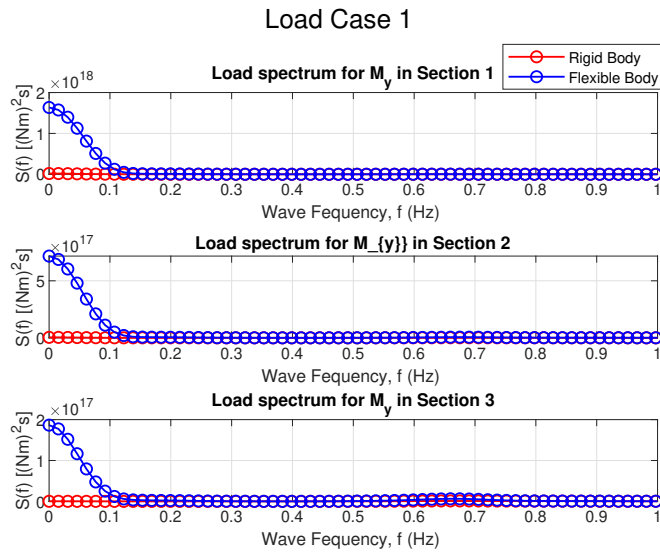


**Figure 7.14:** Bending Moment Spectrum,  $M_y$  in LC1

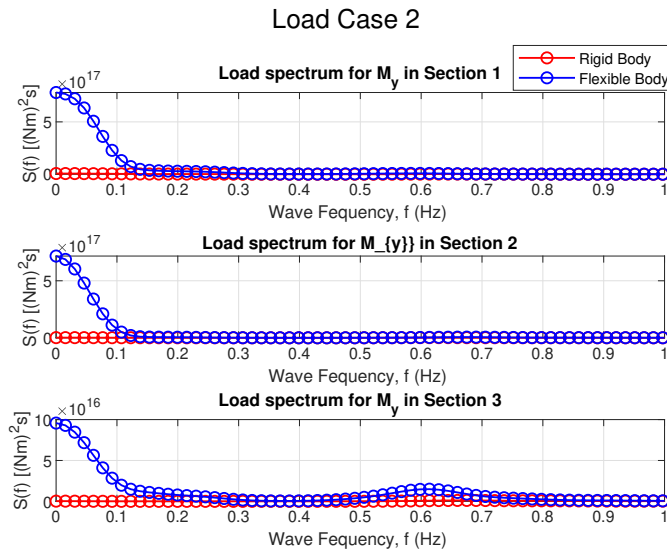


**Figure 7.15:** Bending Moment Spectrum,  $M_y$  in LC2

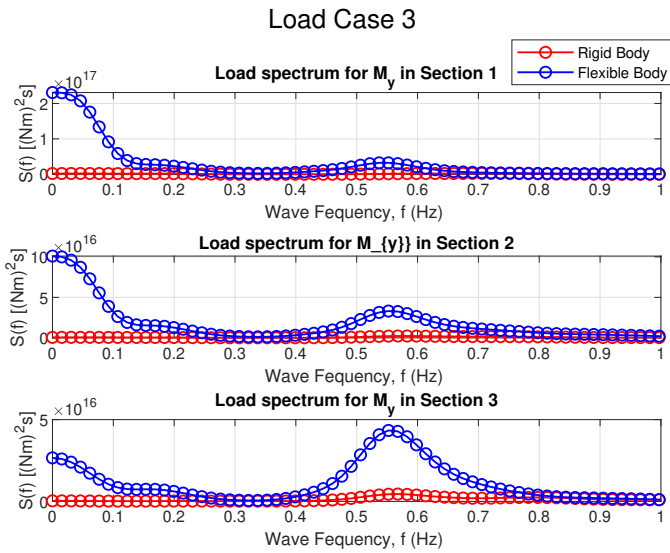


**Figure 7.16:** Bending Moment Spectrum,  $M_y$  in LC3

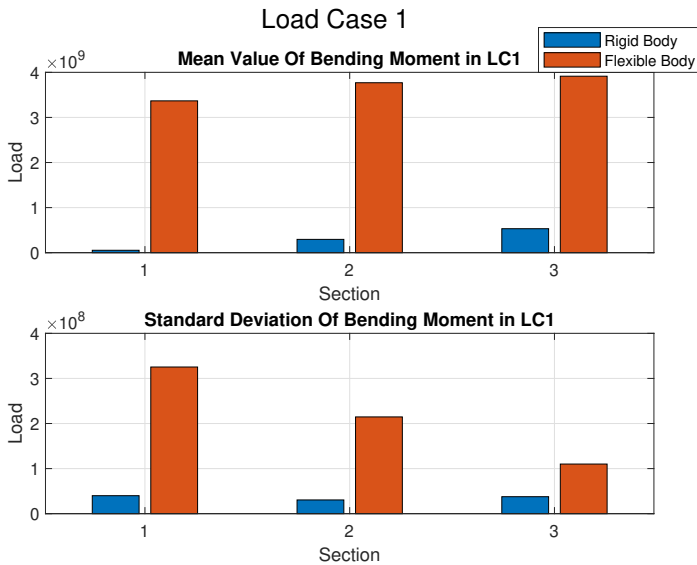


**Figure 7.17:** Bending Moment Statistics,  $M_y$  in LC1

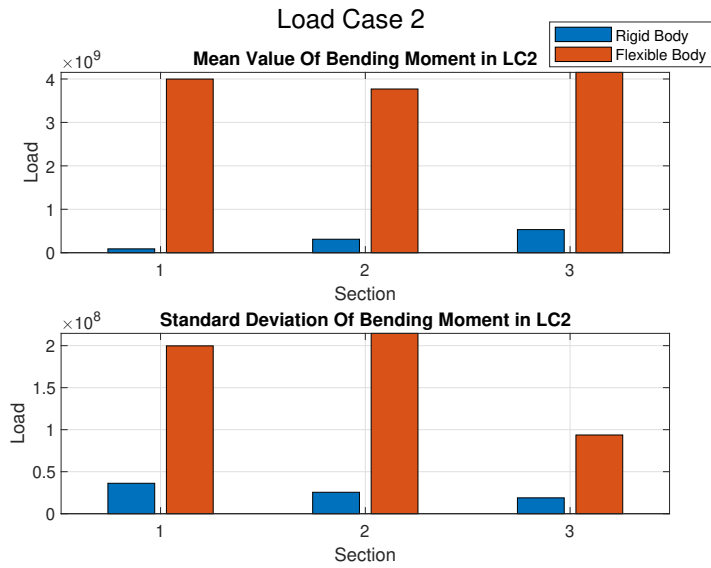


**Figure 7.18:** Bending Moment Statistics,  $M_y$  in LC2

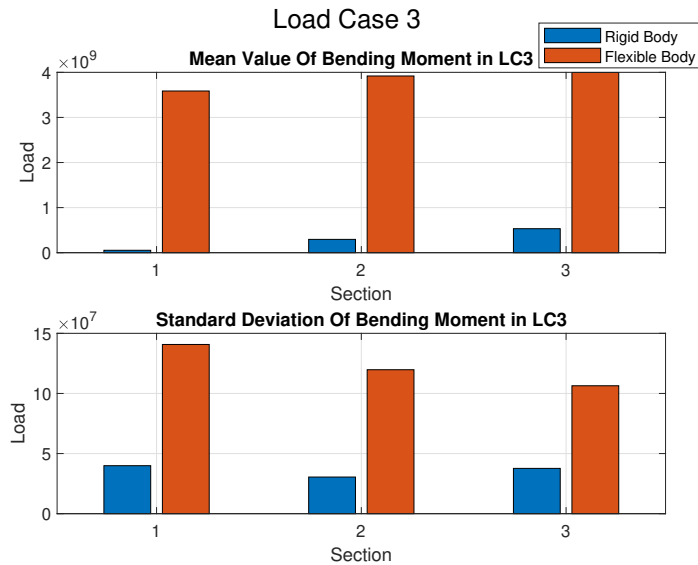


**Figure 7.19:** Bending Moment Statistics,  $M_y$  in LC3





# Chapter 8

## Summary and Conclusion

### 8.1 Summary

The thesis demonstrated an approach to carrying out coupled analysis and transferring the load to the cross-section of the pontoons of the FOWT. The proposed approach has three stages. Stage one is validating the model used in the regular wave and coupled analysis. Stage two validates the proposed approach in a regular wave analysis (wave only). Finally, the model is exposed to a coupled domain in stage three, i.e., simultaneous wind and wave action.

In Stage One, the hydrodynamic properties like added mass, potential damping, and excitation force transfer functions were compared to validate the model used in this thesis work. Their results were reasonably consistent with minor discrepancies. The discrepancies are attributed to the differences in the non-linear damping properties in the models. The SIMA model has a defined mooring line, while mooring lines were not defined in WADAM or WASIM models. The mooring stiffness is accounted for through an additional restoring matrix in WADAM and WASIM. The restoring coefficients in Surge, Sway, and Yaw were obtained from PQ analysis. The PQ analysis results are presented in Appendix [A.3](#).

In Stage Two, the proposed approach is validated by regular wave analysis. The motion response and the sectional loads were compared between the models. The results were reasonably consistent. As expected, there are differences in the resonance zone due to different non-linear damping properties.

In Stage Three, the sectional loads were obtained using the proposed approach. The sectional load's time series and the spectrum were presented. Further, statistical parameters mean and standard deviation of the sectional load were presented.

The proposed approach was compared with a flexible body model. The flexible body model and the rigid body model results were reasonably consistent for the axial load ( $F_x$ ). However, for the bending moment ( $M_y$ ), rigid body and flexible body model results displayed huge variation. The differences could be due to the different pitch motion characteristics of rigid and flexible body models or due to the deformation of the flexible body model.

## 8.2 Conclusion and Future Recommendations

1. The objective of the thesis is to demonstrate a procedure to estimate loads on the cross-section of the FOWT in a coupled domain (simultaneous wind and wave action). The purpose is to account for both wind turbine loads and the hydrodynamic load on the FOWT. The procedure demonstrated, displayed reasonably consistent results. However, the comparison with the flexible body model displayed huge variation, which needs further investigation. Due to lack of time, the motion characteristics of the flexible and rigid body models were not compared. The flexible body model, multi-body representation of the FOWT was developed by a Master's student Mr. Yu Ma, for his Master's Thesis. There could also be a mistake in defining the wind turbulence parameter in Turbsim. In a further study, using the same Turbsim file in both models is recommended. It is recommended to compare the motion characteristics and the wind turbine loads and ensure they are consistent in both rigid and flexible body models. Once the consistency in motion and wind turbine loads are achieved, it is expected for both the flexible body model and the rigid body model to display similar results. If the results are consistent in rigid and flexible body models, flexible body approach in SIMA will be a better technique to estimate loads in the structural member of a FOWT. It offers one stop solution instead of navigating between different numerical tools like WADAM and WASIM in rigid body model approach. Flexible body model also allows to estimate loads in the structural members which are not parallel to the global axes which is a limitation in rigid body approach where cross-sectional loads can be obtained only at the structural members which are parallel to the global axes.
2. In this thesis work, there are minor discrepancies in the resonance region. This is attributed to the differences in non-linear damping properties in SIMA, WASIM, and WADAM models. In SIMA, non-linear damping parameters due to the mooring line are accounted for, while they are not in WADAM and WASIM. In future studies, it is recommended to have consistent damping properties in the different models.
3. Important limitation in the proposed approach is that it is possible only to

estimate the loads at the pontoon aligned with the x-axis. In a further study, it is recommended to develop a procedure to estimate loads in other pontoons which are not parallel to the global axes.

4. Non-linear wave forces are ignored in this thesis work. In a further study, it is recommended to study the effect of non-linear wave forces and investigate the feasibility of including non-linear wave loads in the proposed approach.
5. Due to lack of time, section loads in the side columns were not estimated. In future studies, it is recommended to include the side columns in the load estimation.
6. In a further study, it is recommended to increase the number of load cases and investigate the results for different load cases.
7. The extension of this thesis work be to design the strengthening members of the pontoon based on the estimated load.



# Bibliography

- [1] Gaertner E, Rinker J, Sethuraman L, Zahle F, Anderson B, Barter GE, Abbas NJ, Meng F, Bortolotti P, Skrzypinski W, *et al.*. Iea wind tcp task 37: Definition of the Iea 15-megawatt offshore reference wind turbine ; doi: 10.2172/1603478. URL <https://www.osti.gov/biblio/1603478>.
- [2] Pineda ANI. Wind energy in Europe: Scenarios for 2030. *Wind Europe: Brussels, Belgium* 2017; .
- [3] Arapogianni A, Genachte AB. The next step for offshore wind energy. *A report by European Wind Energy Agency* 2013; .
- [4] Bachynski E. *Offshore wind energy technology Chapter 4. Fixed and Floating OWT support structures*. Wiley, 2018.
- [5] Liu Y, Li S, Yi Q, Chen D. Developments in semi-submersible floating foundations supporting wind turbines: A comprehensive review. *Renewable and Sustainable Energy Reviews* 2016; **60**:433–449, doi:<https://doi.org/10.1016/j.rser.2016.01.109>. URL <https://www.sciencedirect.com/science/article/pii/S1364032116001398>.
- [6] Zhang L, Shi W, Karimirad M, Michailides C, Jiang Z. Second-order hydrodynamic effects on the response of three semisubmersible floating offshore wind turbines. *Ocean Engineering* 2020; **207**:107371, doi:<https://doi.org/10.1016/j.oceaneng.2020.107371>. URL <https://www.sciencedirect.com/science/article/pii/S0029801820304029>.
- [7] *SESAM USER MANUAL WASIM 6.3*.
- [8] Greco M. *TMR 4215: Sea Loads*. 1 edn., NTNU, Marine Technology, 2019.

- [9] Larsen C. Marine dynamics: Tmr4182 marine dynamics. *Akademika forlag Kompendieforlaget, Trondheim* 2014; .
- [10] Chakrabarti S. *Handbook of Offshore Engineering*. 2005.
- [11] Hansen M. *Aerodynamics of wind turbines*. Routledge, 2015.
- [12] *SESAM USER MANUAL WADAM 9.3*.
- [13] Jonkman JM. Loads analysis of a floating offshore wind turbine using fully coupled simulation. *Technical Report*, National Renewable Energy Lab.(NREL), Golden, CO (United States) 2007.
- [14] Bachynski E. *TMR 4505 : Integrated dynamic analysis of wind turbine Lecture slides*. 2021.
- [15] MARINTEK. Simo—theory manual version 4.0 2012.
- [16] Ma Y. Novel modeling and fatigue analysis for early-phase design of a 15-mw fowt 2022.
- [17] Faltinsen O. *Sea Loads on ship and offshore structures*. 1 edn., Cambridge university press, 1990.
- [18] Eriksen R, Engel D, Haugen U, Hodne T, Hovem L, Alvik S, Rinaldo M, *et al.*. Energy transition outlook 2021: Technology progress report 2021; .
- [19] Veers P, Dykes K, Lantz E, Barth S, Bottasso CL, Carlson O, Clifton A, Green J, Green P, Holttinen H, *et al.* ; .
- [20] Why offshore wind energy? *Renewable Energy* 2011; **36**(2):444–450, doi:<https://doi.org/10.1016/j.renene.2010.07.009>. URL <https://www.sciencedirect.com/science/article/pii/S0960148110003332>.
- [21] Bento N, Fontes M. Emergence of floating offshore wind energy: Technology and industry. *Renewable and Sustainable Energy Reviews* 2019; **99**:66–82, doi:<https://doi.org/10.1016/j.rser.2018.09.035>. URL <https://www.sciencedirect.com/science/article/pii/S1364032118306841>.
- [22] Bae Y, Kim M, Im S, Chang I. Aero-elastic-control-floater-mooring coupled dynamic analysis of floating offshore wind turbines. *The Twenty-first International Offshore and Polar Engineering Conference*, OnePetro, 2011.

- [23] *Time Domain Coupled Analysis and Load Transfer for Floating Wind Turbine Structures*, *International Conference on Offshore Mechanics and Arctic Engineering*, vol. Volume 1: Offshore Technology, doi:10.1115/OMAE2018-77880. URL <https://doi.org/10.1115/OMAE2018-77880>, v001T01A027.
- [24] Leble V, Barakos G. A coupled floating offshore wind turbine analysis with high-fidelity methods. *Energy Procedia* 2016; **94**:523–530.
- [25] Jonkman J, Sclavounos P. Development of fully coupled aeroelastic and hydrodynamic models for offshore wind turbines. *44th AIAA Aerospace Sciences Meeting and Exhibit*, 2006; 995.
- [26] Luan C, Gao Z, Moan T. Development and verification of a time-domain approach for determining forces and moments in structural components of floaters with an application to floating wind turbines. *Marine Structures* 2017; **51**:87–109.
- [27] Svendsen KF. Structural design and dynamic analysis of a tension leg platform wind turbine, considering elasticity in the hull. Master's Thesis, NTNU 2016.
- [28] Edwards E. Introduction to linear panel method, WAMIT . MIT ; .
- [29] Hasselmann K, Barnett TP, Bouws E, Carlson H, Cartwright DE, Enke K, Ewing J, Gienapp A, Hasselmann D, Kruseman P, *et al.*. Measurements of wind-wave growth and swell decay during the joint north sea wave project (jonswap). *Ergaenzungsheft zur Deutschen Hydrographischen Zeitschrift, Reihe A* 1973; .
- [30] Hopstad ALH, Argyriadis K, Manjock A, Goldsmith J, Ronold KO. Dnv gl standard for floating wind turbines. *International Conference on Offshore Mechanics and Arctic Engineering*, vol. 51975, American Society of Mechanical Engineers, 2018; V001T01A020.
- [31] As D. Loads and site conditions for wind turbines 2016.
- [32] Moriarty PJ, Hansen AC. Aerodyn theory manual. *Technical Report*, National Renewable Energy Lab., Golden, CO (US) 2005.
- [33] Manwell JF, McGowan JG, Rogers AL. *Wind energy explained: theory, design and application*. John Wiley & Sons, 2010.
- [34] Bhattacharya S. *Design of foundations for offshore wind turbines*. John Wiley & Sons, 2019.



- 
- [35] MARINTEK. Simo—user manual version 4.0 2012.
- [36] MARINTEK. Riflex—user manual version 4.0 2012.
- [37] RP D, *et al.*. Dnv-rp-0286 coupled analysis of floating wind turbines. høvik, norway 2019; .
- [38] RP D, *et al.*. Environmental conditions and environmental loads. høvik, norway 2010; .
- [39] Software D. Sesam workshop: Advanced hydrodynamics– modelling and verification 2019; .

# Appendices





# Appendix A

## A.1 Wind turbine performance curve

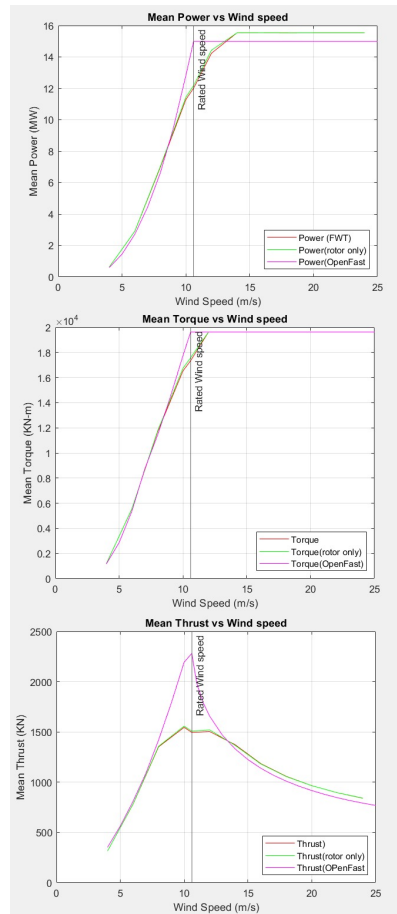


Figure A.1: Wind turbine performance curves

## A.2 Linearized Boundary Value problem

In hydrodynamic load, assessment seawater is assumed to be inviscid and incompressible. A scalar quantity, velocity potential ( $\phi$ ), describes the fluid velocity vector  $\mathbf{V}(x,y,z,t)$ . [17]

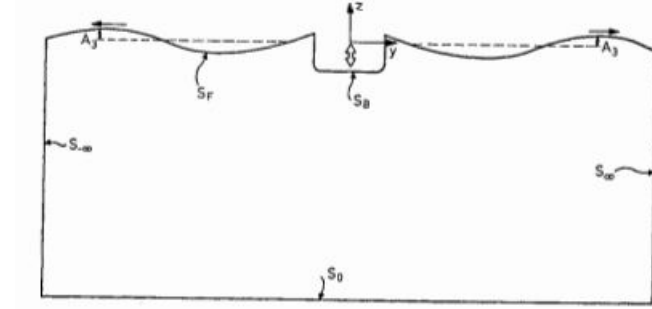


Figure A.2: Control surface in boundary value problem [17]

$$\mathbf{V} = \nabla\phi = \mathbf{i}\frac{\partial\phi}{\partial x} + \mathbf{j}\frac{\partial\phi}{\partial y} + \mathbf{k}\frac{\partial\phi}{\partial z} \quad (\text{A.1})$$

The velocity potential ( $\phi$ ) has to satisfy the following conditions:

1. Laplace equation :

$$\nabla^2\phi = 0 \quad (\text{A.2})$$

2. Boundary conditions:

- (a) Kinematic free surface boundary condition:

The kinematic free surface boundary condition (KFSBC) restricts the water particles from staying at the free surface.

$$\frac{\partial\zeta}{\partial t} = \frac{\partial\phi}{\partial z} \text{ on } z = 0 \quad (\text{A.3})$$

- (b) Dynamic free surface boundary condition:

The dynamic free surface boundary condition (DFSBC) is the water pressure is equal to the atmospheric pressure at the free surface.

$$\frac{\partial\phi}{\partial t} + g\zeta = 0 \text{ on } z = 0 \quad (\text{A.4})$$

(c) Combined free surface boundary condition:

The combined free surface boundary condition is a combination(CFSBC) of KFSBC and DFSBC.

$$\text{Time domain : } \frac{\partial \phi}{\partial t^2} + \frac{g \partial \phi}{\partial z} = 0 \quad \text{on } z = 0 \quad (\text{A.5})$$

$$\text{Frequency domain : } -\omega^2 \phi + g \frac{\partial \phi}{\partial z} = 0 \quad \text{on } z = 0 \quad (\text{A.6})$$

(d) Body boundary condition:

Body boundary condition restricts the body's velocity to be equal to the velocity of water particles.

$$\frac{\partial \phi}{\partial n} = V_n \quad \text{on } S_F \text{ and } S_B \quad (\text{A.7})$$

$$\frac{\partial \phi}{\partial n} = 0 \quad \text{on } S_0 \quad (\text{A.8})$$

1. Solve the boundary value problem,

$$\nabla^2 \phi = 0$$

find  $\phi$  using the boundary conditions.

2. Find the force vector (6X1):

The force vector can be obtained by integrating the linearized Bernoulli equation.

$$p = -\rho \left( \frac{\partial \phi}{\partial t} + gz \right) \quad (\text{A.9})$$

$$F = \int_{SB_0} \frac{\rho \partial \phi \cdot n \cdot dS}{\partial t} + \int_{SB_1} \rho gz \cdot n \cdot ds \quad (\text{A.10})$$

$$F = \underbrace{\int_{SB_0} \frac{\rho \partial \phi \cdot n \cdot dS}{\partial t}}_{\text{hydrodynamic loads}} + \underbrace{\int_{SB_1} \rho gz \cdot n \cdot ds}_{\text{hydrostatic loads}}$$

**Figure A.3:** Hydrodynamic and Hydrostatic loads

### A.3 PQ Analysis

Part 2

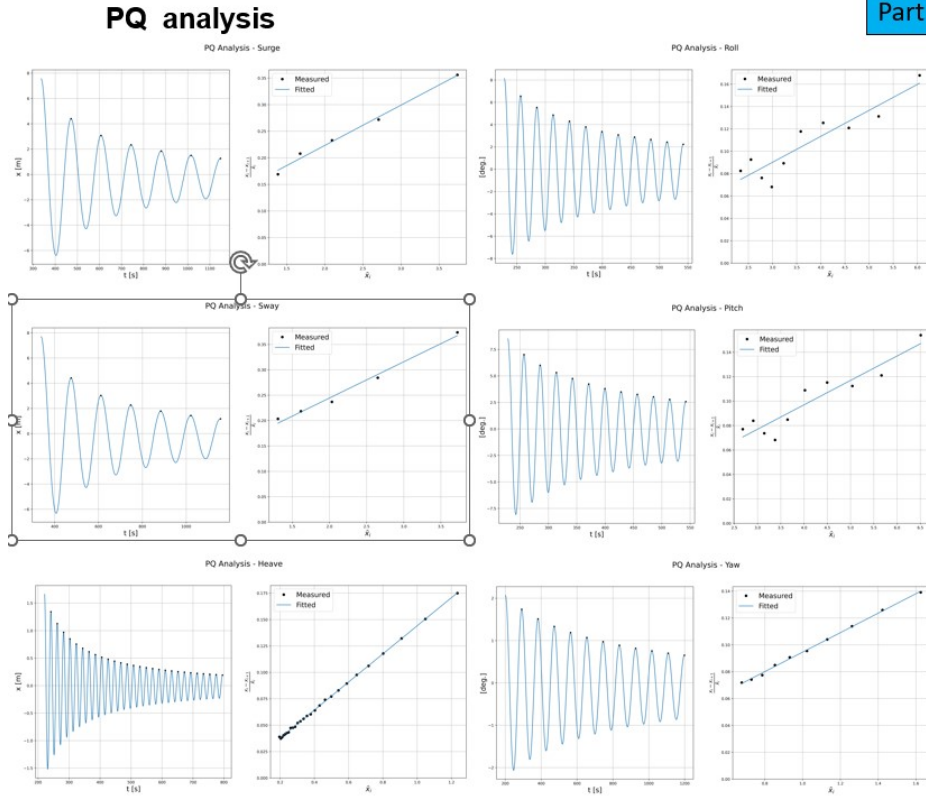


Figure A.4: PQ Analysis

DOF	P	Q	$T_d$	$w_d$	Steady Disp	Applied Moment	K
			s	rad/s	m or deg	kN/kNm	kN/m or kNm/rad
Surge	0.0717	0.0758	135	0.04643	22.766	2250	9.88E+01
Sway	0.1017	0.0714	136	0.04610	27.604	2250	8.15E+01
Heave	0.0112	0.1329	21	0.30628	2.200	10000	4.55E+03
Roll	0.0206	0.0232	29	0.22039	10.792	530000	2.81E+06
Pitch	0.0171	0.0200	29	0.22008	9.290	530000	3.27E+06
Yaw	0.0220	0.0725	91	0.06930	2.182	10000	2.63E+05

Figure A.5: Mooring Stiffness coefficients





# Appendix B

## B.1 Miscellaneous Results in Coupled Analysis

### B.1.1 Motion results

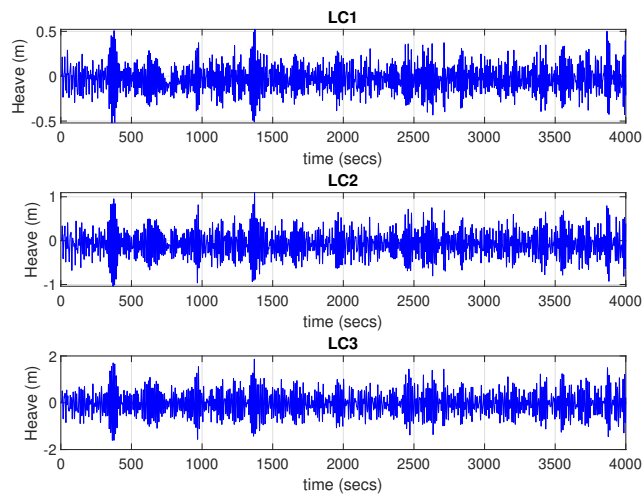
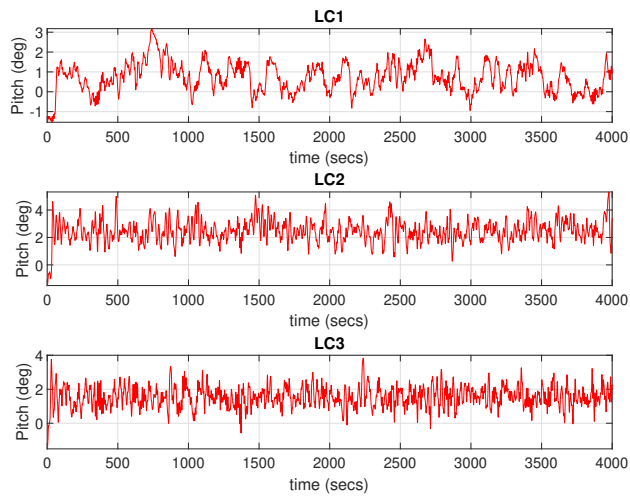
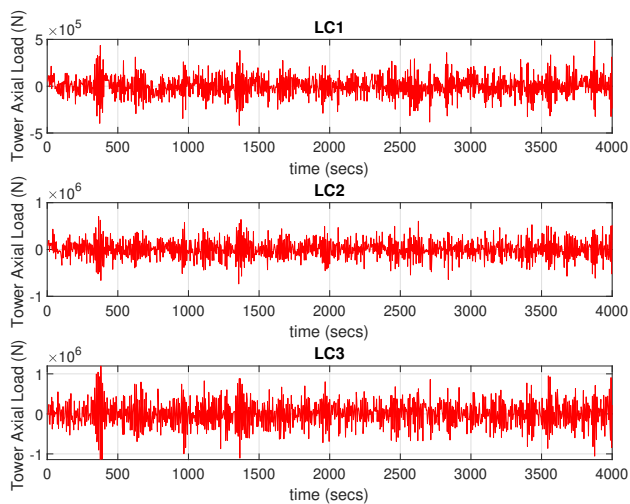


Figure B.1: Heave



**Figure B.2: Pitch**

## B.1.2 Aerodynamic And Mooring Loads



**Figure B.3: Tower Base Axial Loads**

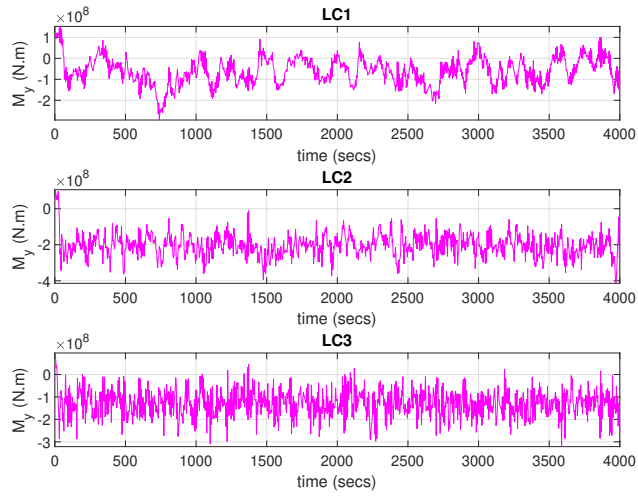


Figure B.4: Tower Base Bending Moment

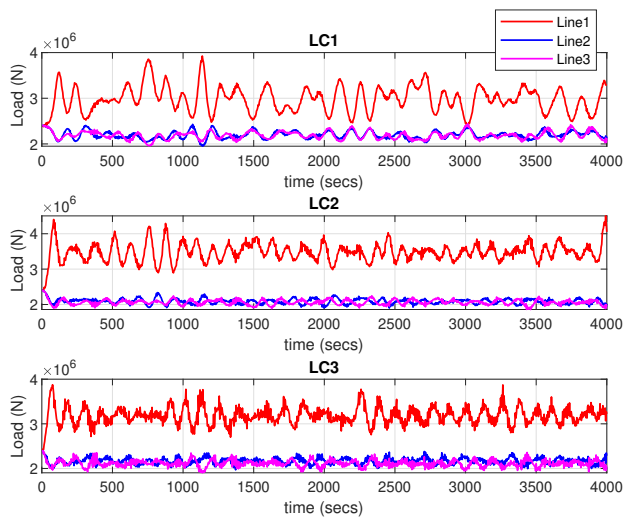


Figure B.5: Mooring Loads

